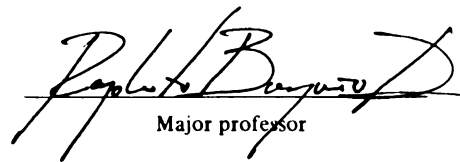This is to certify that the

thesis entitled

Shear Response of Concrete Filled Circular
Fiber-Reinforced-Polymer Composite Tubes

presented by

Kedar Mohan Bhide

has been accepted towards fulfillment
of the requirements for

Master's ____degree in Civil Engineering

Major professor

Date 11/7/02

O-7639   *MSU is an Affirmative Action/Equal Opportunity Institution*

PLACE IN RETURN BOX to remove this checkout from your record.
TO AVOID FINES return on or before date due.
MAY BE RECALLED with earlier due date if requested.

DATE DUE	DATE DUE	DATE DUE

6/01 c:/CIRC/DateDue.p65-p.15

SHEAR RESPONSE OF CONCRETE FILLED CIRCULAR FIBER-REINFORCED-POLYMER COMPOSITE TUBES

By

Kedar Mohan Bhide

A THESIS

Submitted to
Michigan State University
in partial fulfillment of the requirements
for the degree of

MASTER OF SCIENCE

Department Civil and Environmental Engineering

2002

ABSTRACT

SHEAR RESPONSE OF CONCRETE FILLED CIRCULAR FIBER-REINFORCED-POLYMER COMPOSITE TUBES

By

Kedar Mohan Bhide

Concrete filled FRP tubes have been recognized as an efficient hybrid concept for structural members. Recent research projects have led to a good understanding of the axial and flexural behavior of this system. However, the shear response of concrete filled FRP tubes has so far been addressed only in a preliminary way.

An analytical procedure for predicting the shear load-deformation response of concrete filled circular FRP composite tubes with full- and non-composite behavior until first-ply-failure of the FRP composite has thus been developed. The approach is based on a sectional layered analysis with an iterative algorithm to achieve equilibrium and compatibility conditions of the FRP/concrete system. The model follows first order mechanics for the shear behavior of structural members in combination with a smeared shear modulus for cracked concrete and inclusion of extension/shear coupling effects of anisotropic FRP laminates.

Comparisons of the analytical response with available experimental test data were found, in general, to be in good agreement. The correlation of analytical to experimental response indicated the significant influence of shear interaction between the FRP shell and the concrete on the shear load-deformation response. Parametric studies that evaluate the influence of axial load, concrete compressive and tensile strength, and FRP laminate thickness and lay-up were performed.

In memory of my Grandmother and my best friend Saumitra

ACKNOWLEDGMENTS

TABLE OF CONTENTS

LIST OF TABLES

LIST OF FIGURES

KEY TO SYMBOLS

θ	Angle of inclination of principal stresses and strains
ε_i	Off axis components of strain in FRP shell, $i = x, y, xy$
ε_1	Principal tensile strain in concrete
ε_2	Principal compressive strain in concrete
ε_H	Hoop strain in FRP shell
ε_L	Longitudinal strain in FRP shell
ε_r	Radial strain in concrete
γ	Shear strain in FRP shell
σ	Normal stress in concrete
ρ	Reinforcement ratio
τ	Shear stress in FRP shell
ν	Shear stress in concrete
ν_{LT}	Longitudinal Poisson's ratio in FRP shell
ν_{TL}	Transverse Poisson's ratio in FRP shell
A	Cross-sectional area
A_{ij}, B_{ij}, D_{ij}	Plate stiffness matrices
B	Width of section
D	Diameter of section
E_{co}	Modulus of elasticity of concrete (initial tangent stiffness)
E_L	Longitudinal Young's modulus of FRP laminate
E_T	Transverse Young's modulus of FRP laminate
F	Force in concrete fiber
f_{ci}	Stress in concrete fiber, $i = x, y$
f_{cr}	Stress in concrete at cracking
f_r	Modulus of rupture of concrete
f_s	Average stress in reinforcement
G_c	Shear modulus of concrete
G_{eff}	Effective shear modulus

G_{LT}	Longitudinal shear modulus of FRP laminate
h, t	Thickness of laminate
h_i	Distance of the lamina from reference line
I	Moment of inertia of cross-sectional area
M	Bending moment
N	Stress resultant in FRP laminate
Q	First moment of area
Q_{ij}	Stiffness of a unidirectional composite
q	Shear flow
R	Radius of section
S	Longitudinal shear strength.
$S_{m\theta}$	Crack spacing
V	Shearing force in concrete
V_{cimax}	Maximum shear stress in concrete
X_C	Longitudinal compressive strength of FRP laminate
X_T	Longitudinal tensile strength of FRP laminate
y	Co-ordinate of a material point
Y_C	Transverse compressive strength of FRP laminate
Y_T	Transverse tensile strength of FRP laminate

CHAPTER 1: INTRODUCTION

1.1 General

This chapter gives an introduction to the research work presented in this thesis on the shear characterization of concrete filled circular FRP tubes. First, background on past research work on concrete filled circular FRP tubes is discussed. Secondly, a summary on the concrete filled FRP tube as a structural system is provided. The problem statement, research objectives and research significance are then provided. Lastly, the scope of the work is presented.

1.2 Background

The use of Fiber Reinforced Polymer (FRP) composites for new structures in civil infrastructure is expanding. The qualities of FRP composites like high strength-to-weight and high stiffness to weight ratio, high durability, corrosion resistance etc., have made this material attractive. However, while these materials offer unique mechanical properties, their initial cost is still considerably high. This has motivated researchers to develop structural concepts that combine common materials, like concrete and steel, with FRP composites. This has led to the development of concrete/FRP hybrid systems.

Extensive research work on concrete filled FRP tubes has been conducted, and continues to be in progress, led by Sieble *et al.* [14] at the University of California, San Diego (UCSD); by Mirmiran, A. *et al* [10] at the University of Central Florida, University of Cincinati and now at North Carolina State University and by Rizkalla, S. *et al.* [15] at University of Manitoba and now at North Carolina State University. Their

1

active research work in the concept development and structural characterization of concrete filled FRP tubes has provided great understanding on the axial and flexural behavior of this system. Research work at UCSD has led to application of concrete filled FRP tubes as girders in the Kings Stormwater Channel Bridge and as girders and pylons for the new I-5/Gilman Advanced Technology Bridge [17], currently under design.

1.3 Concrete filled FRP tube

The advantages of FRP composites can be better exploited when they are combined with other materials that enhance the performance of the material system combination. Concrete filled FRP tube members consist of three basic components viz. the FRP composite tube, the concrete core and transverse ribs to provide composite action between the two materials. The prefabricated FRP tubes acts as reinforcement and formwork for the concrete. The concrete helps in the compression force transfer and also provides stability to the FRP shell in compression. In addition, the FRP shell provides confinement to the concrete core under compression forces. This confinement enhances the capacity of the concrete core in compression by allowing the concrete to achieve higher strengths and greater ductility. The design of the FRP tubes provides fibers in the longitudinal direction for member bending stiffness and also in the transverse direction for shear and concrete confinement.

1.4 Problem statement

Concrete filled FRP tubes are recognized as a viable option for use as a structural element. However, in order to apply this concept widely, it is necessary to fully

characterize their behavior. The axial and flexural behavior of concrete filled FRP tube is well understood from recent years of research efforts [5]. However the shear behavior of this system has not been fully investigated. The proposed research work focuses on the analytical evaluation of the shear load-deformation response and the shear strength of concrete filled circular FRP composite tubes.

1.5 Objective

The objective of this research work is to develop a rational analycal approach that allows the evaluation of the shear load-deformation response of concrete filled circular FRP composite tubes.

In order to achieve this task, the following specific tasks were defined:

1. Develop an analytical procedure for the shear force distribution between the concrete core and the FRP shell.

2. Include the behavior of concrete under shear loads to measure the shear carrying capacity of cracked concrete based on its shear modulus.

3. Incorporate the extension/shear coupling effects in an existing analytical model for axial and flexure response to capture the influence of anisotropic FRP shell architecture on the shear response

4. Validate the analytical model by comparing the analytical response with experimental data.

5. Conduct parametric studies on the shear behavior of circular concrete filled FRP tubes.

1.6 Research Significance

Concrete filled FRP tubes have started to be used as a primary structural element in civil structures. It is thus necessary to be fully knowledgeable of the axial, flexural, torsion and shear behavior of this structural element. This study will help researchers to understand the shear load–deformation response of circular concrete filled FRP tubes. The work is also expected to provide valuable insight into the shear design of this hybrid system for future applications.

1.7 Scope

This thesis is divided into six chapters and the work is organized as follows: Chapter 2 covers the theoretical considerations in the development of the analytical procedure for the evaluation of the shear response of concrete filled FRP members. It presents an overview on the mechanics of shear stress analysis of prismatic beams. A summary of the mechanics of laminated FRP composite tubes and the failure criteria used is then provided, followed by a discussion on the behavior of concrete filled FRP shells. The chapter also provides an overview on the analytical models for the shear response of other structural members including a detailed discussion of the modified compression field theory.

Chapter 3 covers the analytical procedure for modeling the shear response of concrete filled FRP tubes. A brief summary on the flexural behavior of circular concrete filled FRP tubes, considered as the base model for this work, is provided. The analytical procedure to enhance the available model for anisotropic shell behavior is then described.

Lastly, an analytical procedure to calculate the shear response of concrete filled circular FRP tubes with and without bond between the concrete and the FRP tube is described.

Chapter 4 focuses on the validation of the proposed models and analytical procedure. The analytical results are compared with the experimental response of concrete filled FRP girders. The experimental data was obtained from the research work conducted at the University of California, San Diego [2][4]. Two large-scale tests and two small-scale tests on concrete filled FRP tubes with and without bond details between the concrete core and the FRP tube, respectively, are considered.

Chapter 5 contains parametric studies performed to evaluate the influence of different parameters in the shear behavior of circular concrete filled FRP tubes.

Finally, chapter 6 provides a summary of the work and concluding remarks including recommendations for future research.

CHAPTER 2: THEORETICAL CONSIDERATIONS

2.1 General

This chapter discusses the theoretical considerations in the development of the analytical procedure to evaluate the shear response of concrete filled FRP members. The mechanics of shear stress analysis of structural members are first discussed. Secondly, an overview on the mechanics of laminated FRP composites with an emphasis on in-plane behavior is presented. Then, an overview of previously developed models for concrete filled FRP tubes is provided. Lastly, a discussion on the current methods to evaluate the shear response and strength of structural members composed of reinforced concrete, concrete filled steel tubes and concrete filled FRP tubes is provided.

2.2 Mechanics of shear stress analysis of structural members

An overview on the fundamental strength of materials concept on shear stress distribution across circular prismatic beam sections is covered in this section. The reader is referred to references [7][11][18][22] for more details.

Consider a simply supported circular prismatic beam with diameter d subjected to arbitrary load q and an element of length dx from section A-A as shown in Figure2.2.1. Under differential loading the bending moment will change from M at point A to $M + dM$ at point B with associated shear forces at point A of V and at point B of $V + dV$. We recall the relationship between the shear V and a change in the bending moment M is expressed by:

$$\frac{dM}{dX} = -V \qquad (2.2.1)$$

Due to the bending moment, bending stresses are developed normal to the section.

These bending stresses are given by:

$$\sigma_b = \frac{M \cdot y}{I} \qquad \text{at location A} \qquad (2.2.2)$$

$$\sigma_b = \frac{(M + dM) \cdot y}{I} \qquad \text{at location B} \qquad (2.2.3)$$
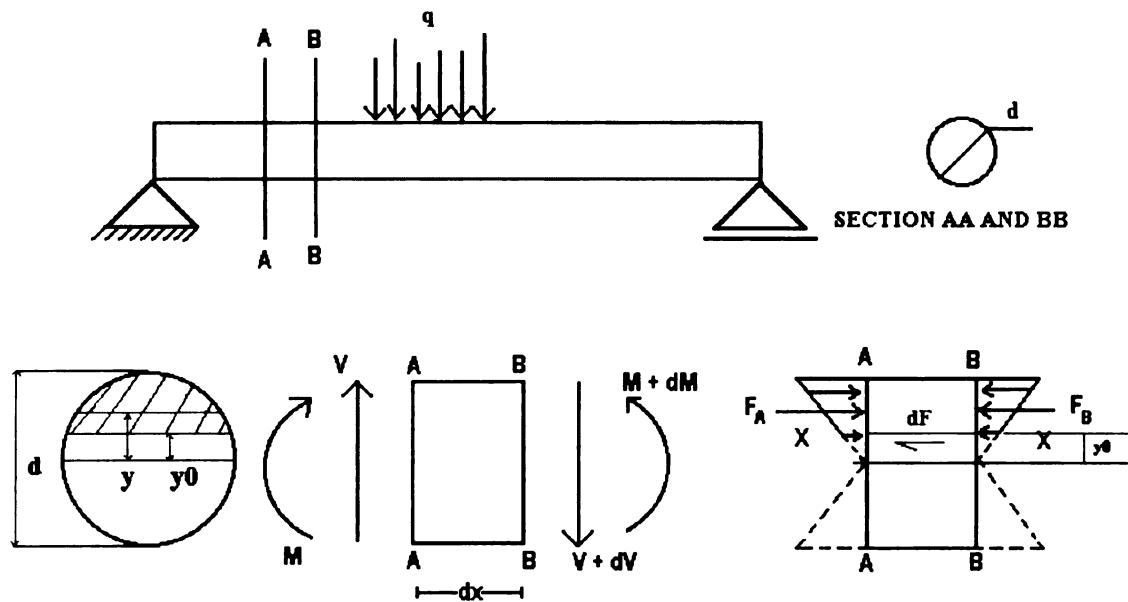
Fig. 2.2.1 Derivation of Shear Stresses in a Circular Prismatic Beam

At a distance y_0 from the section neutral axis, a part of the circle (shaded region) can be isolated from the beam. The resultant forces acting on this segment are shown in Figure 2.2.1 and are calculated as:

$$F_A = \int \frac{M_A \cdot y}{I} dA = \frac{M_A \cdot Q}{I} \qquad (2.2.4)$$

7

$$F_B = \int \frac{M_B \cdot y}{I} dA = \frac{M_B \cdot Q}{I}.$$

(2.2.5)

The force unbalance between the two ends of the section is then given by:

dF = F_B - F_A

(2.2.6)

$$dF = \frac{M_B \cdot Q}{I} - \frac{M_B \cdot Q}{I} = -\frac{dM \cdot Q}{I}.$$

(2.2.7)

For equilibrium, an internal shear force resists the force unbalance. The difference in the force per unit length over the differential segment is then given by equation 2.2.8, where the shear flow q is defined as:

$$q = \frac{dF}{dX} = -\frac{dM \cdot Q}{I \cdot dX} = \frac{VQ}{I}.$$

(2.2.8)

Thus, the shearing stress across the section at the segment location y_0 is obtained by dividing shear flow at the interface by thickness b of the segment at the same location. Therefore,

$$\tau_{xy} = \frac{dF}{dx \cdot b} = \frac{V \cdot Q}{I \cdot b}.$$

(2.2.9)

Equation 2.2.9 represents a uniform vertical shear stress distribution over the area (b t_{eff}) of the fiber. At the periphery of the circular section, vertical shear stresses have components in the tangential and normal directions to the perimeter. As per force equilibrium, the normal component needs to be associated with an equal stress on the periphery, which is clearly absent. Hence shear stresses at the boundary must be calculated tangential to the boundary.

Rigorous solutions on the shear stress distribution for solid circular sections and thick pipes have been developed based on the theory of elasticity. In this research work, a simple approach is used to approximately compute the true shear stresses at the boundary

of the circular FRP shell. First it is assumed that the shear stress found by equation 2.2.9 gives a true *component* of the shear stress acting in the vertical direction. Then, since the shear stresses at the boundary must act tangent to the boundary at any level, the lines of action of these stresses must intersect at a point such as A in Figure 2.2.2. Further, it can be assumed that all shear stresses at a given level act in a direction towards a single point, such A in Figure 2.2.2. It should be further noted that the simple approach described above neglects several conditions such as the two-material system of concrete filled FRP tube and the biaxial stress state on the FRP shell.

Therefore, with reference to Figure 2.2.2, the true tangent shear stress τ_T in the boundary at location C can be estimated by:

$$\tau_T = \frac{\tau_{xy}}{\cos\alpha}$$

(2.2.10)
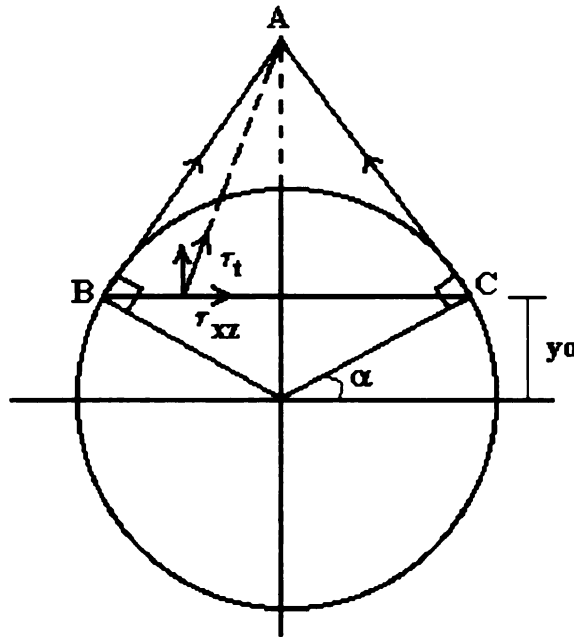
Fig. 2.2.2 Calculation of resultant shear stress across a section of a circular beam

2.3 Laminated FRP Composite Tube

An overview on the mechanics of laminated FRP composites with an emphasis on in-plane behavior is provided in this section. The reader is referred to reference [19] for more details.

Laminated FRP composites are made from the stacking of individual lamina, or plies, having varying fiber orientation. A lamina is a flat or curved arrangement of unidirectional fibers in a matrix. The fibers are the main load-carrying elements. Fibers generally behave linear elastically, thus the response of the fiber-reinforced composite is also essentially linear elastic. The layers of the laminate are bound together by the matrix. A general laminate can be symmetric, asymmetric or anti-symmetric.

Since a laminate may have different effective elastic modulus along the structural axes at every ply, there may be a discontinuity of stresses across the section. Thus unique stress-strain relations cannot be defined. Rather the unit strain and curvature deformations are related to the sum of the stress resultants over the section, viz. axial forces, shear forces and moments. This relationship, called the laminate stiffness, is commonly referred to as the [ABD] matrix and is given by:

$$\begin{Bmatrix} N \\ M \end{Bmatrix} = \begin{bmatrix} A & B \\ B & D \end{bmatrix} \begin{Bmatrix} \varepsilon_x \\ \kappa_x \end{Bmatrix} \tag{2.3.1}$$

where N are the in-plane stress resultants, M are the moment stress resultants, ε are the in-plane strains, and κ are the bending curvatures. From above, it can be observed that, in the [ABD] matrix, the [A] matrix defines the in-plane behavior, the [D] matrix defines

the out of plane behavior and the [B] matrix defines the coupling between in plane and out of plane responses.

Due to the small thickness of the FRP shell in the concrete filled FRP tube system, the imposed deformations are mainly axial strains. Thus, any moments introduced to the shell could only arise from the in plane to out-of plane coupling. However, the concrete restraints the shell from bending or twisting. Thus for the research work, only in-plane behavior of the FRP tube is important. Hence the following discussion focuses on the [A] matrix and in-plane forces in the laminate.

The on-axis stress strain relation for unidirectional fiber reinforced FRP composites in terms of stiffness is given by:

$$\begin{Bmatrix} \sigma_x \\ \sigma_y \\ \tau_{xy} \end{Bmatrix} = \begin{bmatrix} Q_{xx} & Q_{xy} & 0 \\ Q_{yx} & Q_{yy} & 0 \\ 0 & 0 & Q_{ss} \end{bmatrix} \begin{Bmatrix} \varepsilon_x \\ \varepsilon_y \\ \gamma_{xy} \end{Bmatrix} \tag{2.3.2}$$

with,

$$Q_{XX} = mE_L \tag{2.3.3}$$

$$Q_{YY} = mE_T \tag{2.3.4}$$

$$Q_{XY} = mv_{TL}E_L \tag{2.3.5}$$

$$Q_{SS} = G_{LT} \tag{2.3.6}$$

$$m = [1 - v_{LT}v_{TL}]^{-1} \tag{2.3.7}$$

where, E_L = Longitudinal Young's modulus of lamina; E_T = Transverse Young's modulus of lamina; G_{LT} = Longitudinal shear modulus of lamina; v_{LT} = Longitudinal Poisson's ratio and v_{TL} = Transverse Poisson's ratio.

The off-axis stress strain relation for unidirectional composites in terms of stiffness is then given by:

$$
\begin{Bmatrix} \sigma_1 \\ \sigma_2 \\ \tau_{12} \end{Bmatrix} = \begin{bmatrix} \bar{Q}_{11} & \bar{Q}_{12} & \bar{Q}_{16} \\ \bar{Q}_{21} & \bar{Q}_{22} & \bar{Q}_{26} \\ \bar{Q}_{61} & \bar{Q}_{62} & \bar{Q}_{66} \end{bmatrix} \begin{Bmatrix} \varepsilon_{11} \\ \varepsilon_{22} \\ \gamma_{12} \end{Bmatrix} \qquad (2.3.8)
$$

where,

$$
\begin{Bmatrix} \bar{Q}_{11} \\ \bar{Q}_{22} \\ \bar{Q}_{12} \\ \bar{Q}_{66} \\ \bar{Q}_{16} \\ \bar{Q}_{26} \end{Bmatrix} = \begin{bmatrix} m^4 & n^4 & 2m^2n^2 & 4m^2n^2 \\ n^4 & m^4 & 2m^2n^2 & 4m^2n^2 \\ m^2n^2 & m^2n^2 & m^2+n^2 & -4m^2n^2 \\ m^2n^2 & m^2n^2 & -2m^2n^2 & (m^2-n^2)^2 \\ m^3n & -mn^3 & mn^3-m^3n & 2(mn^3-m^3n) \\ mn^3 & -m^3n & m^3n-mn^3 & 2(m^3n-mn^3) \end{bmatrix} \begin{Bmatrix} Q_{xx} \\ Q_{yy} \\ Q_{xy} \\ Q_{ss} \end{Bmatrix} \qquad (2.3.9)
$$

with, $m = \cos\theta$ and $n = \sin\theta$.

The in-plane stress resultant acting on the laminate are thus defined as:

$$
\begin{Bmatrix} N_{xx} \\ N_{yy} \\ N_{xy} \end{Bmatrix} = \begin{bmatrix} A_{11} & A_{12} & A_{16} \\ A_{21} & A_{22} & A_{26} \\ A_{61} & A_{62} & A_{66} \end{bmatrix} \begin{Bmatrix} \varepsilon_x \\ \varepsilon_y \\ \gamma_{xy} \end{Bmatrix} \qquad (2.3.10)
$$

The A_{ij} coefficients are determined with equation 2.3.11 below with reference to Figure2.3.1 by:

$$
A_{ij} = \sum_{i=1}^{n} (\bar{Q}_{ij})_k (h_k - h_{k-1}) \qquad (2.3.11)
$$

12
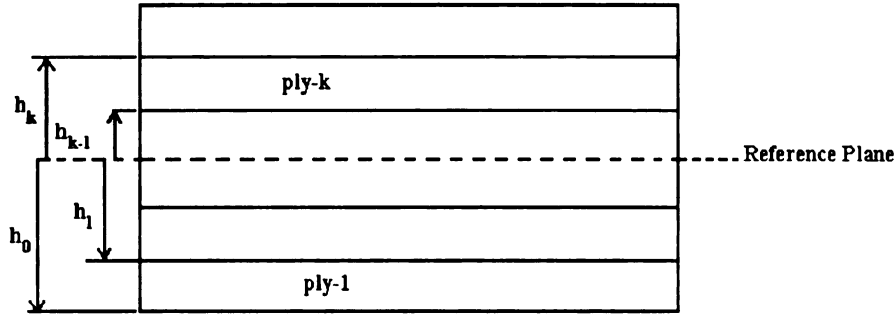
Fig. 2.3.1 Laminated composite configuration (Carbon Fiber Bridge column retrofit, Engineer Training Course; UCSD, May 1996)

Examination of equation 2.3.9 shows that for a symmetric laminate the $\bar{Q}_{16}$ and $\bar{Q}_{26}$ terms become zero. Correspondingly, the terms A_{16} and A_{26} will also be zero. This reduces the in-plane stress-strain relations to an equivalent orthotropic behavior. Equivalent engineering constants can then be computed form the stiffness matrix as follows:

$$E_L = \frac{(A_{11}A_{22} - A_{12}A_{21})}{(A_{22} \cdot h)} \qquad (2.3.12)$$

$$E_T = \frac{(A_{11}A_{22} - A_{12}A_{21})}{(A_{11} \cdot h)} \qquad (2.3.13)$$

$$G = \frac{A_{66}}{h} \qquad (2.3.14)$$

$$v_{21} = \frac{A_{12}}{A_{11}} \qquad (2.3.15)$$

$$v_{21} = \frac{A_{12}}{A_{22}} \qquad (2.3.16)$$

where, E_L = In-plane longitudinal modulus of laminate; E_T = In-plane transverse modulus of laminate; G = In-plane shear modulus of laminate; $v21$ = In-plane Poisson's ratio; h = Thickness of the laminate.

It should be noted that non-symmetric laminates would lead to a fully populated [A] matrix. Hence equivalent engineering properties cannot be defined and coupling between the in-plane shear and extension behavior exists. This issue is further discussed in Chapter 3.

2.4   Failure Criteria

Failure of a material occurs when strength carrying capacity reaches its maximum value. Maximum tensile, compressive and shear strength of material are determined based on failure criteria. For FRP lamina, failure theories are developed assuming a bi-axial stress state, a homogeneous material assumption, and experimentally measured material (ply) strengths.

Several failure theories have been developed to evaluate the strength of FRP laminates. The most common are the Maximum Stress Theory, the Maximum Strain Theory, and the Tsai-Hill quadratic criterion [8]. This work has implemented the Tsai-Hill failure theory. Tsai-Hill's quadratic failure theory considers the biaxial stress interaction that might be present in a given lamina. The failure envelope is given by:

$$\frac{\sigma_1^2}{X^2} + \frac{\sigma_2^2}{Y^2} - \frac{\sigma_1\sigma_2}{X^2} + \frac{\tau_{12}^2}{S^2} = 1 \qquad (2.4.1)$$

where, when material is subjected to tension

X = X_T = Longitudinal tensile strength

Y = Y_T = Transverse tensile strength

When material is subjected to Compression

X = X_C = Longitudinal compressive strength

Y = Y_C = Transverse compressive strength

S = Longitudinal shear strength.

2.5 Concrete filled FRP Shells

In concrete filled FRP tubes, two different materials are involved viz. plain concrete and an FRP laminated composite. These two materials complement each other due to the compression carrying capacity of concrete and the tension carrying capability of FRP composites. The following section provides an overview of the behavior of concrete and the FRP laminate and the interaction between concrete and the FRP composite shell. This material is a summary of the research conducted at the University of California, San Diego by Davol [4] and Burgueño [2].

Concrete behavior:

The strength and ductility of concrete can be improved by the presence of tri-axial compression. This is achieved by providing confinement to the concrete. In the FRP/Concrete hybrid system, it is the FRP shell that provides confinement to the concrete core. In this system, the FRP shell is an elastic material. Thus, when under compression, the confinement pressure applied to the concrete from the FRP shell is linearly proportional to the expansion of the core. An incremental approach, using Mander model for confined concrete by Mander *et al.* is used to calculate stress strain behavior of confined concrete based on the radial dilation of the concrete core [2]. The dilation of the concrete core is evaluated with the one-dimensional model by Elwi and Murray [6] based

on a variable Poisson's ratio for concrete. The confining pressure in the model is then calculated assuming the FRP shell as a thin shell acting as a pressure vessel. Once the confining pressure is known, Mander's confined concrete model is used to calculate the concrete axial stress for that level of axial strain and confining pressure.

FRP shell behavior

The FRP shell consists of a thin FRP laminated composite tube. However, for analysis purposes, the FRP tube is modeled as a flat laminated FRP plate with equivalent orthotropic properties as described in Section 2.3. Classical lamination theory is used to define equivalent plate properties based on the laminate architecture and lamina properties.

Concrete-FRP interaction

The FRP tubes used in the UCSD research program were manufactured by filament winding and provided with internal helicoidal ribs to achieve composite behavior between the concrete and the FRP shell. The UCSD research assumes that the helicoidal ribs on the inside of the FRP shell makes the system to behave compositely [5].

2.6   Shear response of Structural Elements

Extensive work has been conducted on the shear response of reinforced concrete members. The following summary is provided in order to highlight recent developments in the shear modeling of reinforced concrete elements, concrete filled steel tubes and concrete filled FRP tubes.

2.6.1 Reinforced concrete members

The American Concrete Institute [1] design guidelines recommend that the *shear strength* of non pre-stressed members be calculated as:

$$V_n = V_C + V_S \tag{2.6.1}$$

where V_n is the total nominal shear strength, V_c is the shear strength provided by concrete and V_s is the shear strength provided by the transverse steel.

The shear resistance of a reinforced concrete member is thus based on the concrete compressive strength, the tensile steel ratio, and the presence of axial load. Priestley *et al.* [12][14] proposed a multi-component additive model to calculate the *shear strength* of reinforced concrete members under cyclic loads. The model takes into an account the concrete degradation at high ductility levels and the effect of axial load. The shear strength of the reinforced concrete element is then given by sum of three components:

$$V_n = V_c + V_s + V_p \tag{2.6.2}$$

where V_c is the concrete component, depending on the level of member ductility, V_s is the transverse steel reinforcement component, and V_p is the component created by the axial load and the member aspect ratio.

2.6.2 Concrete filled Steel Tubes

The work done on predicting the shear strength and shear response of concrete filled steel tubes (CFT) is limited. It is commonly accepted that the shear strength of CFT members be calculated by considering either the steel tube and concrete shear strength contributions separately or only shear strength contribution of the steel tube alone. For

steel-jacketed reinforced concrete columns, an additional component from the steel tube for estimating the member shear strength was proposed by Priestley et al. [13][14]. An additional term V_j is added to equation 2.5.3 to include the steel jacket contribution to the shear strength of the member leading to the following expression for the member shear strength:

$$V_n = V_C + V_S + V_P + V_J.$$ (2.6.3)

2.6.3 FRP/Concrete members

In the development of the concrete filled FRP concept, preliminary work was done by Seible *et al.* [16] to obtain guidelines for the design and calculation of shear strength of concrete filled multi-directional FRP shells for bridge piers. A simple approach was followed in the shear strength calculations by considering a multiple component additive model similar to the one developed by Priestley *et al.* [14]. The shear strength of concrete filled FRP members was thus considered as the addition of three components: a concrete component V_c, which depends on level of member ductility, an axial load component V_p, which depends on the column aspect ratio and axial load and a truss component V_j, which is modified from Priestley's model to incorporate the FRP laminate. The shear resistance of the FRP shell is then calculated as

$$V_j = \Sigma \ 0.5 \ \pi \ Dt_i \ \phi \ [0.5 \ f_{\theta+\alpha-i} + 0.5 \ f_{\theta+\alpha+i}] \ Cot \ \theta$$ (2.6.4)

where α = lamina angle; θ = crack angle; n = total number of laminas angles; D = overall section diameter; f_α = ultimate tensile strength at an orientation angle α; t = thickness of the laminate. In this model, total laminate strength depends on the addition of the

decoupled individual ply strength at different ply orientations. This model does not take into account the biaxial stress state of the FRP laminate or the curvature of the shell.

2.7 Modified Compression Field Theory

The modified compression field theory (MCFT) [20] uses an integrated approach to calculate the shear stresses in reinforced concrete members. In addition, an analytical model has been developed using this theory, that is capable of predicting the *complete load-deformation response* of reinforced concrete elements subjected to in-plane shear and normal stresses as shown in Figure 2.7.1. Cracked concrete is considered as a "new material" and its stress-strain characteristics were experimentally developed. Modified compression field theory assumes that the principal stress axes and the principal strain axes coincide. Equilibrium, compatibility and stress-strain relationship are formulated in terms of average principal stresses and average principal strains.

The compatibility conditions with respect to Mohr's circle of strains (see Figure 2.6.2) are defined as follows. The change in the concrete strain is accompanied by an equal change in the steel strain.

$$\varepsilon_x = \varepsilon_{sx} = \varepsilon_{cx} \qquad\qquad (2.7.1)$$

$$\varepsilon_y = \varepsilon_{sy} = \varepsilon_{cy}. \qquad\qquad (2.7.2)$$
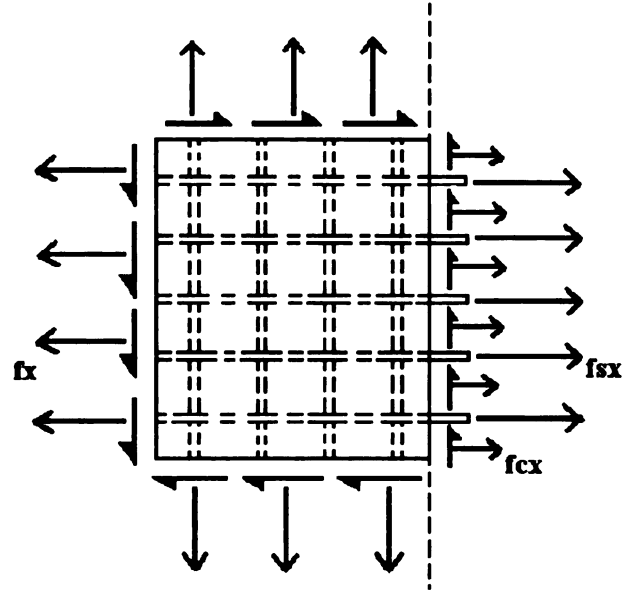
Fig. 2.7.1 Free body diagram of part of element (Vecchio and Collins, 1986)
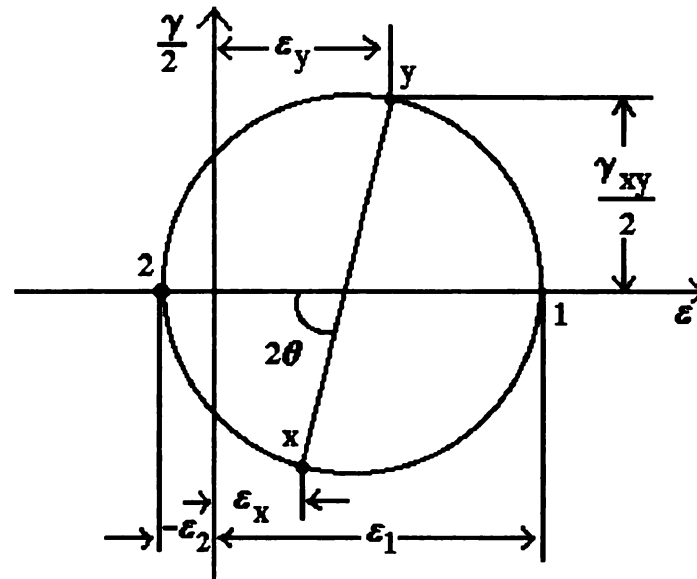
Fig. 2.7.2 Compatibility conditions for cracked elements (Vecchio and Collins, 1986)

The strain in any direction can be obtained if the three strain components ε_x, ε_y and γ_{xy} are known by using Mohr's circle (see Figure 2.7.2)

$$\gamma_{XY} = \frac{2(\varepsilon_X - \varepsilon_Y)}{\tan\theta} \tag{2.7.3}$$

$$\varepsilon_{x'} + \varepsilon_{Y} = \varepsilon_{1} + \varepsilon_{2} \tag{2.7.4}$$

$$\tan^{2}\theta = \frac{(\varepsilon_{X} - \varepsilon_{2})}{(\varepsilon_{Y} - \varepsilon_{2})} = \frac{(\varepsilon_{1} - \varepsilon_{Y})}{(\varepsilon_{1} - \varepsilon_{X})} = \frac{(\varepsilon_{X} - \varepsilon_{2})}{(\varepsilon_{1} - \varepsilon_{X})} = \frac{(\varepsilon_{1} - \varepsilon_{Y})}{(\varepsilon_{Y} - \varepsilon_{2})}. \tag{2.7.5}$$

The forces applied to the reinforced concrete elements are resisted by the stresses in the concrete and stresses in the reinforcement. The equilibrium conditions are determined with respect to Figure 2.7.1 as follows.

$$f_{x} = f_{cx} + f_{sx} \cdot \rho_{sx} \tag{2.7.6}$$

$$f_{y} = f_{cy} + f_{sy} \cdot \rho_{sy} \tag{2.7.7}$$
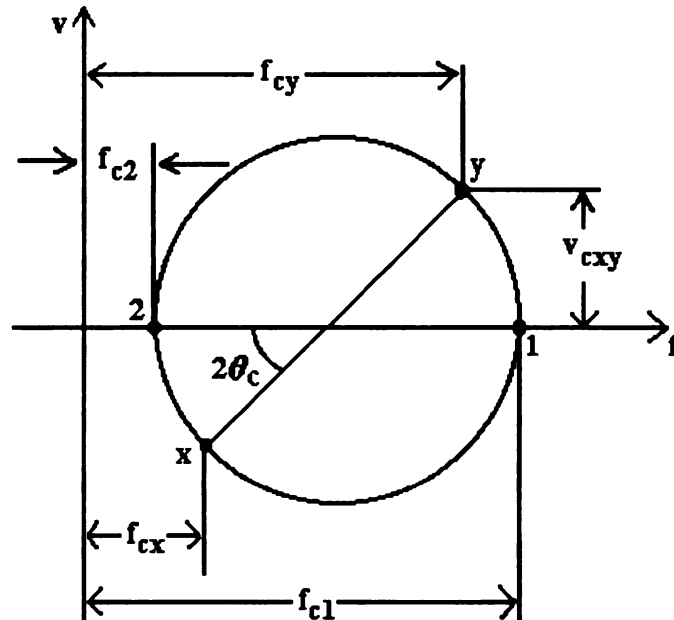
Fig. 2.7.3 Mohr's Circle for Average Concrete Stresses (Vecchio and Collins, 1986)

By using Mohr's circle of stress (see Figure 2.7.3), the two-dimensional stress state is defined as:

$$f_{cx} = f_{c1} - \tau_{cxy} / \tan\theta \tag{2.7.8}$$

$$f_{c2} = f_{c1} - \tau_{cxy}(\tan\theta + 1/\tan\theta) \tag{2.7.9}$$

$$f_{c2} = f_{cx} - \tau_{cxy} \cdot \tan\theta \ .$$

(2.7.10)

The principal compressive stress in the concrete f_{c2} is defined as a function of the principal compressive strain ε_2 and the principal tensile strain ε_1. The principal stress-strain relationship for cracked concrete is given by the following model [20]:

$$f_{c2} = f_{c2\,\text{max}}[2(\frac{\varepsilon_2}{\varepsilon_c}) - (\frac{\varepsilon_2}{\varepsilon_c})^2]$$

(2.7.11)

$$f_{c2\,\text{max}} = \frac{f_c'}{(0.8 - 0.34 \cdot \varepsilon_1 / \varepsilon_c)} \leq 1.0 \ .$$

(2.7.12)

The relationship between the average principal tensile stress in the concrete and the average principal tensile strain is linear up to cracking and is given by [6]:

$$f_{c1} = E_c \cdot \varepsilon_1 \ .$$

(2.7.13)

The average principal tensile stress value after cracking is assumed to decrease with increasing values of the principle tensile strain ε_1 according to the following model [6]:

$$f_{c1} = \frac{f_{cr}}{(1 + (500 \cdot \varepsilon_1)^{0.5})} \ .$$

(2.7.14)

Based on the above considerations, the modified compression field theory is capable of predicting the complete response of reinforced concrete elements subjected to in-plane shear and axial stresses by using compatibility conditions, equilibrium conditions and stress-strain relations expressed in terms of average stresses and strains.

2.8 Predicting the response of Reinforced Concrete Beams Subjected to shear Using Modified Compression Field Theory

The Modified Compression Field Theory provides a framework for the sectional analysis of reinforced concrete elements subjected to shear moment and axial loads. A layered sectional approach has been successfully used by Vecchio and Collins [21] to analyze the *shear response* of reinforced concrete beams. The analytical procedure is summarized below.

An element cross-section is divided into a number of layers with individual width b and depth h. The longitudinal strain in each concrete layer and reinforcement is fixed by defining top concrete fiber strain and a section curvature. Force equilibrium requirements are imposed to balance the shear force, axial force and bending moment acting on the section. Compatibility and equilibrium conditions in the section layers (steel reinforced concrete) are controlled by the modified compression field theory. The procedure follows these steps.

1. Define the longitudinal strain profile

2. Estimate shear flow distribution across the concrete section

3. The stresses in the reinforcement are calculated as per a bilinear uni-axial behavior for the steel reinforcement. The stresses in the concrete layer are calculated based on the modified compression field theory. The longitudinal compressive stress f_{cx} is calculated for each layer given the longitudinal strain and the assumed shear flow distribution. The resultant stresses must balance the sectional forces and therefore satisfy the following conditions:

$$N = \sum_{i=1}^{m} f_{cxi} \cdot b_i \cdot h_i + \sum_{j=1}^{n} f_{sxj} \cdot A_{sj} \qquad (2.8.1)$$

23

$$M = \sum_{i=1}^{m} f_{cxi} \cdot b_i \cdot h_i \cdot (y_{ci} - \bar{y}) + \sum_{j=1}^{n} f_{sxj} \cdot A_{sj} \cdot (y_{cj} - \bar{y}) \qquad (2.8.2)$$

$$V = \sum_{i=1}^{m} v_{ci} \cdot b_i \cdot h_i \qquad (2.8.3)$$

where N, M, and V are the axial load, moment, and shear acting about the centroid of the section. If the equilibrium conditions are not satisfied, the longitudinal strain profile is changed until equilibrium is achieved.

4. The average shear stress acting on the vertical face of concrete layer k is calculated as

$$v_k = \frac{V_k}{b_k \cdot h_k} \qquad (2.8.4)$$

where V_k is the normal shear force at layer k.
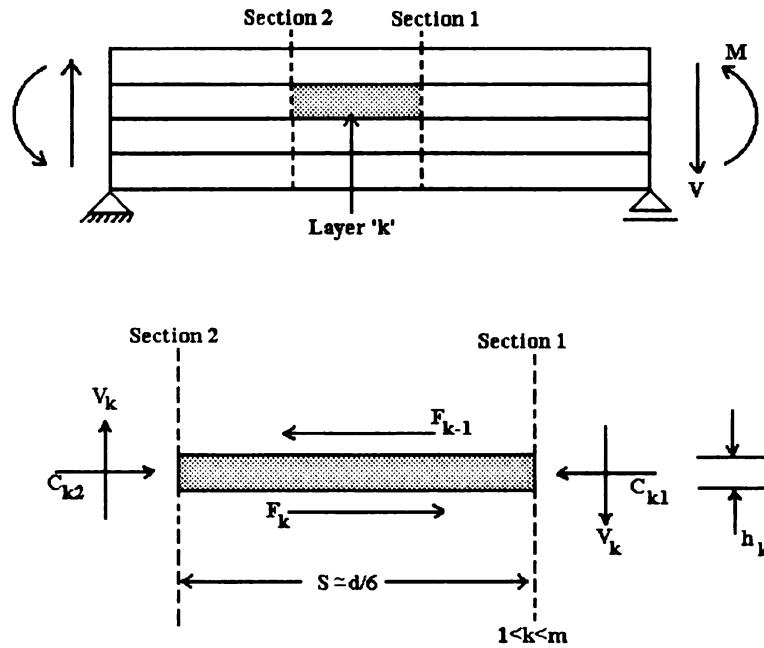
Fig. 2.8.1 Free body diagram for concrete layer k (Vecchio and Collins, 1988)

24

The calculated shear stress distribution is checked against the assumed shear stress distribution. The shear flow distribution is revised and the analysis is repeated until convergence is obtained.

This analytical procedure makes possible the rational analysis of reinforced concrete sections subjected to combined flexure, shear and axial loads. The procedure integrates compatibility and equilibrium conditions and uses realistic stress–strain relationships of cracked concrete based on experimental results. Thus, the model takes into account the degradation of cracked concrete in compression and the stiffening effects of cracked reinforced concrete in tension. In addition, because the concrete section is analyzed layer-wise, it is possible to analyze members with general cross-sections.

CHAPTER 3: SHEAR BEHAVIOR OF CONCRETE FILLED FRP CIRCULAR TUBES

3.1 General

This chapter presents an analytical procedure for modeling the complete *shear response* of concrete filled FRP tubes. Firstly, a brief summary is provided on the flexural analysis of circular concrete filled FRP tubes as developed by Davol *et al.* [5]. Secondly, an extension to this model to capture the influence of anisotropic FRP shell architecture on the shear response is provided. Lastly, an analytical procedure to calculate the shear response of circular concrete filled FRP tubes is described in detail.

3.2 Flexural behavior of circular concrete filled FRP tubes

An experimental and analytical work was conducted by Davol [4] and Burgueño [2] at the University of California, San Diego to characterize the axial and flexural behavior of concrete filled FRP tubes. The following assumptions and relations were proposed:

1. Plane sections remain plane.

2. Longitudinal and hoop strain compatibility between the concrete core and the FRP shell is assumed.

$$\varepsilon_L = \varepsilon_x \qquad (3.2.1)$$

$$\varepsilon_T = \varepsilon_r \qquad (3.2.2)$$

3. The FRP shell is modeled as a plate with equivalent orthotropic properties as given by classical lamination theory (see Sect. 2.3). Thus, the stress-strain relations for an equivalent orthotropic plate are given by:

$$\begin{Bmatrix} \varepsilon_L \\ \varepsilon_T \\ \gamma_{LT} \end{Bmatrix} = \begin{bmatrix} 1/E_L & -v_{LT}/E_L & 0 \\ -v_{TL}/E_T & 1/E_T & 0 \\ 0 & 0 & 1/G_{LT} \end{bmatrix} \begin{Bmatrix} \sigma_L \\ \sigma_T \\ \tau_{LT} \end{Bmatrix} \qquad (3.2.3)$$

4. The compression behavior of the concrete core confined by the elastic FRP shell is achieved through an active confinement modeling procedure. Davol [4] developed a model for the FRP confined lightweight concrete by experimentally defining relations for an incremental tangent Poisson's ratio and tangent modulus for the confined concrete. Burgueño [2] proposed the use of a general model for steel-confined concrete used incrementally for changing confinement pressures that depend on the modeling of concrete dilation by a uni-axial model. *This later approach is used in this work.*

5. For modeling the FRP shell/concrete interaction in compression, the concrete core is modeled as an isotropic elastic cylinder. The stress-strain behavior of an isotropic cylinder is given by:

$$\begin{Bmatrix} \varepsilon_x \\ \varepsilon_r \end{Bmatrix} = \begin{bmatrix} 1/E_c & -v_c/E_c \\ -v_c/E_c & (1-v_c)/E_c \end{bmatrix} \begin{Bmatrix} \sigma_x \\ \sigma_r \end{Bmatrix} \qquad (3.2.4)$$

6. The FRP tube is considered as a thin shell, in which its bending stiffness is neglected. Following this assumption, its restraining effect onto the expanding core is taken similar to that of a pressure vessel. The hoop stresses in FRP shell of average radius R and thickness t due to the internal expansion of the concrete core (σ_r) is given by:

$$\sigma_T = -\frac{\sigma_r \cdot R}{t} \qquad (3.2.5)$$

7. Based on assumptions 2,3,5 and 6 above, Davol [4] proposed an approach to model the interaction between the concrete core and the FRP shell. The following relations were proposed:

$$\varepsilon_r = \frac{\varepsilon_X((v_c E_c R(1 - v_{LT} v_{TL}) + v_{LT} E_T t(1 - v_c - 2v_c^2))}{(-E_T t(1 - v_c - 2v_c^2) - E_c R(1 - v_{LT} v_{TL}))} \tag{3.2.6}$$

$$\sigma_r = -\frac{(\varepsilon_r + v_{LT} \varepsilon_X)}{(1 - v_{LT} \cdot v_{TL})R} \tag{3.2.7}$$

$$\sigma_L = E_L(\varepsilon_L - \sigma_r v_{TL} R / E_T t) \tag{3.2.8}$$

8. The axial tension behavior of concrete was modeled as a linear elastic material up to cracking. The radial behavior was modeled assuming the concrete as an elastic material restraining the contraction of the FRP shell due to the Poisson's ratio. The following relations were proposed [4]:

$$\sigma_r = \varepsilon_H \cdot Eco \tag{3.2.9}$$

$$\varepsilon_H = \frac{\varepsilon_L(E_H t v_{LT})}{(v_{LT} v_{TL} E_c R - E_H t - E_c R)} \tag{3.2.10}$$

3.3 Anisotropic shell behavior of FRP laminate

As presented in section 3.2, the modeling proposed by Davol et al [5] assumes the FRP shell to behave as an equivalent orthotropic plate. In general, as discussed in section 2.3, the in plane behavior of a laminated plate can behave anisotropically, with coupling between the in-plane extension and shear responses. The model developed by Davol et al. [5] is thus expanded herein to include the influence of shear coupling. To incorporate the extension/shear coupling effect on the previously developed model, the proposed

28

equations by Davol et al. [5] are rewritten next in terms of in-plane stiffness coefficients A_{ij}.

For an equivalent orthotropic plate, the equivalent engineering properties in terms of in-plane stiffness coefficients are given by [8]:

$$E_L = \frac{(A_{11}A_{22} - A_{12}A_{21})}{(A_{22}t)} \tag{3.3.1}$$

$$E_T = \frac{(A_{11}A_{22} - A_{12}A_{21})}{(A_{11}t)} \tag{3.3.2}$$

$$G_{LT} = \frac{A_{66}}{h} \tag{3.3.3}$$

$$\nu_{TL} = \frac{A_{12}}{A_{11}} \tag{3.3.4}$$

$$\nu_{LT} = \frac{A_{12}}{A_{22}}. \tag{3.3.5}$$

Recall that, in calculating the equivalent engineering constants, the coupling coefficients A_{16}, A_{26}, A_{61} and A_{62} are considered zero. Using equations 3.3.1 to 3.3.5 in equations 3.3.11 to 3.3.13 and 3.3.15 lead to:

$$\sigma_r = -\frac{(\varepsilon_r A_{22} + \varepsilon_x A_{12})}{R} \tag{3.3.6}$$

$$\varepsilon_r = \varepsilon_x \frac{(\nu_c E_c R + A_{12}(1 - \nu_c - 2\nu_c^2))}{(A_{22}(1 - \nu_c - 2\nu_c^2) + E_c R)} \tag{3.3.7}$$

$$\varepsilon_H = -\frac{(\varepsilon_L A_{12})}{(A_{22} + E_c R)} \tag{3.3.8}$$

Inclusion of the anisotropic effects in the formulation requires that the models developed by Davol et al. [5] be expressed in terms of stress resultant {N} instead of stresses {σ}.

Recalling from section 2.3, the in-plane behavior of a general laminate plate is given by:

$$\left\{ \begin{array}{c} N_L \\ N_T \\ N_{LT} \end{array} \right\} = \left[\begin{array}{ccc} A_{11} & A_{12} & A_{16} \\ A_{21} & A_{22} & A_{26} \\ A_{61} & A_{62} & A_{66} \end{array} \right] \left\{ \begin{array}{c} \varepsilon_L \\ \varepsilon_T \\ \gamma_{LT} \end{array} \right\}. \qquad (3.3.9)$$

Equation 3.2.4 can then be rewritten as:

$$N_T = -\sigma_r R. \qquad (3.3.10)$$

Therefore, using equation 3.3.10 with equation 3.3.9 gives:

$$\sigma_r = -(A_{21}\varepsilon_L + A_{22}\varepsilon_T + A_{26}\varepsilon_{LT})/R. \qquad (3.3.11)$$

An expression for ε_r can now be obtained as follows from equation 3.2.3 giving:

$$\varepsilon_r = (1 - v_C - 2v_C^2)\sigma_r / E_C - v_C \varepsilon_X. \qquad (3.3.12)$$

Using equation 3.3.11 with equation 3.3.12 gives:

$$\varepsilon_r = -\frac{(\varepsilon_X((1 - v_C - 2v_C^2)A_{21} + RE_C v_C) + (A_{26}(1 - v_C - 2v_C^2)\varepsilon_{XY})}{(A_{22}(1 - v_C - 2v_C^2) + RE_C)}. \qquad (3.3.13)$$

Finally, equation 3.3.11 leads to an equation for the transverse shell strain:

$$\varepsilon_T = -\frac{(\sigma_r R_{avg} + A_{21}\varepsilon_L + A_{26}\varepsilon_{LT})}{A_{22}}. \qquad (3.3.14)$$

Inspection of the equations derived above shows the inclusion of the extension-shear coupling terms A_{16} and A_{26} as well as shear strain γ_{LT} in the formulation. Additionally, it can be readily proven that the above expressions reduce to the previous equations by Davol et al. [5] when the A_{16} and A_{26} terms are equal to zero.

The FRP shell and concrete interaction under tensile stresses can be expresses as a function of stiffness coefficients using equations 3.3.9 and 3.3.10 as:

$$\varepsilon_H = -\frac{(\varepsilon_L A_{12} + A_{26}\varepsilon_{xy})}{(A_{22} + E_c R)} \qquad (3.3.15)$$

3.4 Concrete model in tension

The flexural models for concrete filled tubes developed by Davol et al. [5] neglected the tension stiffening effect of concrete as it was found to be not significant for the flexural response [4]. However the tension stiffening effect can be considerable for the evaluation of the shear stresses in the concrete.

Several models have been proposed for the tensile strength enhancement of confined concrete. However, the confinement generated by the FRP shell onto the concrete is minimal. Thus, the tensile behavior of concrete in this work follows the model developed by Vecchio and Collins [20] for unconfined concrete. In addition, this model includes the tension stiffening effects of cracked reinforced concrete. The stress-strain response of concrete in uni-axial tension is linear up to cracking and is given by:

$$f_t = E_{co}\varepsilon_x. \qquad (3.4.1)$$

After cracking, the average tensile stress in the concrete is calculated as:

$$f_t = \frac{f_r}{1 + (500\varepsilon_x)^{0.5}}; \qquad \text{For } \varepsilon_x > \varepsilon_r \qquad (3.4.2)$$

where $\varepsilon_r = f_r / E_c$ is the strain corresponding to the modulus of rupture f_r. There exists considerable scatter on the available data to model the concrete modulus of rupture. ACI-318 [1] recommends that the modulus of rupture be calculated by:

$$f_r = 0.63\lambda\sqrt{f_c'} \quad (\text{MPa}) \ [\ f_r = 7.5\lambda\sqrt{f_c'} \quad (\text{psi})] \tag{3.4.3}$$

where $\lambda=1.0$ for normal weight concrete and $\lambda=0.75$ for light weight concrete. The tensile concrete model is shown in Figure 3.4.1. In spite of the codified recommendation mentioned above, different values have been proposed by researchers, which range from

$$f_r = 0.33\lambda\sqrt{f_c'} \ \text{to} \ f_r = 0.75\lambda\sqrt{f_c'} \quad (\text{MPa}) \ [\ f_r = 4\lambda\sqrt{f_c'} \ \text{to} \ f_r = 9\lambda\sqrt{f_c'} \quad (\text{psi})]$$
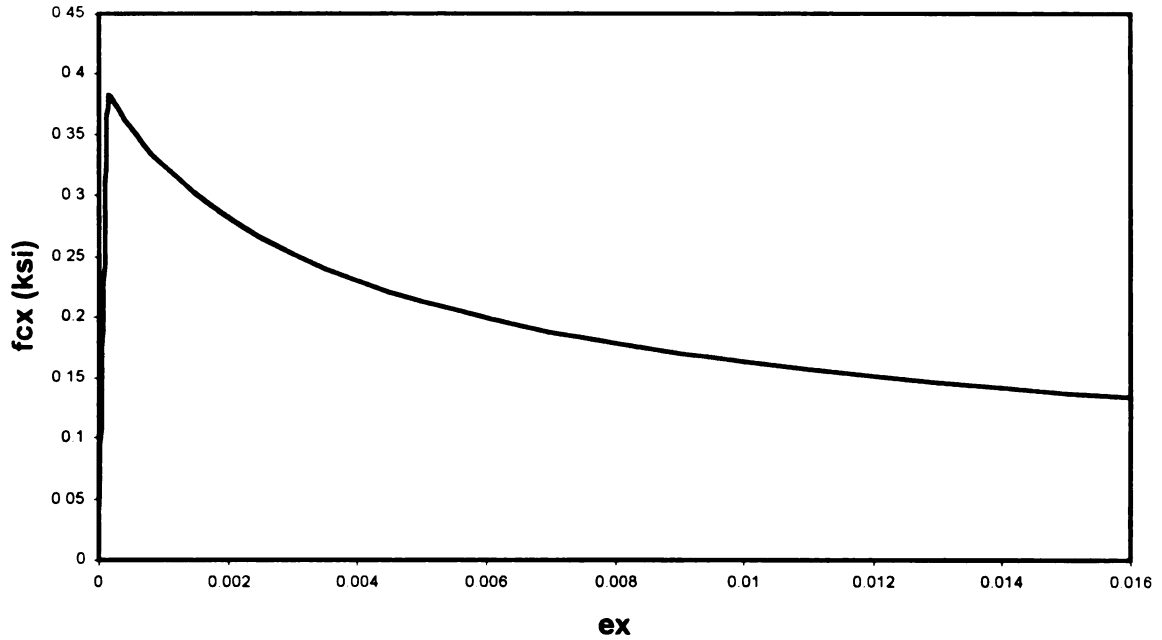
Fig. 3.4.1 Tensile concrete model

The proposed methodology for evaluating the shear stress behavior on concrete filled FRP shells found great dependence on the modulus of rupture parameter. An evaluation of the influence of this parameter on shear stress distribution response is discussed in Chapter 5.

As per Vecchio and Collins [20], the shear capacity of the concrete core is controlled by the ability of the member to transmit forces across the cracks. At higher shear forces, local shear stresses, v_{ci}, are required to transmit tension forces at the crack

interface. Based on the work done by Vecchio and Collins [20], the limiting value of f_{cl} (principal tensile stress in concrete) for the FRP/concrete system is calculated as follows.

Consider a sandwich element where the faces consist of an FRP laminate and the core is composed of plain concrete as shown in Fig 3.4.2. The FRP laminates have equal thickness t and the concrete element has an effective width b. The element is then assumed to be subjected to a set of in plane stresses f_x, f_y and v_{xy}.
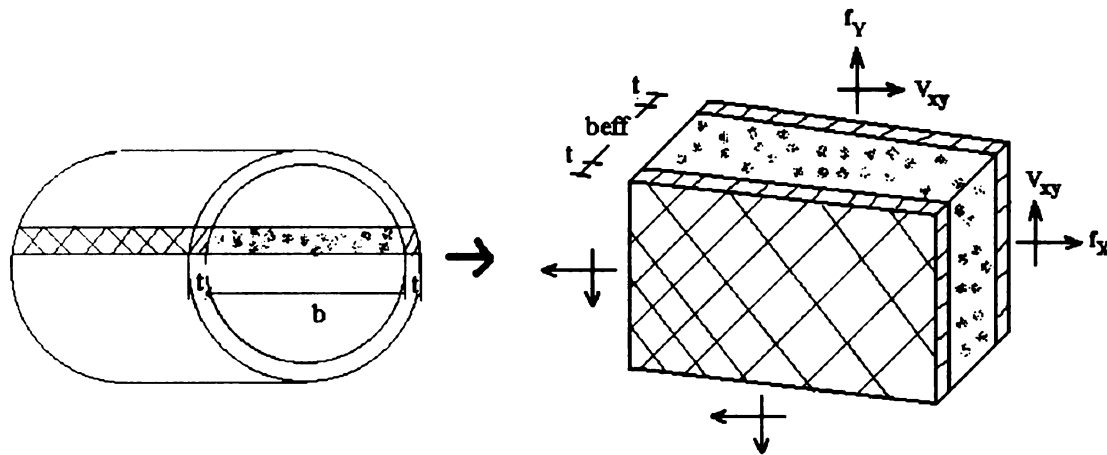
Fig. 3.4.2 Stresses applied in the cracked concrete region

The average stresses in the concrete core and the FRP shell are calculated along a principal angle plane (1-1), assumed to be parallel to the concrete cracking direction as shown in Fig 3.4.3. The actual stresses along a given crack plane (2-2) do not involve average calculated values but rather concentrated forces across the crack interface as shown in Fig 3.4.4.

33
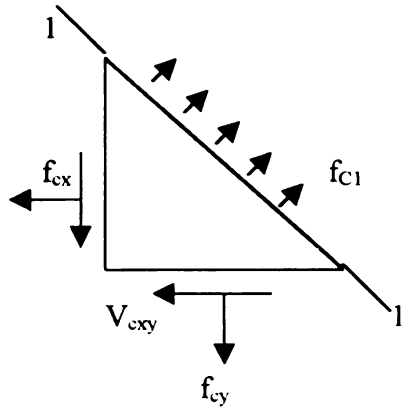
(a) Average stresses in concrete   (b) Average stresses in FRP shell
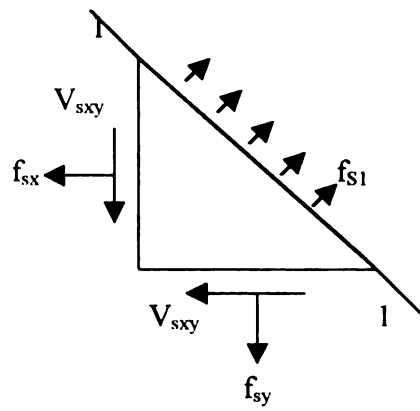
Fig. 3.4.3 Calculated average stresses
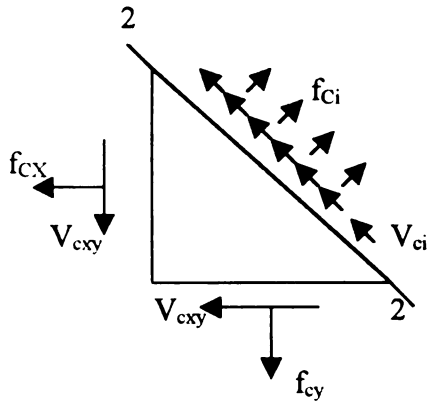
(a) Local stresses at crack in concrete   (b) Local stresses at crack in shell
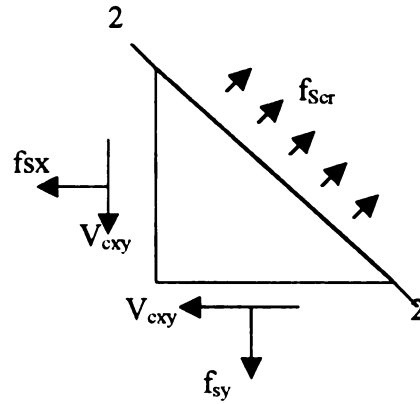
Fig. 3.4.4 Local stresses at a crack plane

Clearly, both stress states (plane 1-1 and plane 2-2) must satisfy equilibrium with the external in-plane forces. Therefore, the two sets of stresses shown in Fig 3.4.3 and Fig 3.4.4 must be statically equivalent.

Hence, considering horizontal and vertical equilibrium we get:

$$\rho_s f_{sx} + f_{c1} \cdot \sin \theta = \rho_s f_{sxcr} - f_{ci} \cdot \sin \theta - V_{ci} \cdot \cos \theta \qquad (3.4.6)$$

34

$$\rho_s f_{sy} + f_{cl} \cdot \cos\theta = \rho_s f_{sycr} - f_{ci} \cdot \cos\theta + V_{ci} \cdot \sin\theta \qquad (3.4.7)$$

Solving for f_{cl} form equations 3.4.6 and 3.4.7, respectively, we obtain:

$$f_{cl} = (\rho_s (f_{sxcr} - f_{sx}) - f_{ci} \cdot \sin\theta - V_{ci} \cdot \cos\theta)/\sin\theta \qquad (3.4.8)$$

$$f_{cl} = (\rho_s (f_{sycr} - f_{sy}) - f_{ci} \cdot \cos\theta + V_{ci} \cdot \sin\theta)/\cos\theta \qquad (3.4.9)$$

Equations (3.4.8) and (3.4.9) can be satisfied with no shear stress on the crack and no compressive stresses in the crack only if,

$$\frac{\rho_s (f_{sxcr} - f_{sx})}{\sin\theta} = \frac{\rho_s (f_{sycr} - f_{sy})}{\cos\theta} \qquad (3.4.10)$$

Neglecting f_{ci}, the maximum value of f_{cl} can be obtained from considerations of vertical force equilibrium as:

$$f_{cl\,max} = \frac{\rho_s (f_{sycr} - f_{sy})}{\cos\theta} + V_{ci\,max} \tan\theta \qquad (3.4.11)$$

The ability of a crack interface to transmit shear stresses depends on the crack width w and the maximum aggregate size a. The limiting value of vci is calculated as [20],

$$V_{ci\,max} = \frac{2.16\sqrt{f_c'}}{0.3 + (\dfrac{24w}{(a+0.63)})} \qquad (3.4.12)$$

The average crack width spacing is calculated as proposed by Collins and Vecchio [6] as:

$$w = \varepsilon_1 \cdot S_{m\theta} \qquad (3.4.13)$$

$$S_{m\theta} = \frac{1}{\dfrac{\sin\theta}{S_{mx}} + \dfrac{\cos\theta}{S_{my}}} \qquad (3.4.14)$$

35

The horizontal and vertical crack spacing equations proposed by Collins and Mitchel [3] were preliminarily modified as follows for the concrete filled circular FRP member:

$$S_{mx} = 2(c_x + s_x / 10) + 0.25 k_1 d_{bx} / \rho_x \qquad (3.4.15)$$

$$S_{my} = 2(c_y + s_y / 10) + 0.25 k_1 d_{by} / \rho_y \qquad (3.4.16)$$

where,

$c_x = c_y = r$ (internal radius)

$s_x = s_y$ = maximum spacing of longitudinal bars but $\leq 15\ d_b$

$d_b = t_S$ (Thickness of laminate)

$k_1 = 0.4$

$$\rho_x = \frac{4 t_s}{D_{avg}} \qquad (3.4.17)$$

$$\rho_y = \frac{2 t_s}{D_{avg}}. \qquad (3.4.18)$$

3.5 Shear Response of Concrete Filled Circular FRP tubes – Full Shear Interaction

A methodology following the principles of modified compression field theory (MCFT) was implemented to evaluate the shear response of concrete filled circular FRP tubes. The analysis procedure implements MCFT for calculation of the shear load-deformation response within the layered sectional analysis approach for flexural response developed by Burgueño [2]. Following the general discussion of Section 2.2 on the derivation of shear stresses for a circular prismatic beam, consider the circular concrete filled FRP tube in Fig 3.5.1. The beam is subjected to four point bending creating regions of constant shear and linear varying moments at both ends.

36
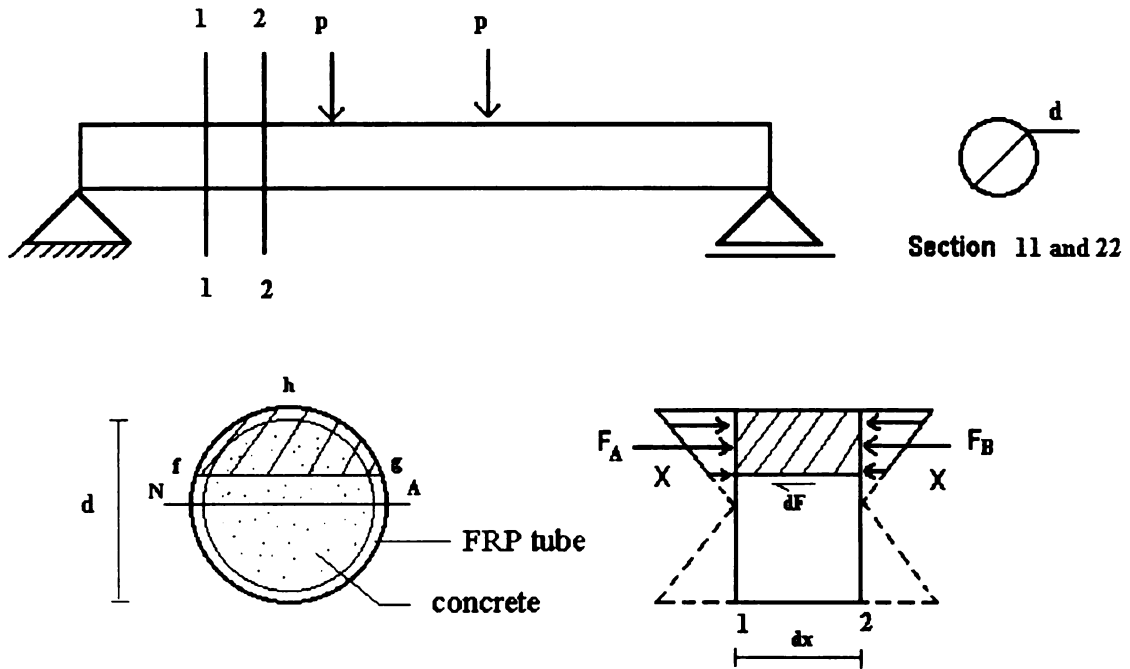
Fig. 3.5.1 Shear Stresses in Concrete Filled FRP Circular Tube

The following assumptions are made:

1. Plane sections remain plane (Bernoulli-Euler hypothesis)

2. Full composite action between the FRP tube and the concrete core is assumed for tubes with internal ribs. Complete strain compatibility between the two materials is thus assumed.

3. The flexural behavior of the FRP/concrete structural member is modeled as proposed by Davol [4] and Burgueño [2] (see Section 2.5 and Section 3.2).

4. In-plane anisotropic behavior (extension/shear coupling) of the FRP shell is considered (see Section 3.3).

5. Modified compression field theory principles are employed to calculate the shear response of the concrete filled FRP member.

6. The degradation of shear stress carrying capability of the concrete core with increased cracking is modeled by the incremental evaluation of an averaged (smeared) shear modulus for the cracked concrete.

7. Contribution of the FRP shell and the concrete core towards the shear stress resistance is taken in proportion to their instantaneous shear stiffness.

The shear stresses in the concrete core and the FRP shell for composite systems are calculated based on the following analytical procedure:

1. The concrete properties, FRP ply properties and laminate architecture of FRP shell are first defined. The stiffness coefficients of FRP shell are then calculated using equation 2.3.11.

2. A longitudinal strain profile ε_x and shear strain profile ε_{xy} are defined across the section.

3. Based on the longitudinal strain profile, the longitudinal stress σ_x and radial stress σ_y in the concrete in each cross-section fiber "i" are calculated using the confined concrete model by Mander *et al.* [9] incrementally for the concrete in compression. The longitudinal force f_{cx} in each segment is then simply calculated by multiplying longitudinal stress by the area of corresponding fiber.

$$F_{cx}(i) = \sigma_c(i) \cdot A_{Concrete}(i) \tag{3.5.1}$$

The FRP shell is divided into fibers of thickness t at $0.5°$ increments around the perimeter. The resultant force in each fiber is calculated using equations 3.3.12. The longitudinal force in each fiber is calculated by:

$$F_{Shell}(i) = \frac{N_L(i) \cdot D_{avg} \cdot 0.5}{720}.$$ (3.5.2)

For the section in tension, the longitudinal stress σ_x and the radial stress σ_y in each concrete fiber are calculated using equations 3.4.1, 3.4.2 and 3.2.4. The longitudinal force f_{cx} in each fiber is calculated using equation 3.5.1. As described above, The FRP shell is divided into fibers at 0.5° increments around the perimeter and the resultant force in each fiber is calculated using equations 3.3.12. The longitudinal force in each segment is then calculated using equation 3.5.2.

4. After calculating longitudinal force in concrete and FRP shell in all fibers, force equilibrium of the entire section is checked. If force equilibrium is not achieved then the longitudinal strain profile, or curvature, is changed until force equilibrium is obtained.

5. The summation of forces of concrete and FRP shell above each layer are calculated as follows:

$$F(k) = \sum_{i=1}^{k} f_{cx}(i) + F_{shell}(i)$$ (3.5.3)

6. If the concrete fiber is in compression, the average shear modulus of the fiber is calculated as follows [20]:

From the normal stresses and strains, principal stresses and strains are calculated as:

$$f_{c1} = \frac{\sigma_{cx} + \sigma_{cy}}{2} + \sqrt{(\frac{\sigma_{cx} - \sigma_{cy}}{2})^2 + \tau_{xy}^2}$$ (3.5.4)

$$f_{c2} = \frac{\sigma_{cx} + \sigma_{cy}}{2} - \sqrt{(\frac{\sigma_{cx} - \sigma_{cy}}{2})^2 + \tau_{xy}^2}$$ (3.5.5)

39

$$\varepsilon_1 = \frac{\varepsilon_x + \varepsilon_y}{2} + \sqrt{(\frac{\varepsilon_x - \varepsilon_y}{2})^2 + (\frac{\gamma_{xy}}{2})^2} \qquad (3.5.6)$$

$$\varepsilon_2 = \frac{\varepsilon_x + \varepsilon_y}{2} - \sqrt{(\frac{\varepsilon_x - \varepsilon_y}{2})^2 + (\frac{\gamma_{xy}}{2})^2} \qquad (3.5.7)$$

From the principal stresses and strains, the average shear modulus is then calculated as,

$$G_C(i) = \frac{f_{c1} - f_{c2}}{2(\varepsilon_1 - \varepsilon_2)} \qquad (3.5.8)$$

7. If the concrete segment is in tension, the principal tensile stress f_{c1} and tensile strain ε_1 and principal compressive stress f_{c2} and compressive strain ε_2 are calculated from the corresponding normal stresses and stains. The principal tensile stress f_{c1} is compared to its limit, $f_{c1limit}$, as described in Section 3.4. If it exceeds the calculated limit, then the revised principal compressive stress f_{c2} is calculated based on equilibrium as:

$$f_{c2} = f_{cx} + f_{cy} - f_{c1\,limit} \qquad (3.5.9)$$

The shear modulus of the corresponding fiber is then calculated with equation 3.5.8.

8. To compute the effective shear stiffness, concrete fibers are converted into equivalent shell fibers to deal with only one material. The height of each segment is kept same while the thickness of each concrete segment is converted into an equivalent shell thickness by:

$$b_{Concrete(New)} = \frac{b_{Concrete} \cdot E_C}{E_{Shell}} \qquad \text{(For each fiber)} \qquad (3.5.10)$$

$$b_{eff} = b_{Shell} + b_{Concrete} \frac{E_C}{E_{Shell}} \qquad \text{(For each fiber)} \qquad (3.5.11)$$

The effective average shear modulus of the hybrid system is calculated as

$$G_{eff}(i) = \frac{G_C(i)A_C(i) + G_{Shell}(i)A_{Shell}(i)}{A_C(i)\frac{E_C}{E_{Shell}} + A_{Shell}(i)} \qquad (3.5.12)$$

$$G_{eff}(i) = \frac{G_C(i)b_{Concrete}(i) + G_{Shell}(i)b_{Shell}(i)}{b_{Concrete}(i)\frac{E_C}{E_{Shell}} + b_{Shell}(i)}. \qquad (3.5.13)$$

9. The shear stresses in the transformed section are then calculated as:

$$\tau_{hybrid}(i) = \frac{dF}{(dx \cdot b_{eff})} \qquad (3.5.14)$$

where,

$$dF = F_2 - F_1 = (f_{cx}(i) + F_{Shell}(i))_2 - (f_{cx}(i) + F_{Shell}(i))_1 \qquad (3.5.15)$$

The tangential shear stresses along the FRP shell circular periphery are then calculated (see Section 2.2) by:

$$\tau_T(i) = \frac{\tau_{hybrid}(i)}{\cos\alpha}. \qquad (3.5.16)$$

These tangential shear stresses are calculated for the section in compression and the section in tension while the concrete is in the elastic range. When the concrete in tension cracks, the shear force is distributed primarily along the thin shell of the FRP tube. The error induced in using the vertical shear stress instead of the tangential shear stress for the thin walled members is considered negligible. The shear stresses in the FRP shell in the tension region of the section are thus not

41

corrected. The error introduced clearly reduces as the D/t ratio of the section increases.

The shear strain in transferred section is calculated as

$$\gamma_{hybrid}(i) = \frac{\tau_{hybrid}(i)}{G_{eff}(i)} \cdot$$

(3.5.17)

10. From the transformed (hybrid) shear stresses, shear stresses in the concrete and FRP shell in each segment are calculated as:

$$\tau_{Concrete}(i) = \frac{\tau_{hybrid}(i) \cdot G_C(i)}{G_{eff}(i)}$$

(3.5.18)

$$\tau_{Shell}(i) = \frac{\tau_{hybrid}(i) \cdot G_{Shell}(i)}{G_{eff}(i)}$$

(3.5.19)

From concrete shear stresses, concrete shear strains are calculated as:

$$\gamma_{Concrete}(i) = \frac{\tau_{Concrete}(i)}{G_C(i)}$$

(3.5.20)

$$\gamma_{Concrete}(i) = \frac{\tau_{hybrid}(i) \cdot G_C(i)}{G_{eff}(i) \cdot G_C(i)}$$

(3.5.21)

$$\gamma_{Concrete}(i) = \frac{\tau_{hybrid}(i)}{G_{eff}(i)}$$

(3.5.22)

$$\gamma_{Concrete}(i) = \gamma_{hybrid}(i)$$

(3.5.23)

Also from FRP shell shear stresses, FRP shell shear strains are calculated as:

$$\gamma_{Shell}(i) = \frac{\tau_{Shell}(i)}{G_{Shell}(i)}$$

(3.5.24)

$$\gamma_{Shell}(i) = \frac{\tau_{hybrid}(i) \cdot G_{Shell}(i)}{G_{eff}(i) \cdot G_{Shell}(i)}$$

(3.5.25)

$$\gamma_{Shell}(i) = \frac{\tau_{hybrid}(i)}{G_{eff}(i)}$$ (3.5.26)

$$\gamma_{Shell}(i) = \gamma_{hybrid}(i)$$ (3.5.28)

Thus, equations 3.5.23 and 3.5.28 satisfy the assumption of strain compatibility between shell and concrete.

i.e. $\gamma_{Concrete}(i) = \gamma_{Shell}(i) = \gamma_{hybrid}(i)$ (3.5.29)

11. The calculated shear strain values in shell and concrete are compared with the assumed shear strain values in Step 2. If they don't agree, then the assumed shear strain profile is replaced with the calculated shear strain values and steps 3 to 9 are repeated until the force equilibrium and strain compatibility is achieved.

12. The vertical shear stress distribution is checked for equilibrium as follows:

$$V = \sum_{I=1}^{n} \tau_{Shell}(i) \cdot A_S(i) + \tau_{Concrete}(i) \cdot A_C(i)$$ (3.5.30)

A solution algorithm for the analytical procedure just described is summarized in Figure 3.5.2.

Flowchart

```
            ┌──────────────────────────┐
            │   Define Ply Properties  │
            └────────────┬─────────────┘
                         │
                         ▼
            ┌──────────────────────────┐
            │ Define Concrete Properties│
            └────────────┬─────────────┘
                         │
                         ▼
            ┌──────────────────────────┐
    ◄───────│      For J = 1,Nstep     │
            └────────────┬─────────────┘
                         │
                         ▼
            ┌───────────────────────────────┐
            │ Define Longitudinal strain profile │◄──────
            └────────────┬──────────────────┘
                         │
                         ▼
            ┌──────────────────────────┐
            │ Define Shear strain profile exy │
            └────────────┬─────────────┘
                         │
                         ▼
            ┌──────────────────────────┐
    ◄───────│       For N = 1,Nseg     │◄──────────────
            └────────────┬─────────────┘
                         │
                         ▼
            ┌──────────────────────────┐
            │ Calculate stresses and Radial │
            │     strain in Concrete   │
            └────────────┬─────────────┘
                         │
                         ▼
            ┌──────────────────────────┐
            │ Calculate stresses in FRP shell │
            └────────────┬─────────────┘
                         │
                         ▼
            ┌──────────────────────────┐
            │ Calculate Force in Concrete layer │
            └────────────┬─────────────┘
                         │
                         ▼
                 ┌──────────────┐
    ────────────►│   Continue   │
                 └───────┬──────┘
                         │
                         ▼
            ┌──────────────────────────┐
    ◄───────│     For Theta = 0,360    │
            └────────────┬─────────────┘
                         │
                         ▼
            ┌──────────────────────────┐
            │ Calculate Force in FRP shell │
            └────────────┬─────────────┘
                         │
                         ▼
                 ┌──────────────┐
    ────────────►│   Continue   │
                 └───────┬──────┘
                         │
                         ▼
   ┌─────┐         ┌─────────┐        ┌─────┬─────┐
   │  1  │         │    A    │        │  2  │  5  │
   └─────┘         └─────────┘        └─────┴─────┘
```

change strain profile

Fig. 3.5.2 Flowchart of Shear stress analysis of circular concrete filled FRP tube

with composite behavior

44

```
        ┌─────────┐                              ┌─────────┐
        │    A    │                              │    2    │
        └─────────┘                              └─────────┘
             │                                        ▲
             ▼                                        │
    ┌──────────────────┐                              │
    │  For N = 1,Nseg  │◄─────────┐                   │
    └──────────────────┘          │                   │
             │                    │                   │
             ▼                    │                   │
    ┌──────────────────────────┐  │                   │
    │ Check for force equilibrium│ │                  │
    └──────────────────────────┘  │                   │
             │                    │                   │
             ▼                    │                   │
    ┌──────────────┐              │                   │
    │   Continue   │◄─────────────┘                   │
    └──────────────┘                                  │
             │                                        │
             ▼                               N        │
    ┌──────────────────────┐  ──────────────────────►
    │   Is Sum( F ) =0.0   │
    └──────────────────────┘
             │ Y
             ▼
    ┌──────────────────────────┐
    │  Calculate M, V, Curvature │
    └──────────────────────────┘
             │
             ▼
    ┌──────────────────┐
    │  For N = 1,Nseg  │◄─────────────┐
    └──────────────────┘              │
             │                        │
             ▼                        │
    ┌──────────────────┐              │
    │   For I = 1,N    │◄────────┐    │
    └──────────────────┘         │    │
             │                   │    │
             ▼                   │    │
    ┌──────────────────────────┐ │    │
    │ Calculate Fx = Fc + Fshell│ │    │
    └──────────────────────────┘ │    │
             │                   │    │
             ▼                   │    │
    ┌──────────────┐             │    │
    │   Continue   │◄────────────┘    │
    └──────────────┘                  │
             │                        │
             ▼                        │
    ┌──────────────┐                  │
    │   Continue   │◄─────────────────┘
    └──────────────┘
             │
             ▼
    ┌──────────────────┐
    │  For N = 1,Nseg  │◄────────┐
    └──────────────────┘         │
             │                   │
       ┌─────┴─────┐             │
       ▼           ▼             │
   ┌───────┐   ┌───────┐
   │   3   │   │   B   │
   └───────┘   └───────┘
```

Fig. 3.5.2 (Continued-1)

45

Fig. 3.5.2 (Continued-2)

46

```
                          ┌─────────┐
                          │    C    │
                          └────┬────┘
                               ▼
        ┌────────────┌──────────────────┐
        │            │  For N = 1,Nseg   │
        │            └────────┬─────────┘
        │                     ▼
        │        ┌───────────────────────────────┐
        │        │ teff = t(shell) + t(conc). Ec / Es │
        │        └──────────────┬────────────────┘
        │                       ▼
        └──────────────▶┌──────────────┐
                        │   Continue    │
                        └───────┬──────┘
                                ▼
        ┌────────────┌──────────────────┐
        │            │  For N = 1,Nseg   │
        │            └────────┬─────────┘
        │                     ▼
        │     ┌─────────────────────────────────────┐
        │     │ Geff =(t(shell).Gs+t(conc).Gc)/ tef │
        │     └──────────────┬──────────────────────┘
        │                    ▼
        └─────────────▶┌──────────────┐
                       │   Continue    │
                       └───────┬──────┘
                               ▼
        ┌────────────┌──────────────────┐
        │            │  For N = 1,Nseg   │
        │            └────────┬─────────┘
        │                     ▼
        │        ┌───────────────────────────┐
        │        │  T(hyb) = dF / (L .teff)   │
        │        └────────────┬──────────────┘
        │                     ▼
        │        ┌───────────────────────────┐
        │        │  e(hyb) = T(hyb) / Geff    │
        │        └────────────┬──────────────┘
        │                     ▼
        └─────────────▶┌──────────────┐
                       │   Continue    │
                       └───────┬──────┘
                               ▼
              ┌────┌──────────────────┐
              │    │  For N = 1,Nseg   │
              │    └────────┬─────────┘
              │             ▼
              │   ┌───────────────────────────┐
              │   │  Tc = T(hyb) . Gc / Geff   │
              │   └────────────┬──────────────┘
              ▼                ▼
          ┌───────┐        ┌───────┐
          │   4   │        │   D   │
          └───────┘        └───────┘
```

Fig. 3.5.2 (Continued-3)

47

```
┌─────┬─────┐              ┌───────┐                    ┌─────┐
│  1  │  4  │              │   D   │                    │  5  │
└─────┴─────┘              └───────┘                    └─────┘
   ▲     │                     │                           ▲
   │     │              ┌──────────────────────┐           │
   │     │              │ Ts = T(hyb) . Gs / Geff │         │
   │     │              └──────────────────────┘           │
   │     │                     │                           │
   │     │              ┌──────────────────────┐           │
   │     │              │ ec = Tc / Gc, es = Ts / Gs │      │
   │     │              └──────────────────────┘           │
   │     │                     │                           │
   │     └──────────────►┌──────────┐                      │
   │                     │ Continue │                      │
   │                     └──────────┘                      │
   │                          │                            │
   │                     ┌──────────────┐                  │
   │                     │ For N = 1,Nseg │                │
   │                     └──────────────┘                  │
   │                          │                            │
   │              N           ▼                            │
   │        ◄────────────┌──────────┐                      │
   │        │            │ IS es = exy │                   │
   │        │            └──────────┘                      │
   │        │               │ Y                            │
   │        │            ┌──────────┐                      │
   │        │     ◄──────│ Continue │                      │
   │        │     │      └──────────┘                      │
   │        ▼     │                                        │
   │        └─────┼──────►┌──────────┐──────────────────►  │
   │              │       │ exy = es │                      │
   │              │       └──────────┘                      │
   │              │            │                            │
   │         ◄────┘       ┌──────────┐
   └─────────────────────│ Continue │
                         └──────────┘
```

Fig. 3.5.2 (Continued-4)

3.6 Shear Response of Concrete Filled Circular FRP tubes – No Shear Interaction

This section provides an analytical procedure for calculating the shear stresses in the concrete and the FRP shell when no specific means are provided to ensure composite action between the FRP tube and the concrete core (i.e. internal ribs). In spite of the lack of this detail, minimal shear interaction between the FRP tube and the concrete is to be expected. The sources are material adhesion during concrete casting, friction between the two materials, and imperfections (waviness) on the inside of the tube. Thus, composite action is assumed to exist at the early stages of loading.

The strain demands at the tube/core interface will increase most rapidly when wide shear cracks in the concrete core develop. The shell reinforcement will then be responsible for arresting the crack growth. If the shear interaction at the interface is not strong enough, then the materials will slip with respect to one another. After this happens, the two materials will fail to work compositely. Since the concrete core will be essentially un-reinforced (no more composite action) the resistance of the system is reduced to that provided by the FRP tube alone. Hence a full bond between concrete and FRP tube is considered up to the shear strength of plain concrete and no bond is considered between concrete and FRP tube beyond that limit. For this research work, this behavior is considered as a *non-composite action*.

A methodology following the principles of modified compression field theory is used in the analysis to calculate the response of the cracked concrete. All assumptions presented in section 3.5, except #2 are considered to apply to this condition. Additional assumptions include:

1. Full composite action between the FRP tube and the concrete core is assumed until the concrete core exceeds its un-reinforced shear strength.

2. After the concrete core exceeds its shear strength load carrying capacity, the FRP shell is assumed to take all additional shear stress demands and behaves as a thin elastic pipe.

The analytical procedure follows steps 1 through 9 as presented for the composite section behavior in Section 3.5. The following steps are then taken to model the behavior of the non-composite section:

10. After calculating the shear stresses in the concrete fibers, the shear force carried by concrete is calculated as:

$$V_c = \sum_{i=1}^{n} \tau_{concrete}(i) A_{concrete}(i) .$$
(3.6.1)

The shear force carried by concrete is checked against the shear strength load carrying capacity of non pre-stressed plain concrete as per ACI-318 recommendations [1]:

$$V_{allow} = 2\sqrt{f_c'} bd .$$
(3.6.2)

Once the shear carrying capacity of concrete is reached, any additional shear force demands are transferred to the FRP shell. The total shear stress in the FRP tube is calculated as:

$$\tau_{total}(i) = \tau_{Shell}(i) + (\tau_{concrete}(i) - \tau_{allow}(i)) \frac{b_{Concrete}(i)}{b_{Shell}(i)} .$$
(3.6.3)

11. The revised shear strain in the FRP tube is then calculated by:

$$\gamma_{Shell}(i) = \frac{\tau_{total}(i)}{G_{Shell}(i)}.$$ (3.6.4)

The calculated shear strains in the shell are compared with the assumed shear strain values in step 2. If they don't agree, then the assumed shear strain profile is replaced with the calculated shear strain values and steps 3 to 10 are repeated until convergence is obtained.

12. The vertical shear stress values are checked for force equilibrium by:

$$V = \sum_{I=1}^{n} \tau_{Shell}(i) \cdot A_S(i) + \tau_{Concrete}(i) \cdot A_c(i).$$ (3.6.5)

A solution algorithm for the analytical procedure just described is summarized in Figure 3.6.1.

Flowchart

```
┌─────────────────────────────┐
│     Define Ply Properties    │
└─────────────────────────────┘
              │
              ▼
┌─────────────────────────────┐
│   Define Concrete Properties │
└─────────────────────────────┘
              │
              ▼
┌─────────────────────────────┐
│       For J = 1,Nstep        │
└─────────────────────────────┘
              │
              ▼
┌─────────────────────────────┐
│ Define Longitudinal strain profile │
└─────────────────────────────┘
              │
              ▼
┌─────────────────────────────┐
│   Define Shear strain profile exy │
└─────────────────────────────┘
              │
              ▼
┌─────────────────────────────┐
│        For N = 1,Nseg        │
└─────────────────────────────┘
              │
              ▼
┌─────────────────────────────┐
│   Calculate stresses and Radial │
│       strain in Concrete     │
└─────────────────────────────┘
              │
              ▼
┌─────────────────────────────┐
│   Calculate stresses in FRP shell │
└─────────────────────────────┘
              │
              ▼
┌─────────────────────────────┐
│  Calculate Force in Concrete layer │
└─────────────────────────────┘
              │
              ▼
        ┌──────────┐
        │ Continue │
        └──────────┘
              │
              ▼
┌─────────────────────────────┐
│      For Theta = 0,360       │
└─────────────────────────────┘
              │
              ▼
┌─────────────────────────────┐
│    Calculate Force in FRP shell │
└─────────────────────────────┘
              │
              ▼
        ┌──────────┐
        │ Continue │
        └──────────┘
              │
              ▼

  ┌─────┐      ┌─────┐      ┌─────┬─────┐
  │  1  │      │  A  │      │  2  │  5  │
  └─────┘      └─────┘      └─────┴─────┘
```
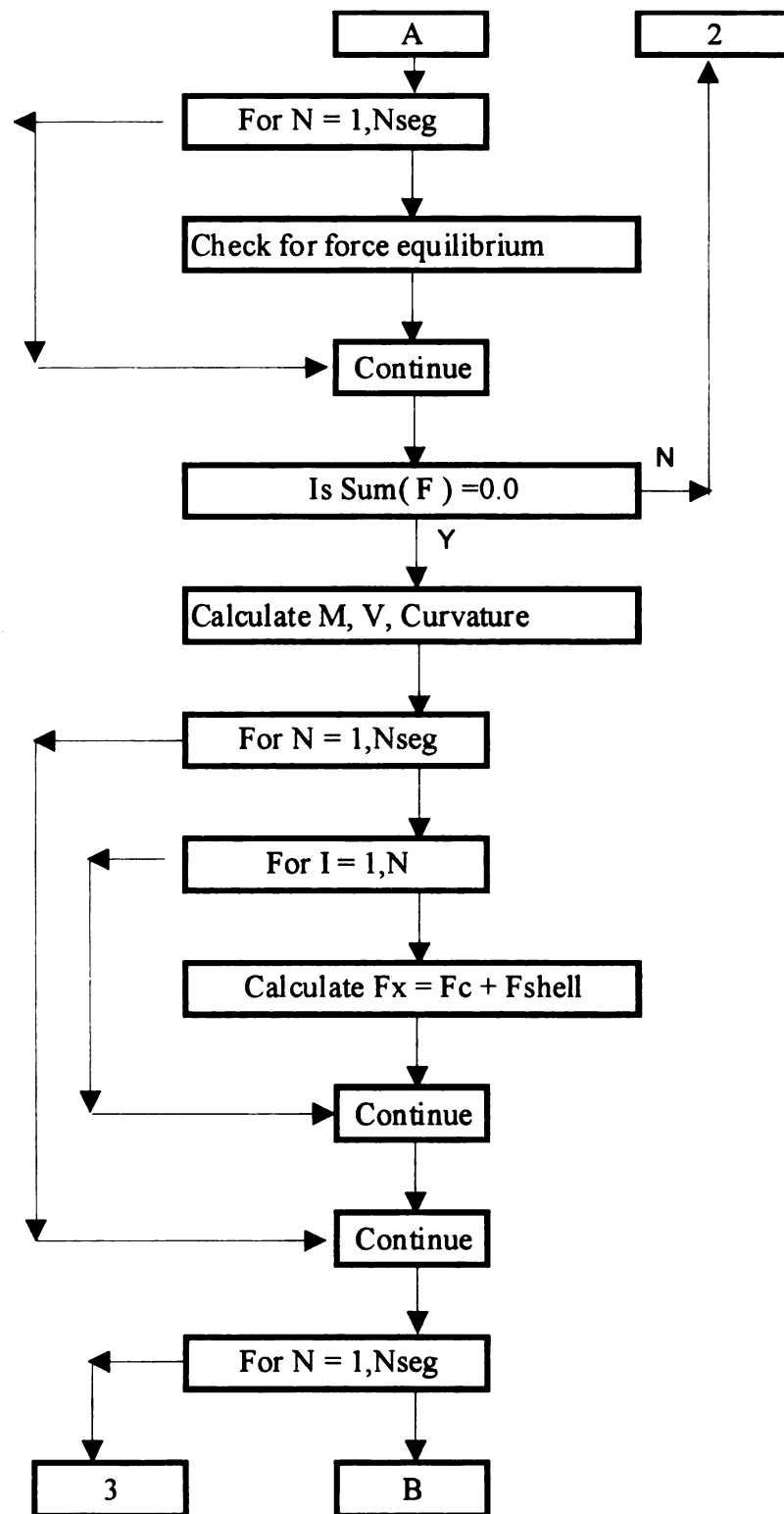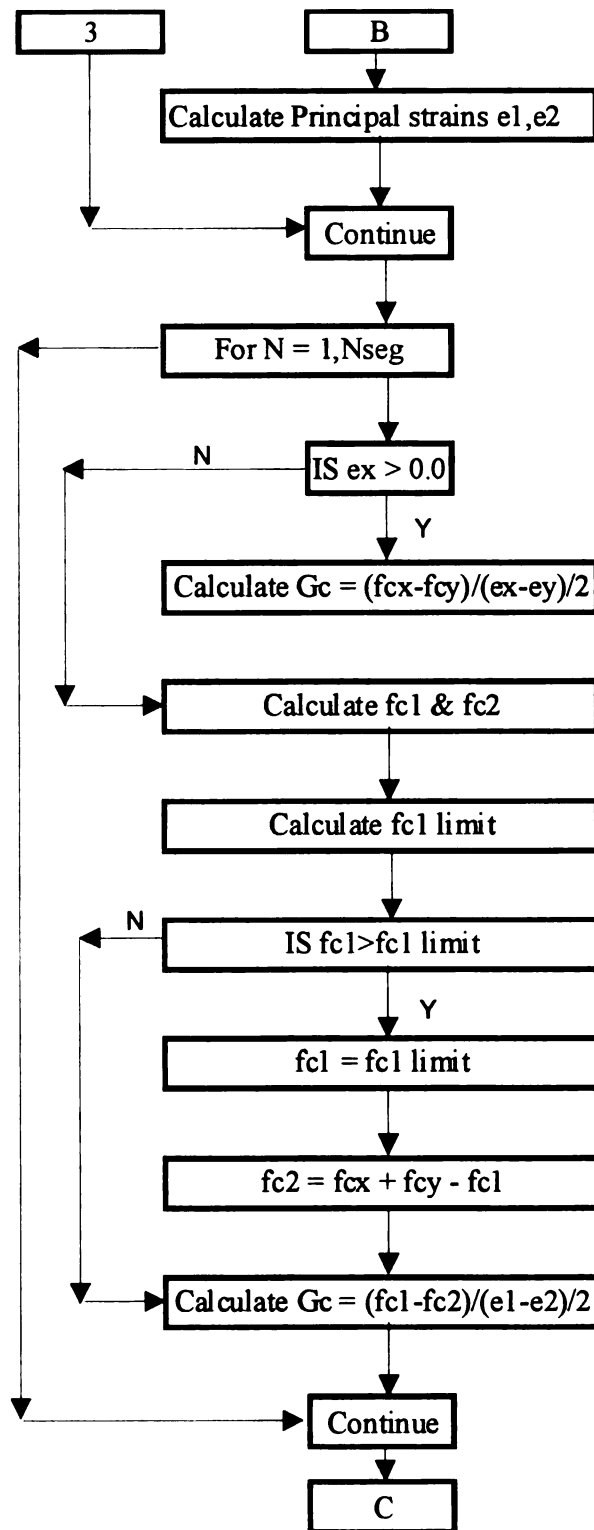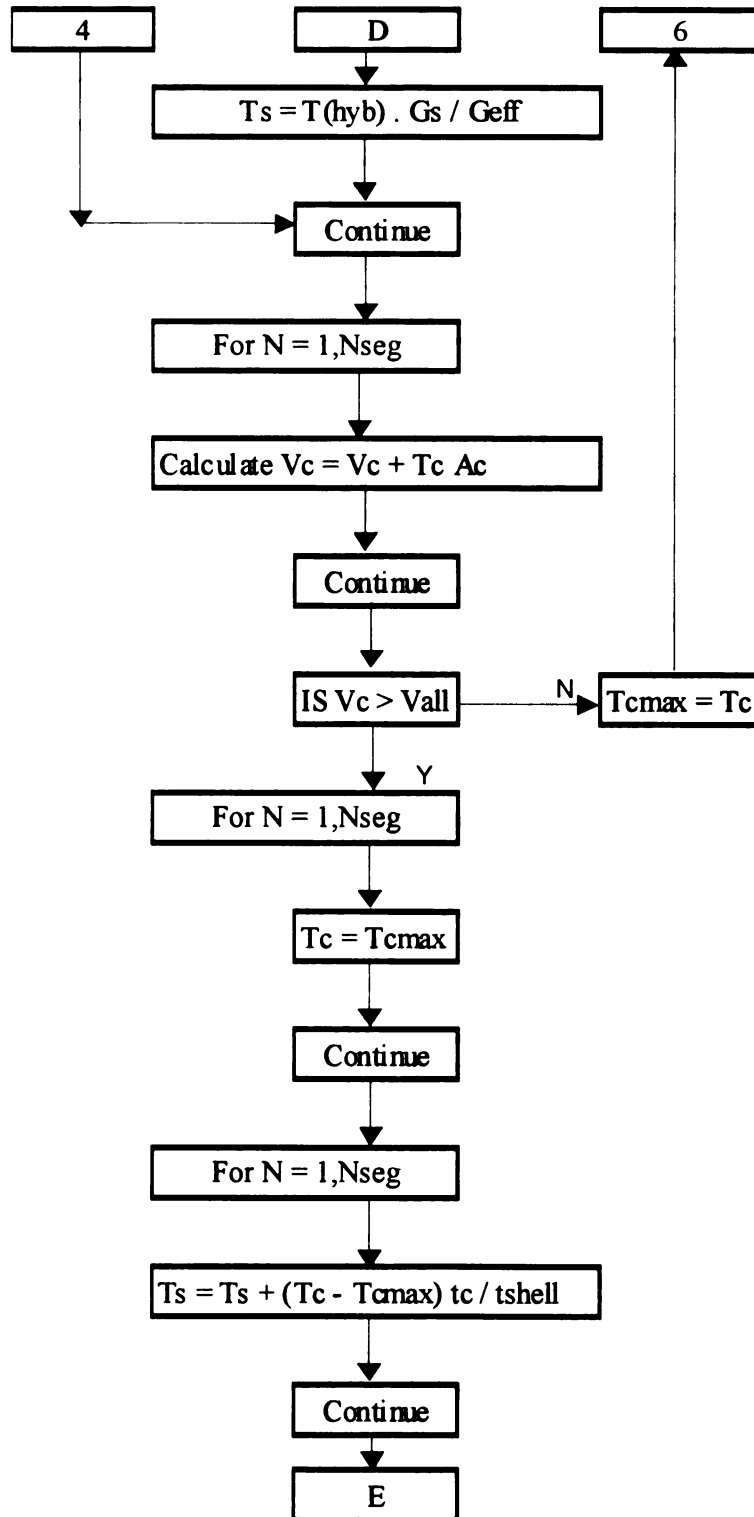
change strain profile

Fig. 3.6.1 Flowchart of Shear stress analysis of circular concrete filled FRP tube
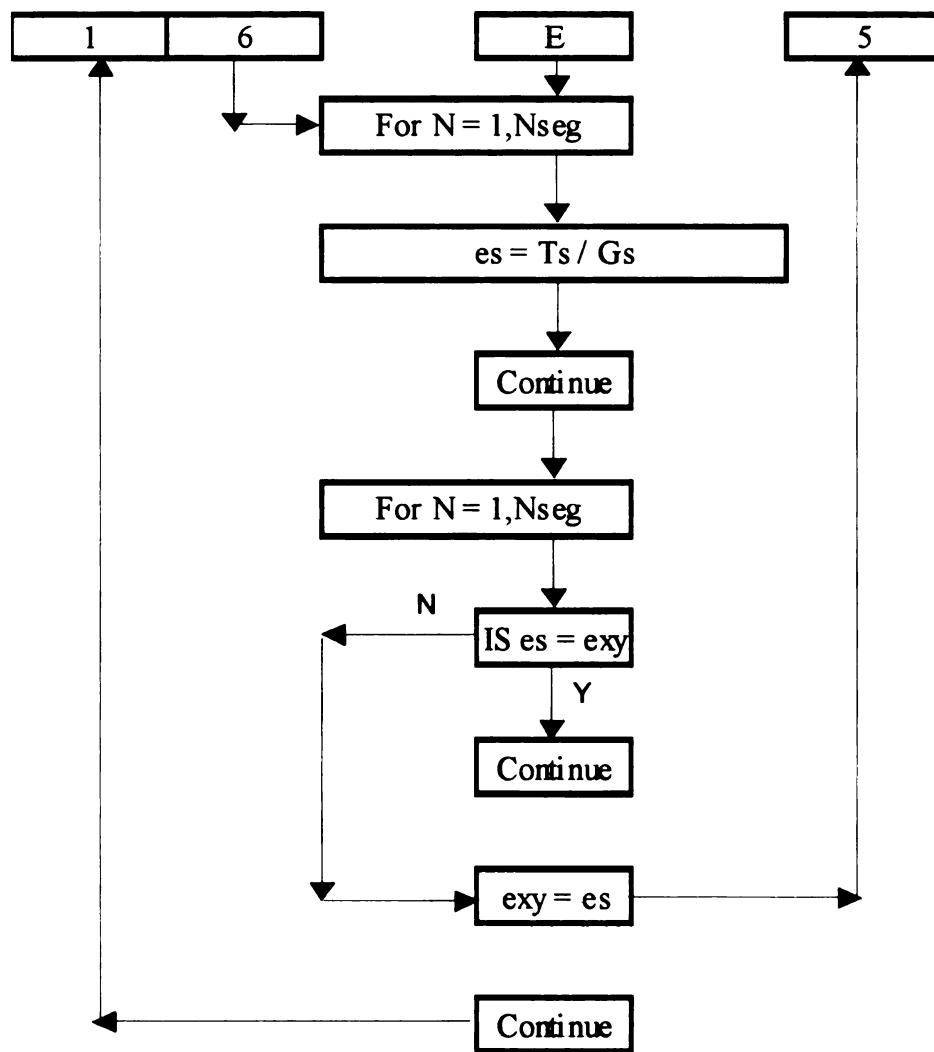
with non-composite behavior

52

```
      ┌─────────┐                    ┌─────────┐
      │    A    │                    │    2    │
      └────┬────┘                    └────▲────┘
           │                              │
      ┌────▼──────────┐                   │
◄─────┤ For N = 1,Nseg│                   │
│     └────┬──────────┘                   │
│          │                              │
│     ┌────▼────────────────────┐         │
│     │ Check for force equilibrium│      │
│     └────┬────────────────────┘         │
│          │                              │
│     ┌────▼────────┐                     │
└────►│  Continue   │                     │
      └────┬────────┘                     │
           │                              │
      ┌────▼────────────────┐   N         │
      │  Is Sum( F ) =0.0   ├─────────────┘
      └────┬────────────────┘
           │ Y
      ┌────▼────────────────────┐
      │ Calculate M, V, Curvature│
      └────┬────────────────────┘
           │
      ┌────▼──────────┐
◄─────┤ For N = 1,Nseg│
│     └────┬──────────┘
│          │
│     ┌────▼────────┐
│ ◄───┤ For I = 1,N │
│ │   └────┬────────┘
│ │        │
│ │   ┌────▼──────────────────────┐
│ │   │ Calculate Fx = Fc + Fshell│
│ │   └────┬──────────────────────┘
│ │        │
│ │   ┌────▼────────┐
│ └──►│  Continue   │
│     └────┬────────┘
│          │
│     ┌────▼────────┐
└────►│  Continue   │
      └────┬────────┘
           │
      ┌────▼──────────┐
  ◄───┤ For N = 1,Nseg│
  │   └────┬──────────┘
  │        │
┌─▼───┐  ┌─▼───┐
│  3  │  │  B  │
└─────┘  └─────┘
```

Fig. 3.6.1 (continued-1)

Fig. 3.6.1 (continued-2)

```
    ┌─────────┐         ┌─────────┐         ┌─────────┐
    │    4    │         │    D    │         │    6    │
    └─────────┘         └─────────┘         └─────────┘
                             │                   ▲
                             ▼                   │
                   ┌─────────────────────┐       │
                   │ Ts = T(hyb) . Gs / Geff │   │
                   └─────────────────────┘       │
                             │                   │
                             ▼                   │
                   ┌──────────────┐              │
         ──────────▶│   Continue   │             │
                   └──────────────┘              │
                             │                   │
                             ▼                   │
                   ┌──────────────┐              │
                   │ For N = 1,Nseg │            │
                   └──────────────┘              │
                             │                   │
                             ▼                   │
                   ┌─────────────────────┐       │
                   │ Calculate Vc = Vc + Tc Ac │ │
                   └─────────────────────┘       │
                             │                   │
                             ▼                   │
                   ┌──────────────┐              │
                   │   Continue   │              │
                   └──────────────┘              │
                             │                   │
                             ▼        N   ┌──────────────┐
                   ┌──────────────┐ ─────▶│ Tcmax = Tc   │
                   │ IS Vc > Vall │       └──────────────┘
                   └──────────────┘
                             │ Y
                             ▼
                   ┌──────────────┐
                   │ For N = 1,Nseg │
                   └──────────────┘
                             │
                             ▼
                   ┌──────────────┐
                   │ Tc = Tcmax   │
                   └──────────────┘
                             │
                             ▼
                   ┌──────────────┐
                   │   Continue   │
                   └──────────────┘
                             │
                             ▼
                   ┌──────────────┐
                   │ For N = 1,Nseg │
                   └──────────────┘
                             │
                             ▼
                   ┌──────────────────────────┐
                   │ Ts = Ts + (Tc - Tcmax) tc / tshell │
                   └──────────────────────────┘
                             │
                             ▼
                   ┌──────────────┐
                   │   Continue   │
                   └──────────────┘
                             │
                             ▼
                   ┌──────────────┐
                   │      E       │
                   └──────────────┘
```

Fig. 3.6.1 (continued-3)

```
┌─────┬─────┐        ┌─────────┐              ┌─────┐
│  1  │  6  │        │    E    │              │  5  │
└─────┴─────┘        └─────────┘              └─────┘
      │                    │                     │
      │              ┌─────────────┐             │
      └─────────────→│ For N = 1,Nseg│           │
                     └─────────────┘             │
                            │                     │
                     ┌─────────────┐             │
                     │  es = Ts / Gs │           │
                     └─────────────┘             │
                            │                     │
                     ┌─────────────┐             │
                     │  Continue   │             │
                     └─────────────┘             │
                            │                     │
                     ┌─────────────┐             │
                     │ For N = 1,Nseg│           │
                     └─────────────┘             │
                            │                     │
              N      ┌─────────────┐             │
          ←──────────│  IS es = exy│            │
                     └─────────────┘             │
                          Y │                     │
                     ┌─────────────┐             │
                     │  Continue   │             │
                     └─────────────┘             │
                            │                     │
                     ┌─────────────┐             │
          ──────────→│  exy = es   │────────────→│
                     └─────────────┘
                            │
                     ┌─────────────┐
      ←──────────────│  Continue   │
                     └─────────────┘
```

Fig. 3.6.1 (continued-4)

3.7 Summary

The modeling and analytical procedure for determining the shear response of circular concrete filled FRP tubes with composite and non-composite interaction were presented in this chapter. The accuracy of the models and procedures is assessed in Chapter 4.

CHAPTER 4: MODEL VALIDATION

4.1 General

This chapter focuses on the validation of the proposed models and analytical procedure for predicting the shear response of concrete filled circular FRP tubes. The analytical response is correlated with experimental results from research conducted by Davol [4] and Burgueño [2] at the University of California, San Diego (UCSD) as a part of the development and characterization of concrete filled carbon shells for new bridge construction. Specifically, the flexural tests carried out on two large-scale and two small-scale circular concrete filled FRP tubes by Davol [2] and Burgueño [4] are used as the benchmark experimental data for the model validation.

4.2 Large scale Flexure Tests

4.2.1 Test Unit Geometry, Properties and Test Set-up

The full-scale experimental tests were carried out on concrete filled filament wound carbon/epoxy circular FRP tubes designed to behave compositely by providing ribs to the inside of the FRP tube. The FRP tube had an inside diameter of 343mm (13.5 in.). Two different laminate designs were used as given in Table 4.2.1. Both tube designs used the same carbon/epoxy material with ply properties given in Table 4.2.2.

Table 4.2.1 Large-Scale FRP Shell Laminate Architecture

	Lay-up	Thickness
Design 1	$[90, \pm 10_2, 90, \pm 10_2, 90]_s$	10 mm (0.38 in.)
Design 2	$[90_2, \pm 10_2, 90_2, \pm 10_2, 90_2, \pm 10, 90_2, \pm 10, 90_3]$	9 mm (0.35 in.)
* Thickness 10^0 ply = 0.5 mm (0.02") and 90^0 ply = 0.25 mm (0.01")		

Table 4.2.2 Carbon/Epoxy Ply Properties

Properties	Values
E_{11}	120.7 GPa (17.5 Msi)
E_{22}	6.89 GPa (1.0 Msi)
G_{12}	4.83 GPa (0.7 Msi)
v_{12}	0.3

Recalling Section 2.2, the in-plane stiffness matrix [A] and the equivalent orthotropic engineering properties for Design 1 are calculated as:

$$[A] = \begin{bmatrix} 945.8 & 45 & 0 \\ 45 & 245.2 & 0 \\ 0 & 0 & 71.6 \end{bmatrix} \text{ [KN/mm]}$$

or

$$[A] = \begin{bmatrix} 0.54E + 0.4 & 0.257E + 03 & 0 \\ 0.257E + 03 & 0.14E + 04 & 0 \\ 0 & 0 & 0.409E + 03 \end{bmatrix} \text{ [Kips/in]} \qquad (4.2.1)$$

Engineering properties: E_L = 97.1 GPa (14086 ksi); E_H = 25.2 GPa (3652 ksi); G_{LH} = 7.4 GPa (1076 ksi)

Similarly, the [A] matrix and Engineering properties for Design 2 are:

$$[A] = \begin{bmatrix} 721.6 & 37.3 & 0 \\ 37.3 & 385.3 & 0 \\ 0 & 0 & 61.6 \end{bmatrix} \text{[KN/mm]}$$

or

$$[A] = \begin{bmatrix} 0.412E+0.4 & 0.213E+03 & 0 \\ 0.213E+03 & 0.22E+04 & 0 \\ 0 & 0 & 0.352E+03 \end{bmatrix} \text{[Kips/in]} \qquad (4.2.2)$$

Engineering properties: E_L = 80.8 GPa (11712 ksi); E_H = 43.1 GPa (6254 ksi); G_{LH} = 6.93 GPa (1005 ksi)

Both test units were pumped-filled with all-lightweight concrete. The concrete properties for each test unit at the day of the test are given in Table 4.2.3

Table 4.2.3 Concrete Properties (Design #1 and Design #2)

	Design 1	Design 2
f'_c	21 MPa (3 ksi)	31 MPa (4.5 ksi)
E_{co} (ksi)	14 GPa (2.1 Msi)	18 GPa (2.6 Msi)
ν_{co}	0.2	0.2

The concrete filled carbon/epoxy FRP tubes were tested in flexure in a four-point bending test setup as shown in Figure 4.2.1. The boundary conditions were designed to replicate a pin and a roller condition, thus avoiding any axial load on the member. To monitor the shear stresses in the FRP shell, a section in the shear span (1.83m [72 in.]

from the support) of the beam (Section A-A) was instrumented. Strain gages around the circumference of section A-A were placed on the carbon/epoxy shell. Biaxial strain gages were used in the extreme compression and tension fibers (locations 1 and 5) and rectangular rosettes were placed at six other locations around the circumference viz. at $+60^0$, $+30^0$, 0^0, -30^0, -60^0 (locations 2,3,4 and 8, 7 and 6, respectively) from the section center-line as shown in Figure 4.2.1.
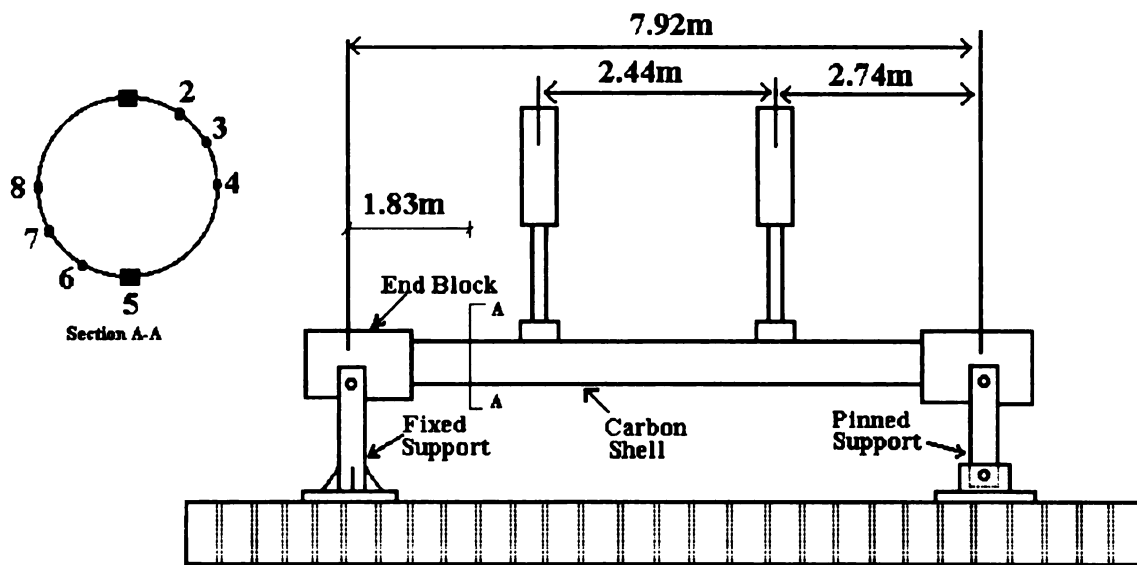
Fig. 4.2.1 Large scale Four point bending Beam Test set-up (Burgueño, R., 1999)

[25.4mm = 1 in]

4.2.2 Comparison of Analytical and experimental results

The shear force against shear strain response histories around the section circumference for the large-scale girder tests are shown in Figure 4.2.2 through Figure 4.2.5. The results for Design #1 are shown in Fig 4.2.2 and Fig 4.2.3. It can be seen that the analytical response agrees well with the experimental traces at all locations except location #3 where higher strains than predicted were measured.

61

The response histories for Design #2 are shown in Fig 4.2.4 and Fig 4.2.5. It can be seen that good agreement between the analytical and experimental traces is obtained for all locations except location #6, where much higher strains were measured than the analytically computed values.
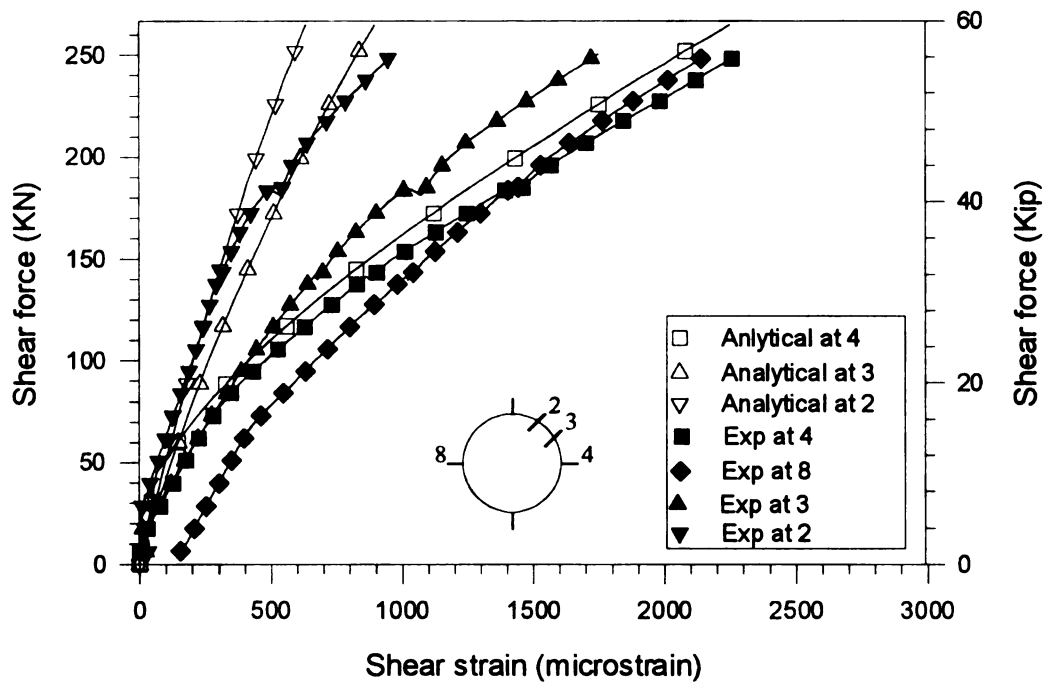
Fig. 4.2.2 Shear Strain Histories for locations 2,3, and 4 (Design #1)
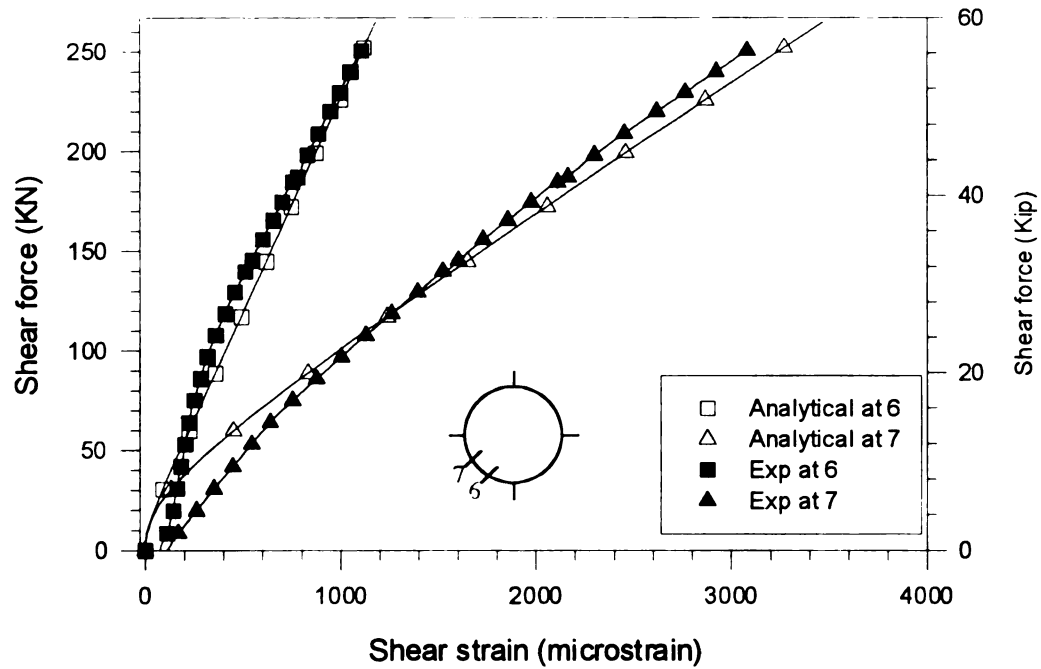
Fig. 4.2.3 Shear Strain Histories for locations 6 and 7 (Design #1)
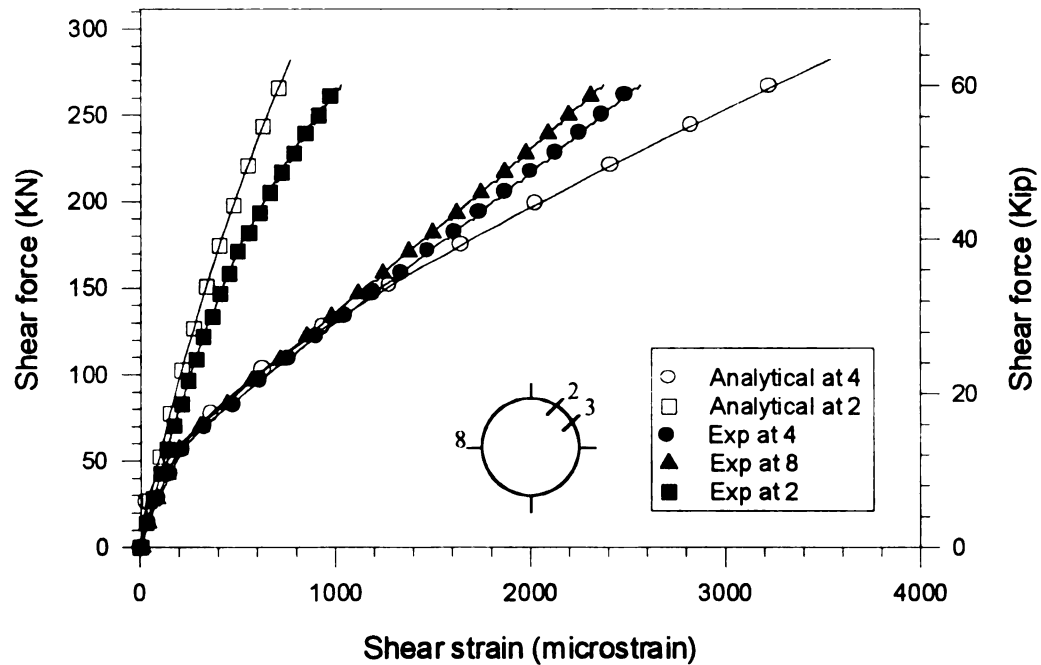
Fig. 4.2.4 Shear Strain Histories for locations 2 and 4 (Design #2)
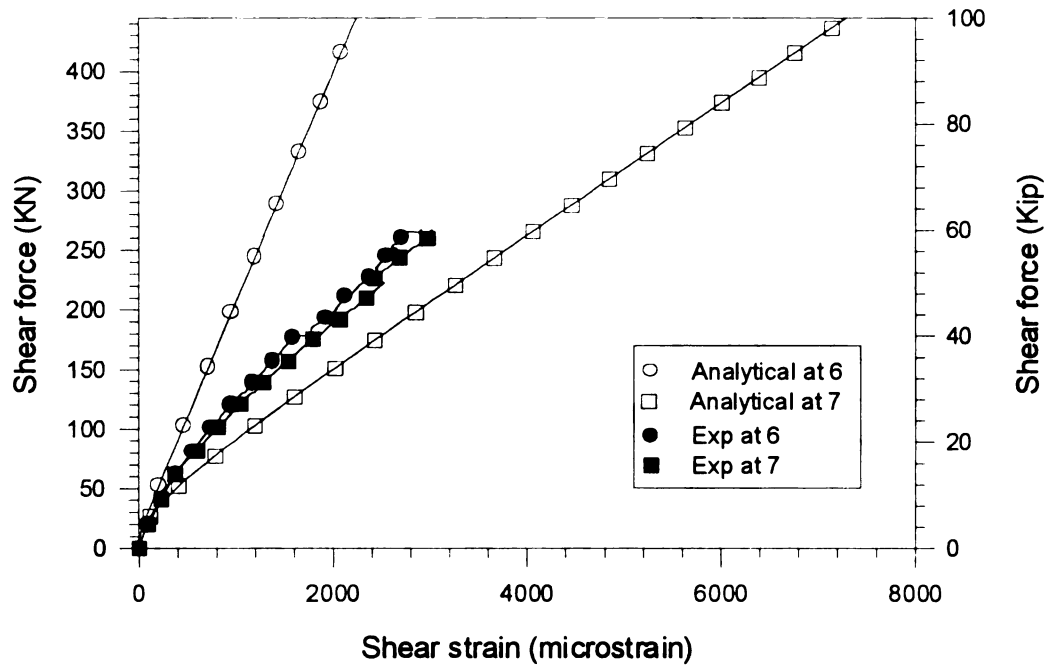
Fig. 4.2.5 Shear Strain Histories for locations 6 and 7 (Design #2)

Cross-section shear strain profiles along the FRP shell periphery throughout the loading history for Design #1 and Design #2 are provided in Figure 4.2.6 and Figure 4.2.7, respectively. The analytical response is shown with hollow symbols connected by a continuous line, while the experimental measurements are shown with equal "unconnected" solid symbols. The profiles are provided at different percentages of response to the ultimate failure load in the experiment.

For both designs, the analytical profiles agree well with the experimental measurements with exception of the locations noted earlier. Despite these disagreements, it can be seen that the shear strain profiles along the cross-section have a consistent trend with the experimental measurements throughout the different load levels.
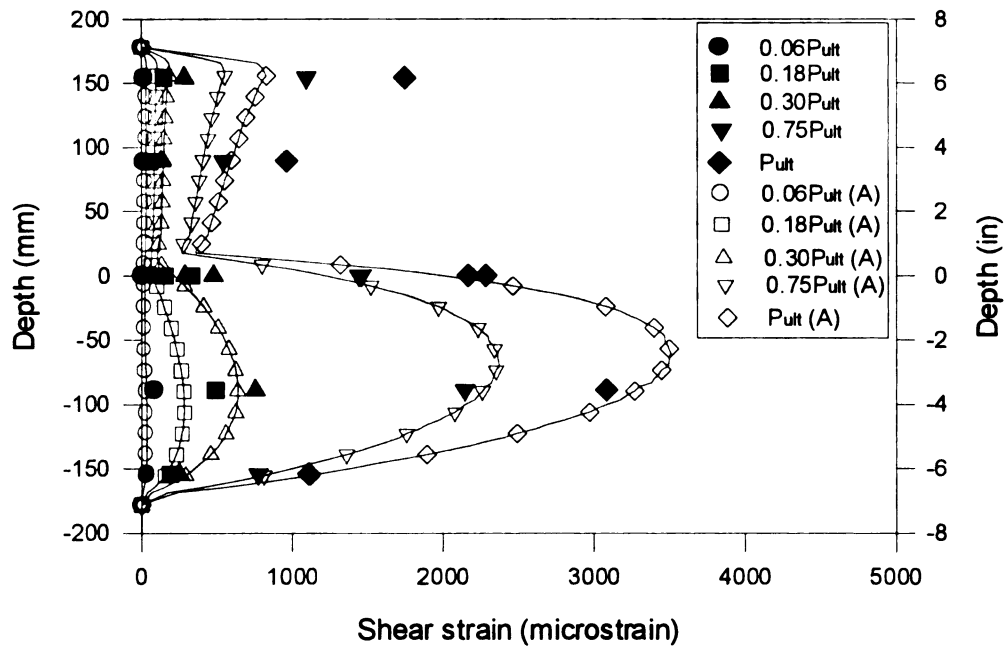
Fig. 4.2.6 Cross-Section Shear Strain Profiles along FRP tube periphery (Design #1)
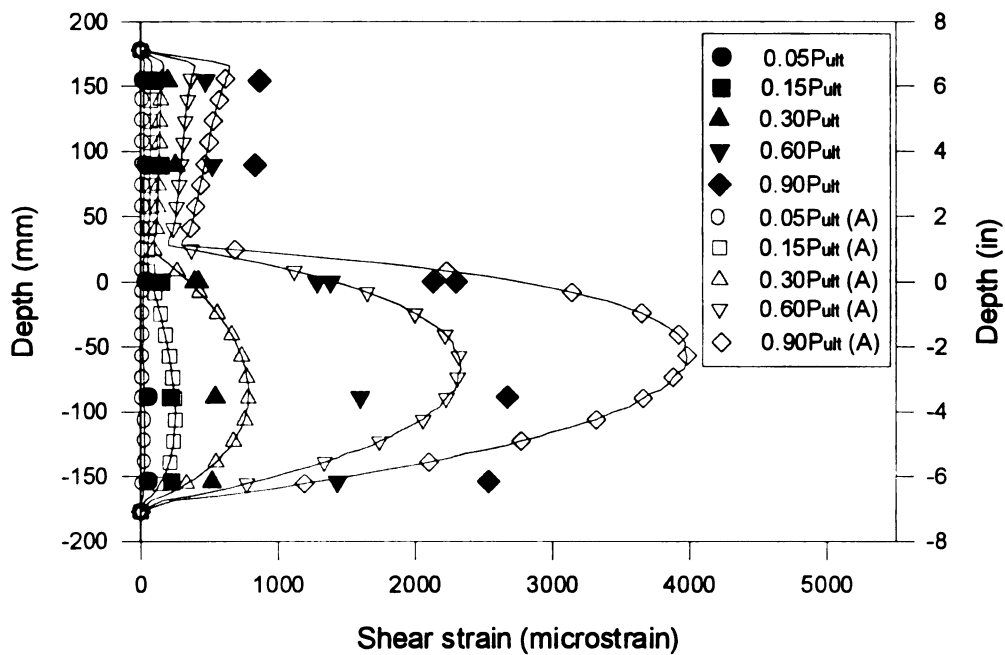
Fig. 4.2.7 Cross-Section Shear Strain Profiles along FRP tube periphery (Design #2)

In summary, the shear force versus shear strain response of the analytical model agrees well with the experimental data. The greatest discrepancies were found at locations 3 (Design #1) and 6 (Design #2), (see Figure 4.2.1 and Figure 4.2.5). At these locations the measured experimental values were greater than the analytical predictions. The analytical shear strain profiles across the section at different stages of loading show similar trends and are in good agreement when compared with the experimental values.

4.2.3 Shear stress section profiles at ultimate conditions

Analytically determined cross-section shear stress profiles for the concrete core and the FRP shell at ultimate conditions for both designs are given in Figure 4.2.8 through 4.2.13. The vertical shear stress profile along the concrete core for Design #1 and Design #2 are given in Fig 4.2.8 and Figure 4.2.11 respectively. It can be clearly seen that the concrete under compressive stresses (top region) carries more shear stresses than the concrete under tensile stresses. This is clearly follows from the reduction of the average concrete shear modulus of the cracked concrete in the tension zone, which reduces its shear stress carrying capacity.
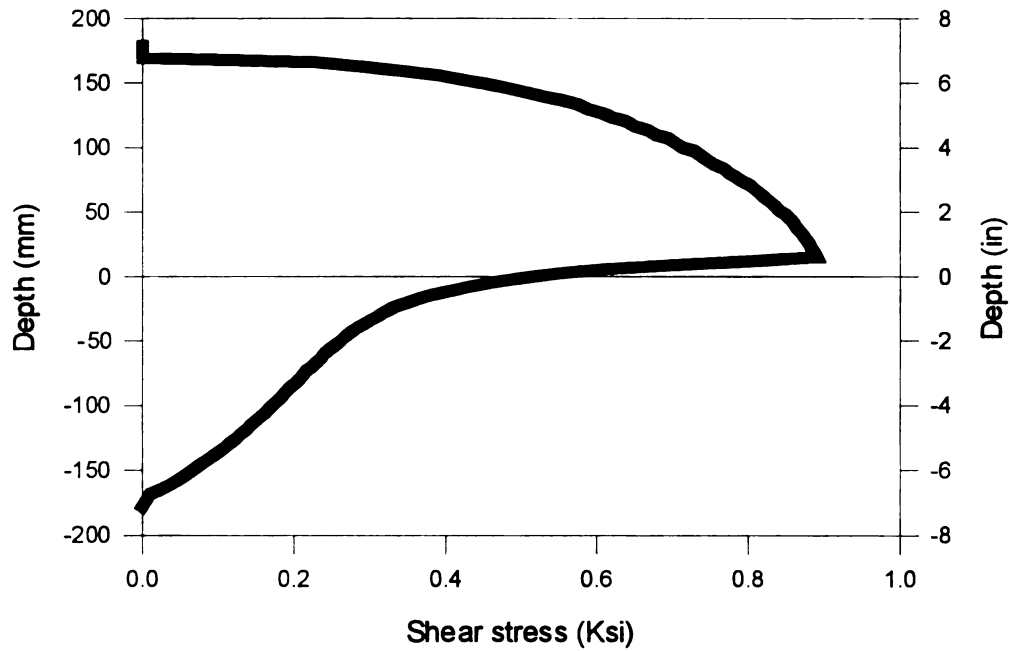
Fig. 4.2.8 Shear stress profile of concrete at failure (Design #1)
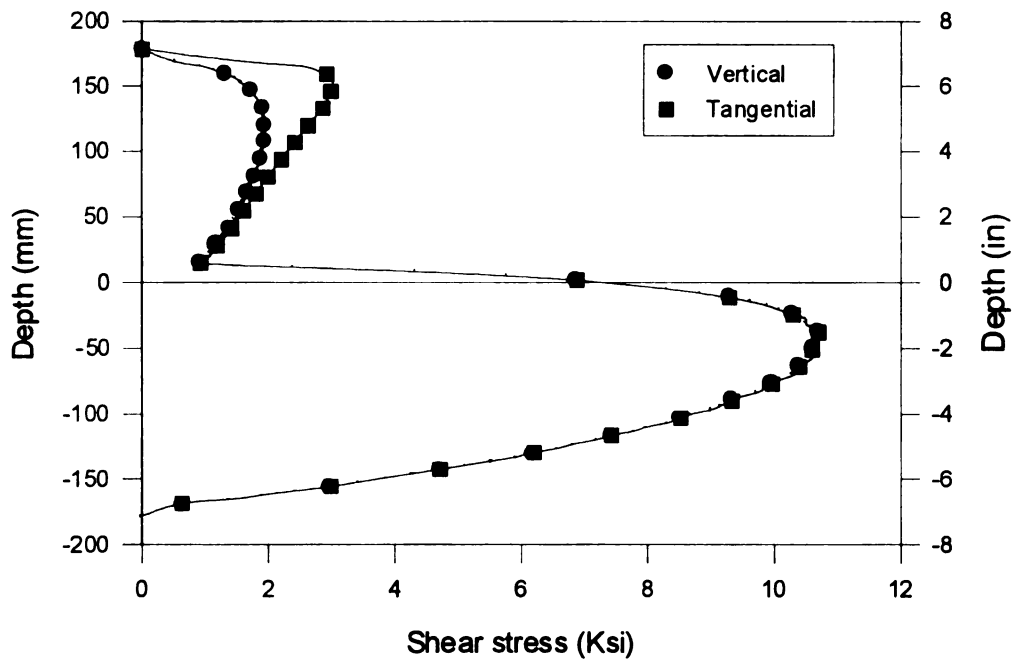
Fig. 4.2.9 Shear stress profile of FRP shell at failure (Design #1)
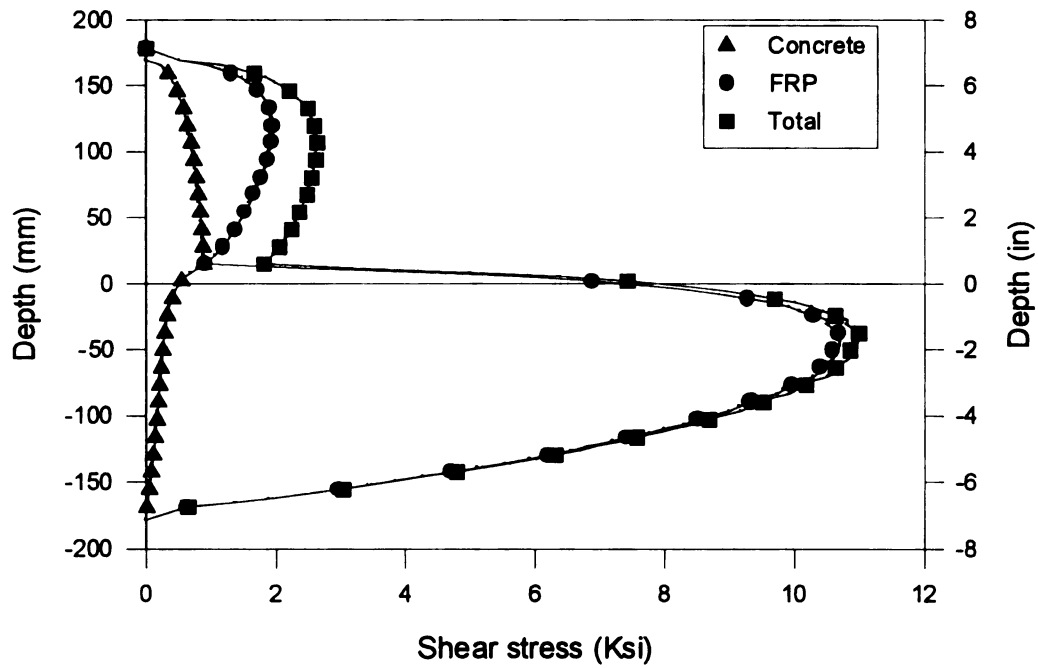
Fig. 4.2.10 Vertical Shear stress contribution of concrete and FRP shell (Design #1)
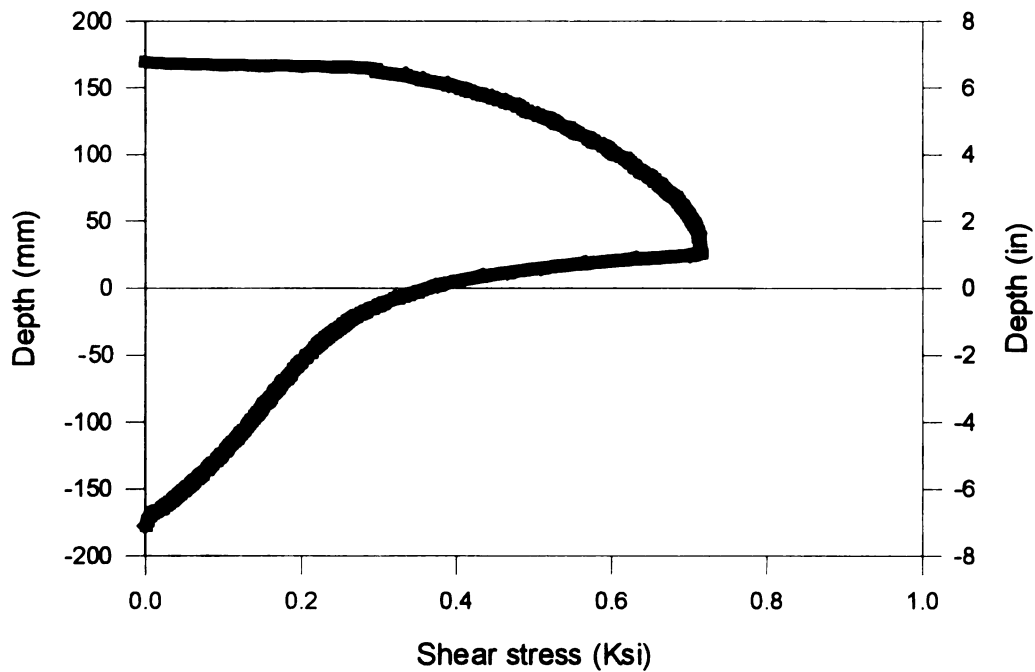
Fig. 4.2.11 Shear stress profile of concrete at failure (Design #2)
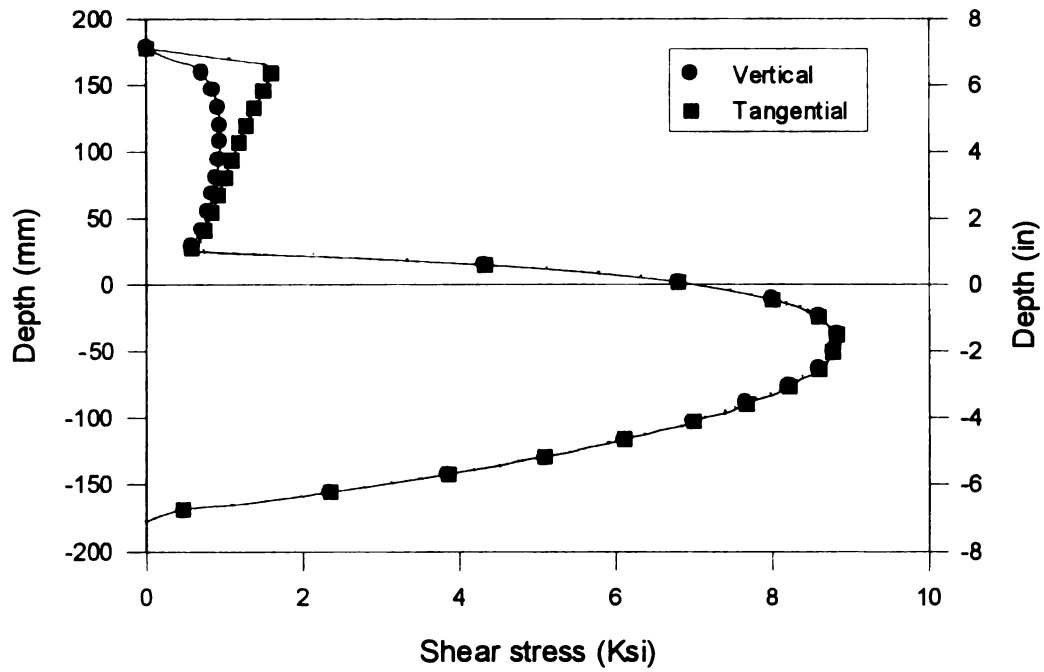
Fig. 4.2.12 Shear stress profile of FRP shell at failure (Design #2)
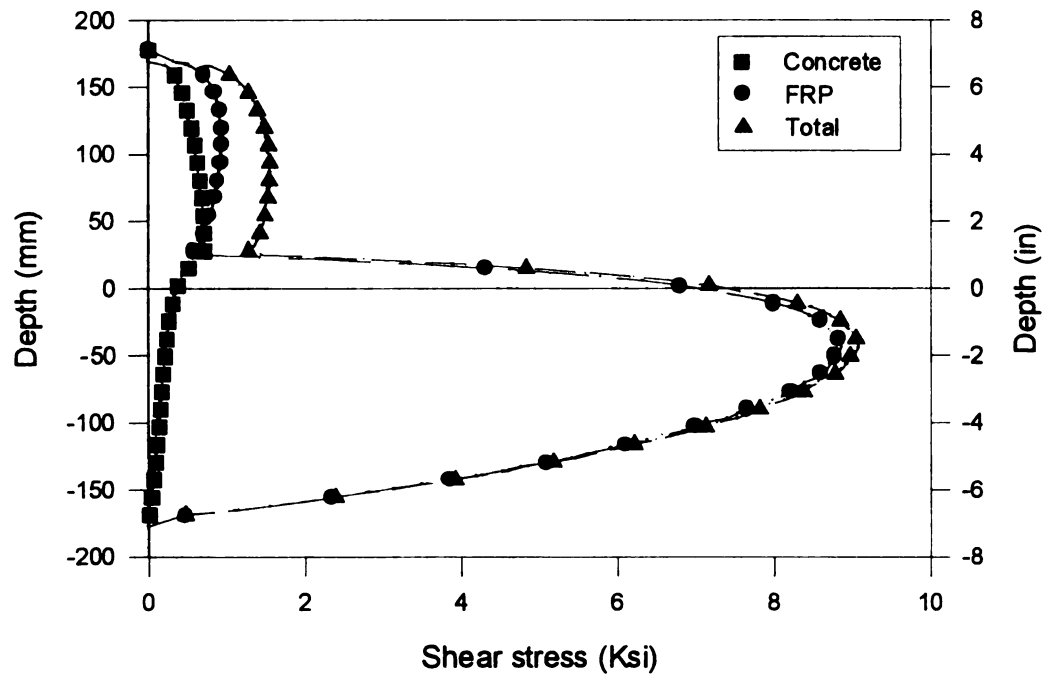
Fig. 4.2.13 Vertical Shear stress contribution of concrete and FRP shell (Design #2)

The vertical and tangential shear stresses on the FRP shell for Design #1 and Design #2 are provided in Figure 4.2.9 and Figure 4.2.12, respectively. It can be seen that in the compression zone, the FRP shell takes less shear as the concrete shear stiffness is greater and thus carries the majority of the shear stresses. Conversely, as the load increases and the shear carrying capacity of the cracked concrete in tension reduces, the FRP shell can be seen taking most of the section shear stresses.

A depiction of the individual and collective *vertical* shear stress distributions in the concrete and the FRP shell for Design #1 and Design #2 are shown in Figure 4.2.10 and Figure 4.2.13, respectively. The figures show the relative magnitude of the shear stresses in both the concrete and FRP shell, and the clearly different behavior of both materials in carrying the shear stresses through the cross-section.

4.2.4 Shear stress profiles of concrete and FRP shell throughout loading history

The analytical vertical shear stress profiles in the concrete core and tangential shear stress profiles in the FRP shell throughout the loading history for Design #1 are shown in Figure 4.2.14 and Figure 4.2.15, respectively. The responses are shown for different loading levels corresponding to percentage fractions of the ultimate failure load in the experiment test.

Similarly, analytical shear stress profiles in the concrete core and the FRP shell throughout the loading history for Design #2 are shown in Figure 4.2.16 and Figure 4.2.17, respectively.
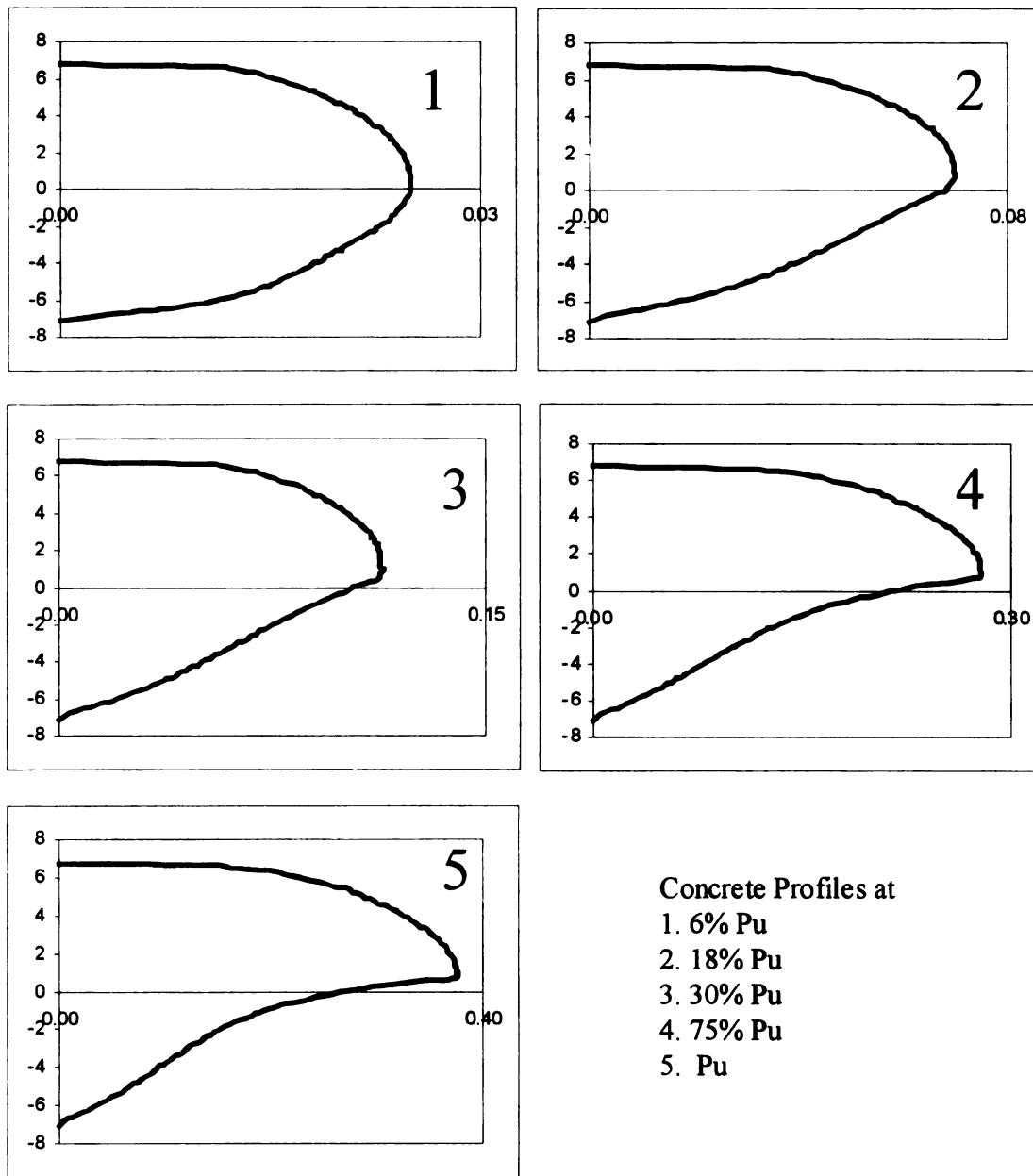
[X-axis: Shear stress (ksi); Y-axis: Depth (in.)] [1 ksi = 6.895 MPa; 1 in. = 25.4 mm]

Fig. 4.2.14 Shear stress profile of concrete throughout the loading history

(Design #1)

71

[X-axis: Shear stress (ksi); Y-axis: Depth (in.)] [1 ksi = 6.895 MPa; 1 in. = 25.4 mm]
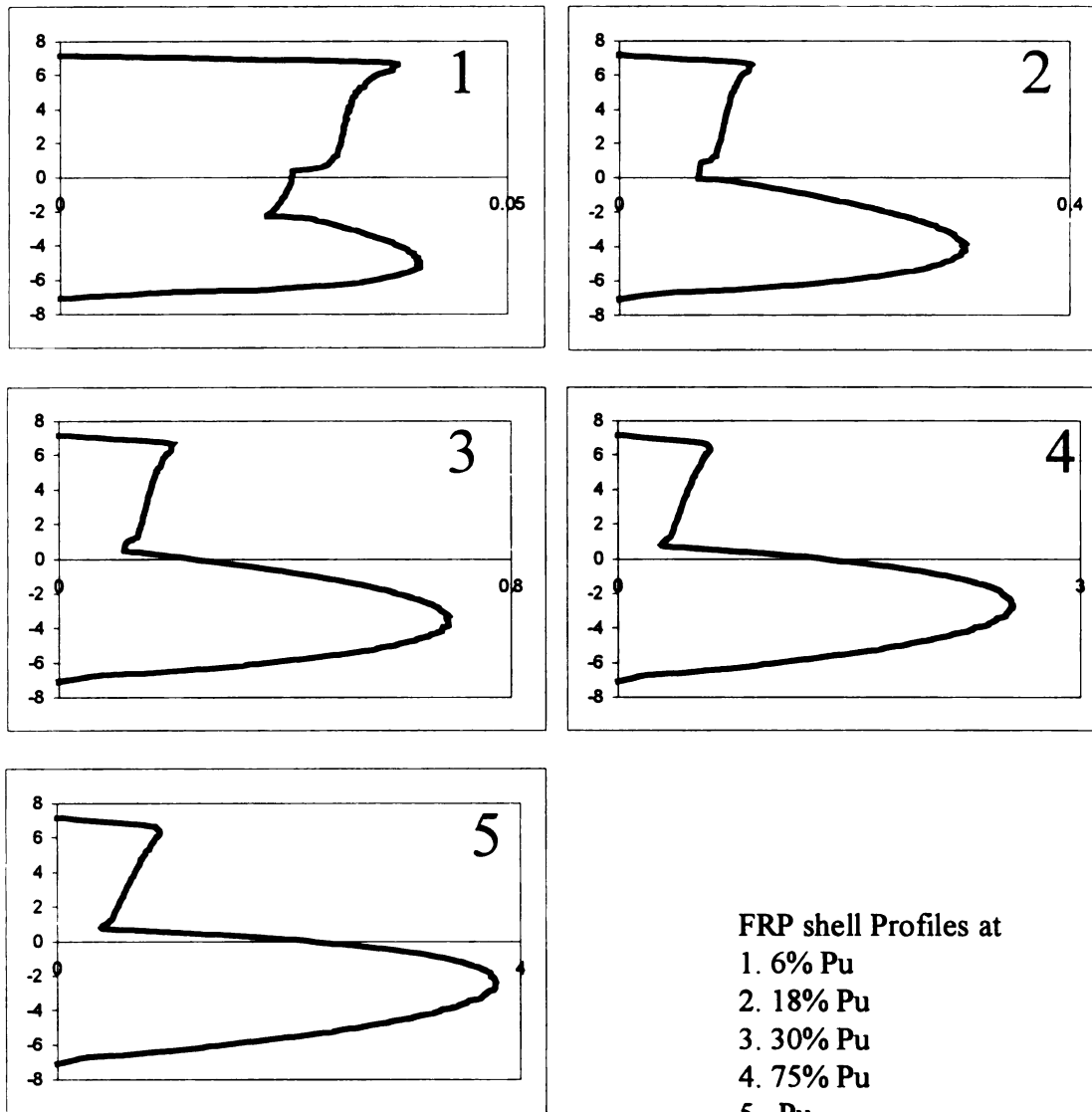
FRP shell Profiles at
1. 6% Pu
2. 18% Pu
3. 30% Pu
4. 75% Pu
5. Pu

Fig. 4.2.15 Shear stress profile of FRP shell throughout the loading history
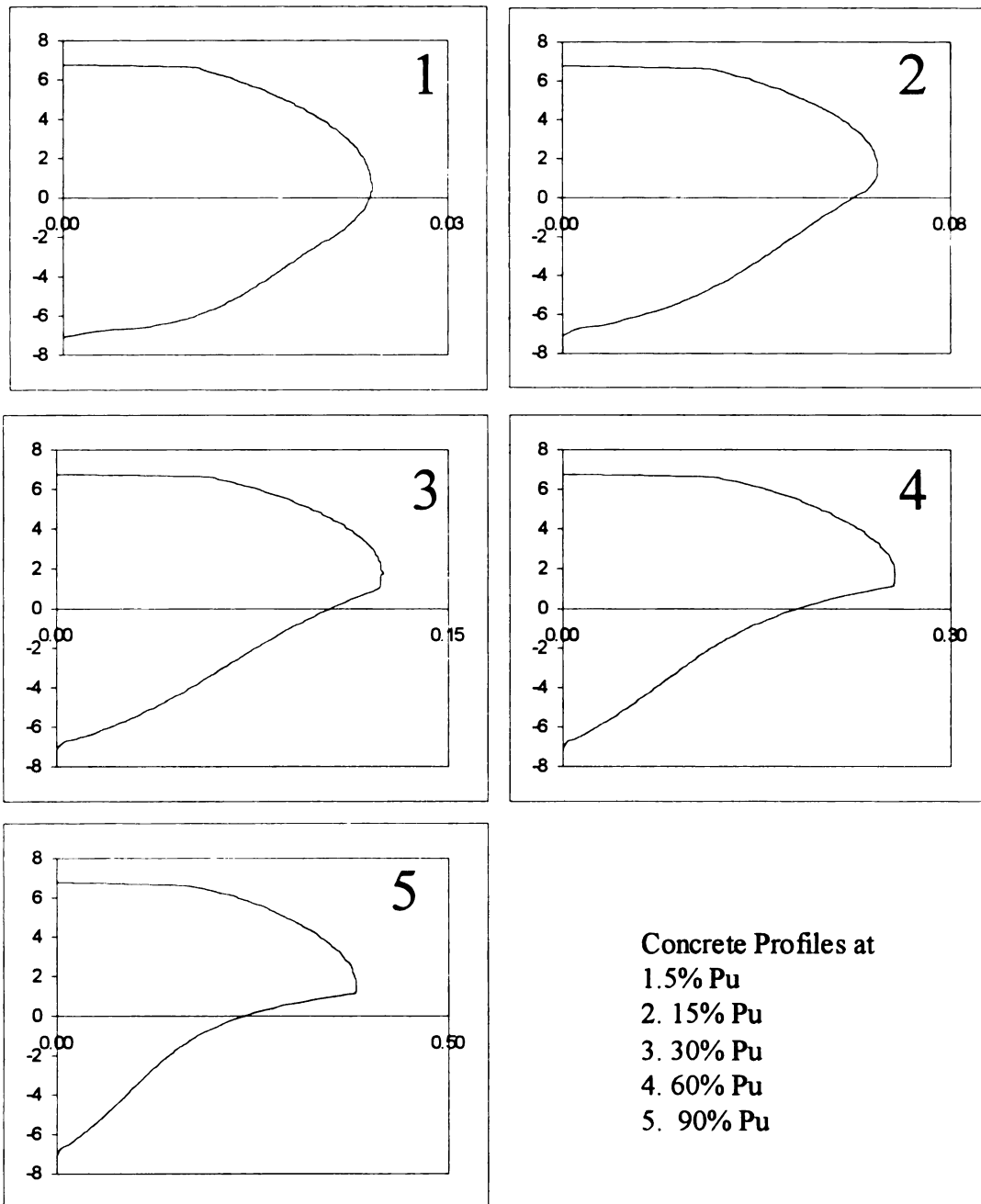
(Design #1)

[X-axis: Shear stress (ksi); Y-axis: Depth (in.)] [1 ksi = 6.895 MPa; 1 in. = 25.4 mm]

Fig. 4.2.16 Shear stress profile of concrete throughout the loading history

(Design #2)

Concrete Profiles at
1. 5% Pu
2. 15% Pu
3. 30% Pu
4. 60% Pu
5. 90% Pu

73
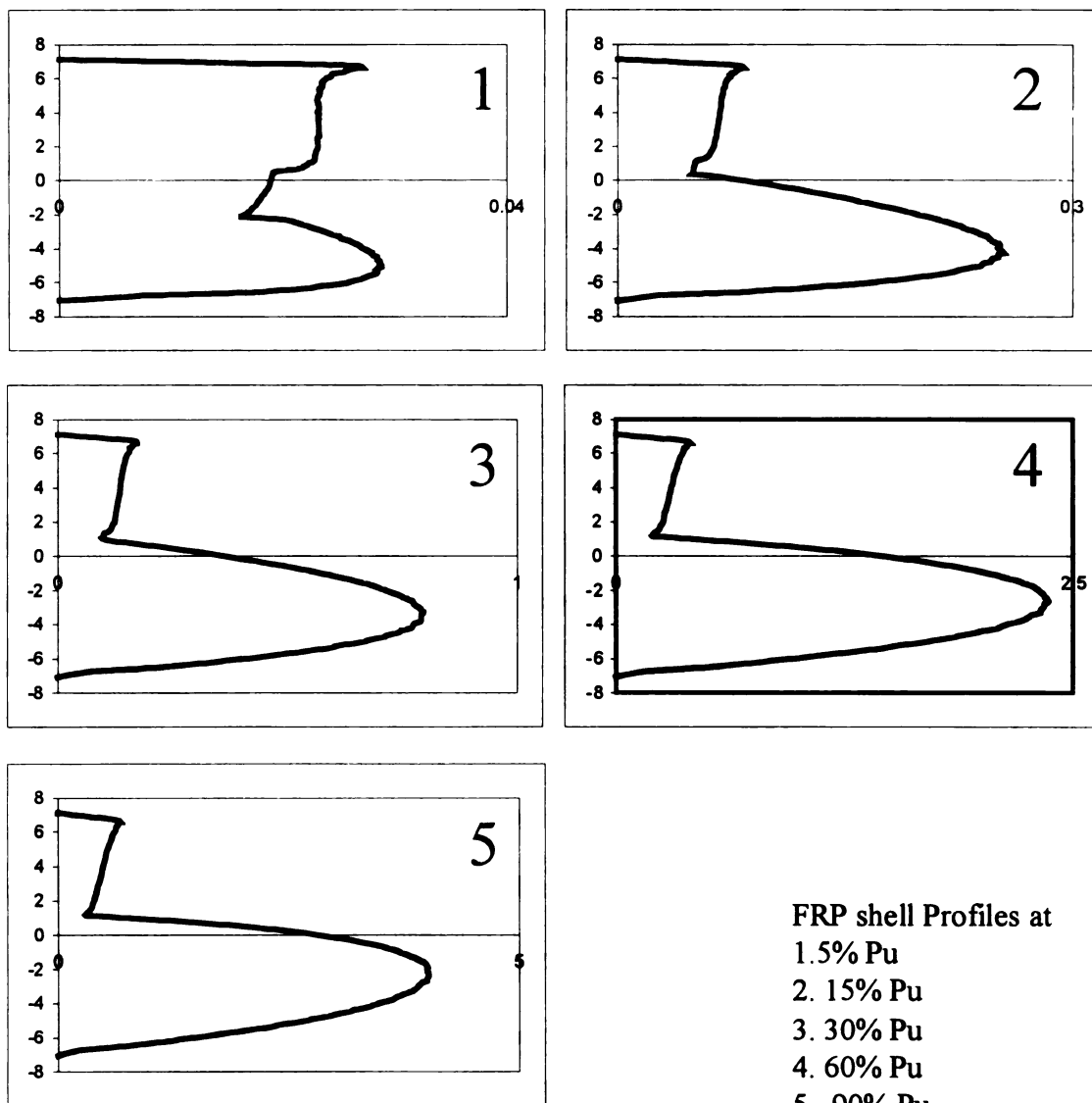
[X-axis: Shear stress (ksi); Y-axis: Depth (in.)] [1 ksi = 6.895 MPa; 1 in. = 25.4 mm]

Fig. 4.2.17 Shear stress profile of FRP shell throughout the loading history

(Design #2)

Careful observation of the profiles shown in Figure 4.2.14 through Figure 4.2.17 indicates how the vertical shear stress distribution in the concrete core is initially very similar to the expected linear elastic behavior. However, it can be seen that as the load demand increases, the cracked concrete in the tension zone is reduced in its shear carrying capacity as shown in Figure 4.2.14 and Figure 4.2.16. This phenomenon increases the shear stress demands on the linear elastic FRP shell in the tension zone of the cross-section, as seen in Figure 4.2.15 and Figure 4.2.17.

4.3 Small scale Flexure Tests

4.3.1 Test Unit Geometry, Properties and Test Set-up

The small-scale experimental tests were carried out on concrete filled carbon/epoxy circular FRP tubes. These FRP tubes were not provided with ribs on the inside of the tube. The FRP tube had an inside diameter of 152mm (6 in.). Two different laminate designs were used as given in Table 4.3.1. Both tube designs used the same carbon/epoxy material with ply properties given in Table 4.2.2.

Table 4.3.1 Laminate properties (Design #3 and Design #4)

	Lay-up	Thickness
Design 3	[90, $\pm$ 10, $\pm$ 10, 90]	2.54 mm (0.1 in.)
Design 4	[90, $\pm$ 10, $\pm$ 10, 90]$_s$	5.08 mm (0.2 in.)
* Thickness 10^0 ply = 0.5 mm (0.02") and 90^0 ply = 0.25 mm (0.01")		

The [A] Matrix and equivalent orthotropic engineering properties of Design #3
are given in equation 4.3.1 below:

$$[A] = \begin{bmatrix} 236.5 & 11.5 & 0 \\ 11.5 & 76.5 & 0 \\ 0 & 0 & 18.6 \end{bmatrix} \quad (KN/m)$$

or

$$[A] = \begin{bmatrix} 0.135E + 0.4 & 0.655E + 02 & 0 \\ 0.655E + 02 & 0.437E + 03 & 0 \\ 0 & 0 & 0.106E + 03 \end{bmatrix} \quad (Kip/in) \tag{4.3.1}$$

Engineering properties:

$E_L = 92.41$ GPa (13400 ksi); $E_H = 29.9$ GPa (4330 ksi); $G_{LH} = 7.31$ GPa (1060 ksi);

$v_{12} = 0.1504$

The [A] Matrix and equivalent orthotropic engineering properties of design #4 are given
in equation 4.3.2 below:

$$[A] = \begin{bmatrix} 472.9 & 22.9 & 0 \\ 22.9 & 152.9 & 0 \\ 0 & 0 & 36.9 \end{bmatrix} \quad (KN/m)$$

or

$$[A] = \begin{bmatrix} 0.270E + 0.4 & 0.131E + 03 & 0 \\ 0.131E + 03 & 0.873E + 03 & 0 \\ 0 & 0 & 0.211E + 03 \end{bmatrix} \quad (Kip/in) \tag{4.3.2}$$

Engineering properties: $E_L = 92.41$ GPa (13400 ksi); $E_H = 29.9$ GPa (4330 ksi); $G_{LH} =$

7.31 GPa (1060 ksi); $v_{12} = 0.1504$

Both test units were pumped-filled with all-lightweight concrete. The concrete

properties for each test unit are given in Table 4.3.3.

Table 4.3.2 Concrete Properties (Design #3 and Design #4)

	Design 3 & 4
f'_c	46 MPa (6.6 ksi)
E_{co} (ksi)	21 GPa (3.09 Msi)
v_{co}	0.2

The concrete filled carbon/epoxy FRP tubes were tested in flexure in a four-point bending test setup as shown in Figure 4.2.2. To monitor the shear stresses in the FRP shell, strain gages around the circumference of section A-A were placed on the carbon/epoxy shell. Biaxial strain gages were used in the extreme compression and tension fibers and rectangular rosettes were placed at four other locations around the circumference viz. at $+45^0$, 0^0, -45^0 from the section centerline. A schematic of the strain gage layout in section A-A is shown in Figure 4.2.2.

1

2

3

7

6

5

A-A

Constant Moment Region

Shear span

711 mm
(28")

406 mm
(16")

(12")

152mm
(6")

Strain Rosettes
1.83 m
(6')
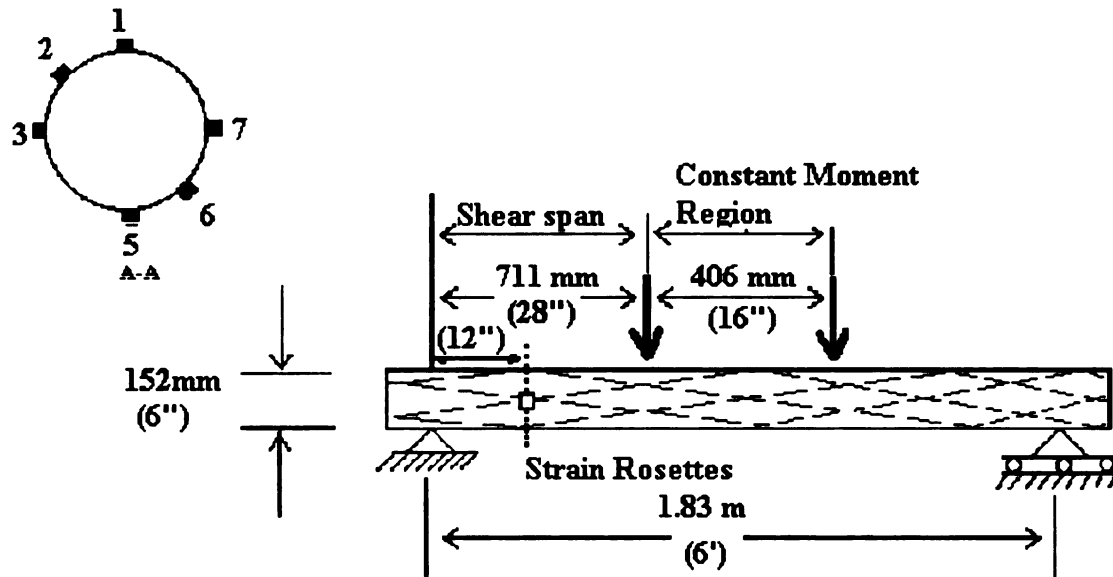
Fig. 4.3.1 Schematic of Four Point Bending Test Setup (Davol, A., 1998)

4.3.2 Comparison of Analytical model with experimental measurements (Design #3 and Design #4)

The shear force against shear strain response histories around the section circumference for the small-scale girder tests for Design #3 and Design #4 are shown in Figure 4.3.2 and Figure 4.3.3, respectively. The analytical response is shown with hollow symbols while experimental response is shown with solid symbols. It can be seen that, for Design #3, the analytical response agrees well with the experimental traces at all locations.
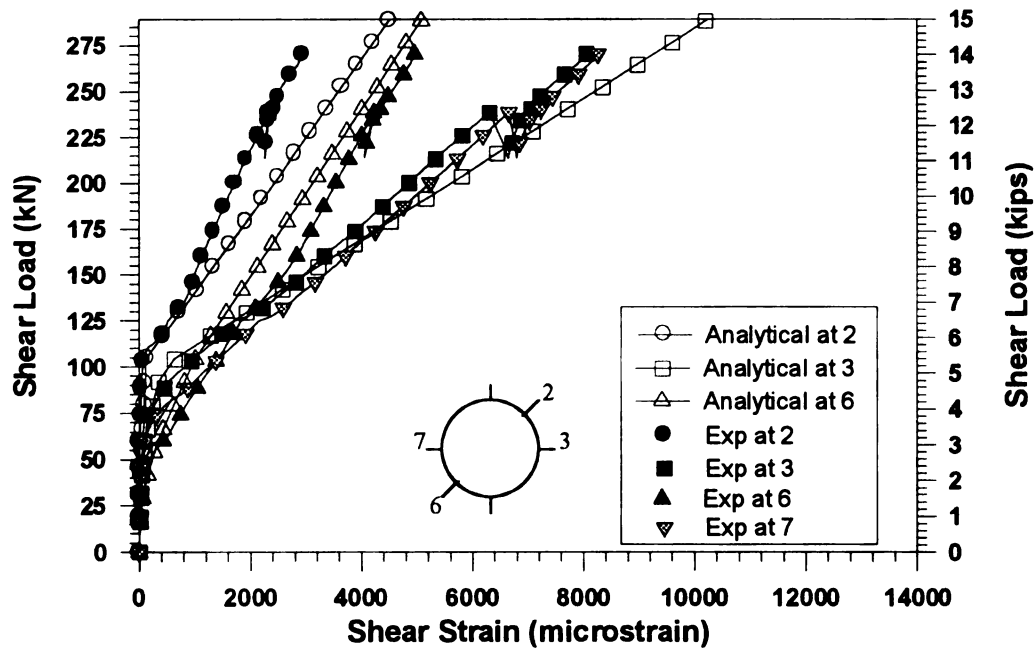
Fig. 4.3.2 Shear Strain Histories for locations 2,3, 6 and 7 (Design #3)

For Design #4, the analytical response after concrete cracking deviates from the experimental response at all the locations except at location 2. Careful observation of the experimental traces, for example location 3, shows that the shear force to shear strain response has two distinct slopes *after* cracking of the concrete. In the analysis, the FRP shell takes the balance shear force once concrete reaches its shear carrying capacity. Thus, the slope of the analytical shear force to shear strain graph after cracking agrees well with the third slope of experimental trace. Therefore, the second slope clearly indicates some level of composite interaction between the concrete and the FRP shell after cracking has occurred. Another important observation is that the experimental shear strain values at location 6 (tension zone) are smaller than experimental shear strain values

79

at location 2. As this should not be the case, it indicates irregularities in the gage readings and makes the experimental trace at this location suspect.
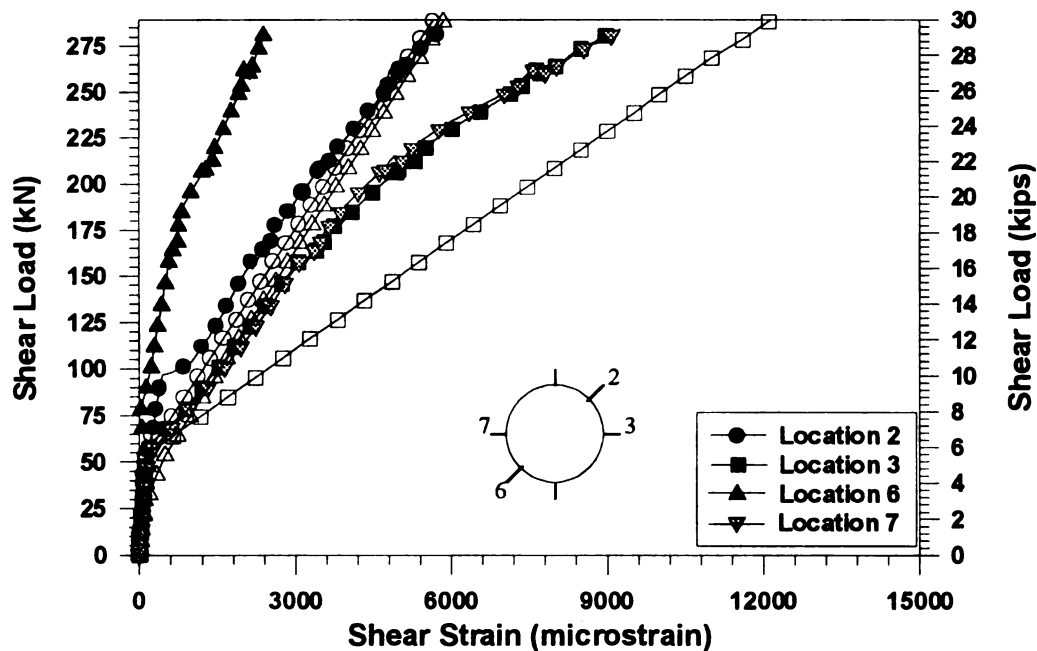
Fig. 4.3.3 Shear Strain Histories for locations 2,3, 6 and 7 (Design #4)

Cross-section shear strain profiles along the FRP shell periphery throughout the loading history for Design #3 and Design #4 are provided in Figure 4.3.4 and Figure 4.3.5, respectively. The analytical response is shown with hollow symbols connected by a continuous line, while the experimental measurements are shown with equal "unconnected" solid symbols. The profiles are provided at different percentages of response to the ultimate failure load in the experiment.

For both designs, the analytical profiles agree well with the experimental measurements with some discrepancies at the locations noted earlier. But, it can be seen that the shear strain profiles along the cross-section have a consistent trend with the experimental measurements throughout the different load levels.
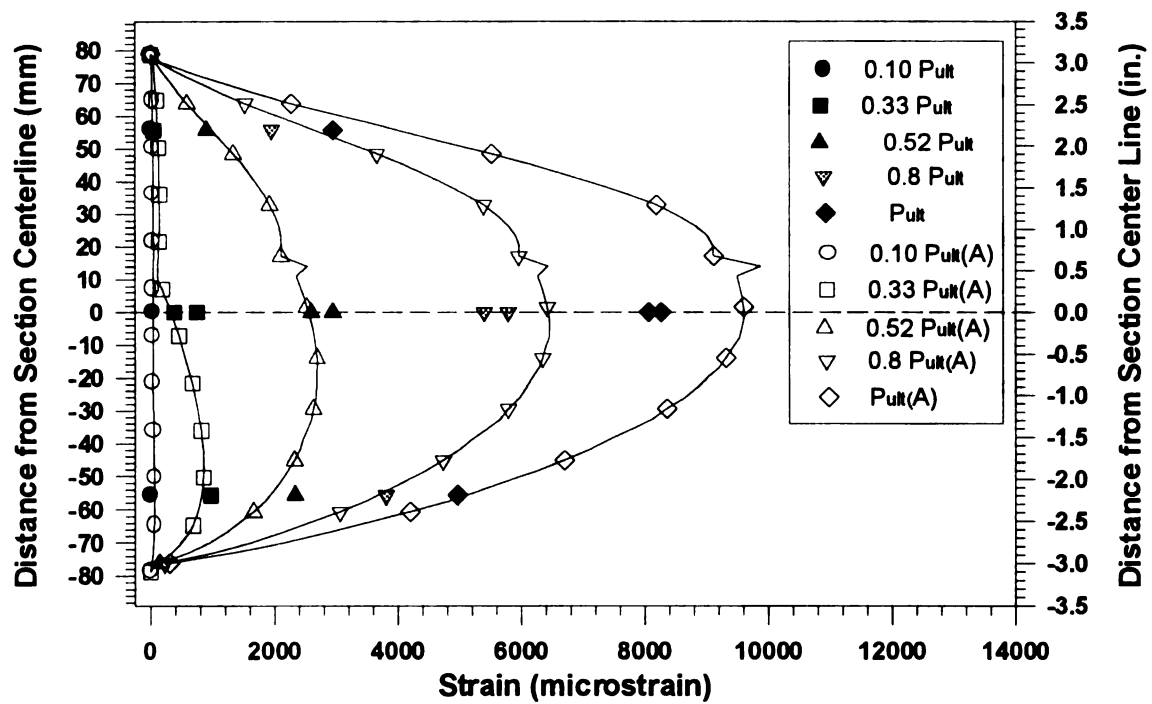
Fig. 4.3.4 Cross-Section Shear Strain Profiles along FRP tube periphery (Design #3)
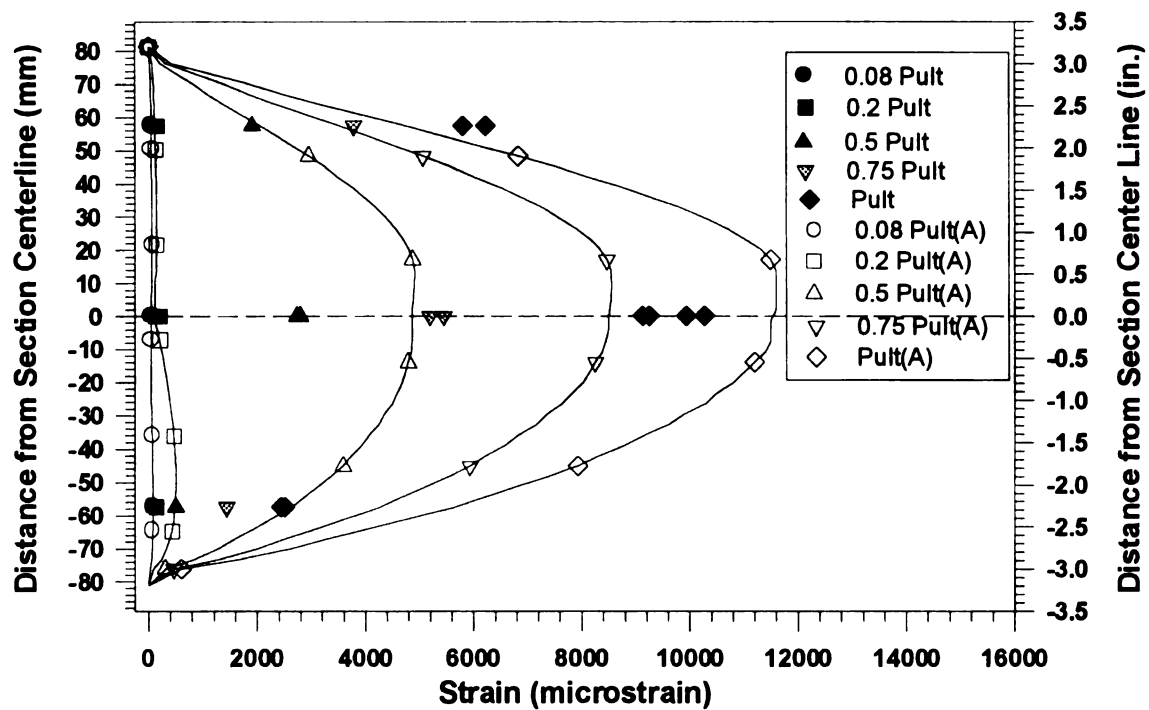
Fig. 4.3.5 Cross-Section Shear Strain Profiles along FRP tube periphery (Design #4)

81

In summary, the shear force versus shear strain response of the analytical model agrees well with the experimental data. The largest discrepancy was observed for Design #4, particularly at location 6 (gage located at -45^0 from the section centerline in the tension side [see Figure 4.3.1]). At this location, the measured experimental values were greater than the analytical prediction. The discrepancy is believed to be due to a faulty gage as discussed in section 4.3.2. The analytical shear strain profiles at different stages of loading show similar trends and are in good agreement when compared with the experimental values.

4.3.3 Influence of composite action

As discussed in the previous section, the shear force to shear strain response of the small-scale girders showed indications of composite action. The influence of composite action behavior is illustrated with reference to the response at location #3 for both tests units in Figure 4.3.6 and Figure 4.3.7, respectively.

The analytical response of Design #3 and Design #4 at location 3 is compared with experimental response as shown in Figure 4.3.6 and 4.3.7, respectively. The analytical response is shown with hollow symbols while the experimental response is shown with solid symbols.
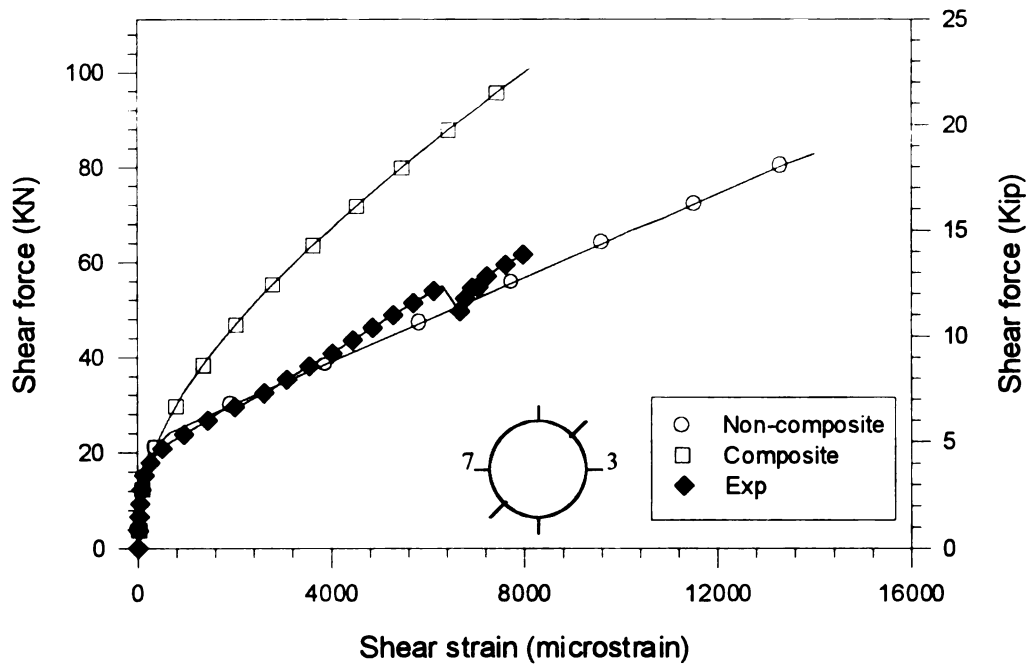
Fig. 4.3.6 Shear Strain History for locations 3 (Design #3)
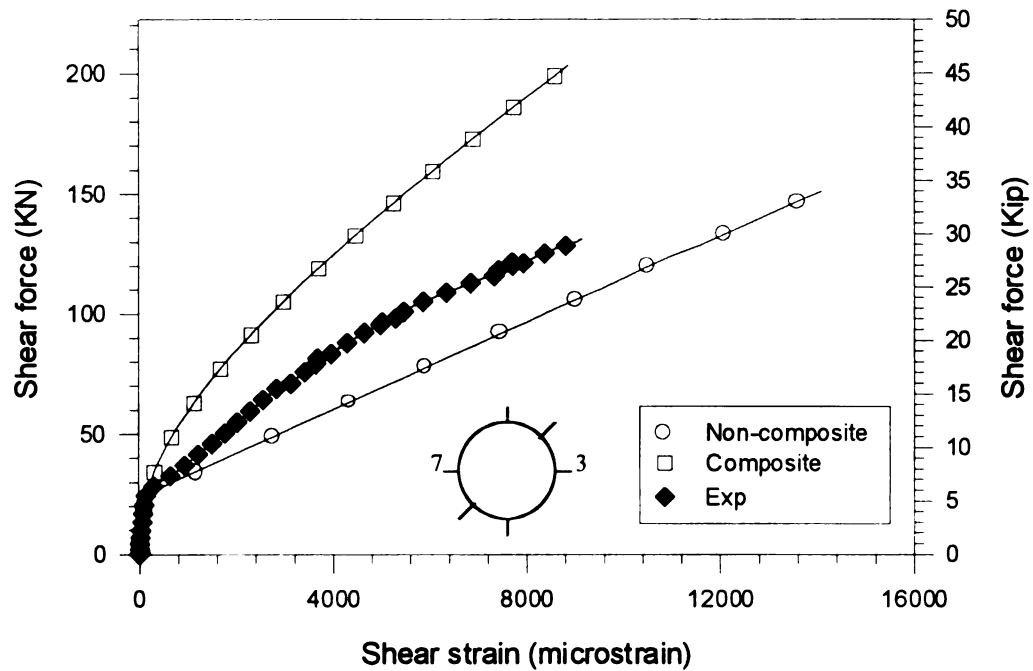
Fig. 4.3.7 Shear Strain History for locations 3 (Design #4)

Figure 4.3.6 shows that for Design #3 (D/t = 60), the analytical response for non-composite action agrees well with the experimental response. However, the experimental response of Design #4 (D/t = 30), shown in Figure 4.3.7, falls in between the composite and non-composite analytical curves. After concrete cracking, it can be seen that the slope of the experimental shear force to shear strain graph is higher than the slope of the analytical curve for the non-composite behavior. This discrepancy shows that the test unit underwent a transition from composite behavior to same residual composite behavior. However, it can also be observed that the slope of response at a later stage (the third slope) approximates the non-composite condition assumed in the analytical model.

CHAPTER 5: PARAMETRIC STUDIES

5.1. General

This chapter presents parametric studies on the shear response of concrete filled circular FRP tubes. The parameters considered are the lamina properties, the laminate type, the effect of axial load and the concrete properties.

5.2 Parameters and Case Studies Description

The following parameters are considered in the studies:

1. Diameter to thickness ratio

2. Axial load

3. Effect of anisotropic shell behavior

4. Concrete modulus of rupture

5. Concrete compressive strength

In order to determine effect of the different parameters on the shear response of concrete filled circular FRP tubes, six examples of circular carbon/epoxy FRP composite tubes with different laminate properties were considered. In all cases, the FRP tube has an inside diameter of 609 mm (24 in.). Composite behavior between concrete and FRP shell is assumed in all the parametric studies.

The laminate architectures for the selected examples are given in Table 5.2.1

Table 5.2.1 FRP Tube Laminate Architecture for Parametric Studies

Ex. No.	Type of laminate	Thickness mm (in)	Lay-up	Lamina Thickness mm (in.)
1	Symm. General Orthotropic	3.05 (0.12)	$[90/\pm10/90]_s$	$90^0 =0.254\ (0.01)$; $10^0 = 0.508\ (0.02)$
2	Symm. General Orthotropic	6.097 (0.24)	$[90/\pm10/90/90/\pm10/90]_s$	$90^0 =0.254\ (0.01)$; $10^0 = 0.508\ (0.02)$
3	Symm. Quasi Isotropic	3.05 (0.12)	$[155/110/65/20]_s$	$155^0=0.38\ (0.015)$; $110^0= 0.38\ (0.015)$; $65^0=0.38\ (0.015)$; $20^0= 0.38\ (0.015)$.
4	Symm. Quasi Isotropic	6.097 (0.24)	$[155/110/65/20/155/110/65/20]_s$	$155^0=0.38\ (0.015)$; $110^0= 0.38\ (0.015)$; $65^0=0.38\ (0.015)$; $20^0= 0.38\ (0.015)$.
5	Symm. In-plane Anisotropic	3.05 (0.12)	$[65/-65/20/110/110/20]_s$	$65^0=0.254\ (0.01)$; $20^0= 0.254\ (0.01)$; $-65^0=0.254\ (0.01)$; $110^0= 0.254\ (0.01)$.
6	Symm. In-plane Anisotropic	6.097 (0.24)	$[65/-65/20/110/110/20/65/-65/20/110/110/20]_s$	$65^0=0.254\ (0.01)$; $20^0= 0.254\ (0.01)$; $-65^0=0.254\ (0.01)$; $110^0= 0.254\ (0.01)$.

The lay-ups were chosen to obtain longitudinal to transverse stiffness ratios that would be typical for beam/column type applications. All of the FRP tubes are assumed to consist of a carbon/epoxy material system with ply properties as given in Table 5.2.2. A summary of the equivalent engineering properties for the selected laminates is given in Table 5.2.3. It should be noted that the values shown for the anisotropic laminates are given only as a reference since equivalent engineering properties are not uniquely defined

(see Section 2.3). Finally, all studies consider that the concrete core consists of normal weight concrete with properties as given in Table 5.2.4.

Table 5.2.2 Material Properties for Carbon/Epoxy plies

Property	Value
Long. Modulus E_{11}	127.1 GPa (18430 ksi)
Trans. Modulus E_{22}	9.5 GPa (1378 ksi)
Shear Modulus G_{12}	4.56 GPa (661.4 ksi)
Poisson's Ration v_{12}	0.263
Ultimate Long. Strain in tension, ε_{XT}	0.01701
Ultimate Trans. Strain in tension, ε_{YT}	0.00703
Ultimate Long. Strain in comp, ε_{XC}	0.01194
Ultimate Trans. Strain in comp, ε_{YC}	0.01743
Ultimate Shear. Strain, ε_{S}	0.01737

Table 5.2.3 Equivalent In-Plane Properties

Ex. No.	E_x GPa (ksi)	E_y GPa (ksi)	G_{xy} GPa (ksi)	v_{xy}
1.	83.45 (12100)	48.83 (7080)	6.78 (983)	0.0964
2.	83.45 (12100)	48.83 (7080)	6.78 (983)	0.0964
3.	49.24 (7140)	49.24 (7140)	18.83 (2730)	0.3083
4.	49.24 (7140)	49.24 (7140)	18.83 (2730)	0.3083
5.	38.83 (5630)*	61.93 (8980)*	18 (2610)*	0.2349*
6.	38.83 (5630)*	61.93 (8980)*	18 (2610)*	0.2349*

*Reference values only (anisotropic laminate)

Table 5.2.4 Concrete Core Properties

Property	Value
Compressive strength, f'_c	34 MPa (5.0 ksi)
Elastic Modulus, E_{co}	29.55 GPa (4286 ksi)
Poisson's Ratio, ν_{co}	0.2

5.3 Effect of Diameter to Thickness Ratio

To evaluate the effect of diameter to thickness ratio (D/t) on the shear response of concrete filled circular FRP tubes, the analytical response of shear load versus maximum shear strain for examples with equal laminate types are compared. The analytical response of the general orthotropic laminates (Ex.1 and Ex.2), the quasi-isotropic laminate (Ex.3 and Ex.4), and the in-plane anisotropic laminates (Ex.5 and Ex.6) are shown in Figure 5.3.1, Figure 5.3.2, and Figure 5.3.3 respectively. A summary of the maximum response quantities for all cases is given in Table 5.3.1.
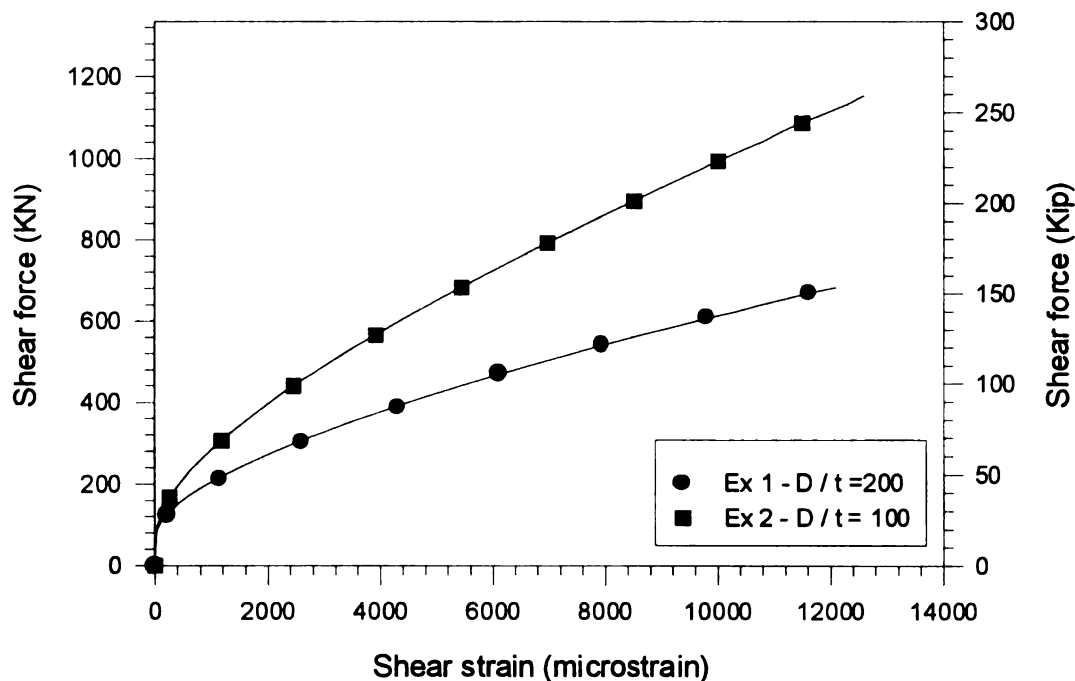
Fig. 5.3.1 Effect of Diameter to Thickness Ratio on General Orthotropic Laminates
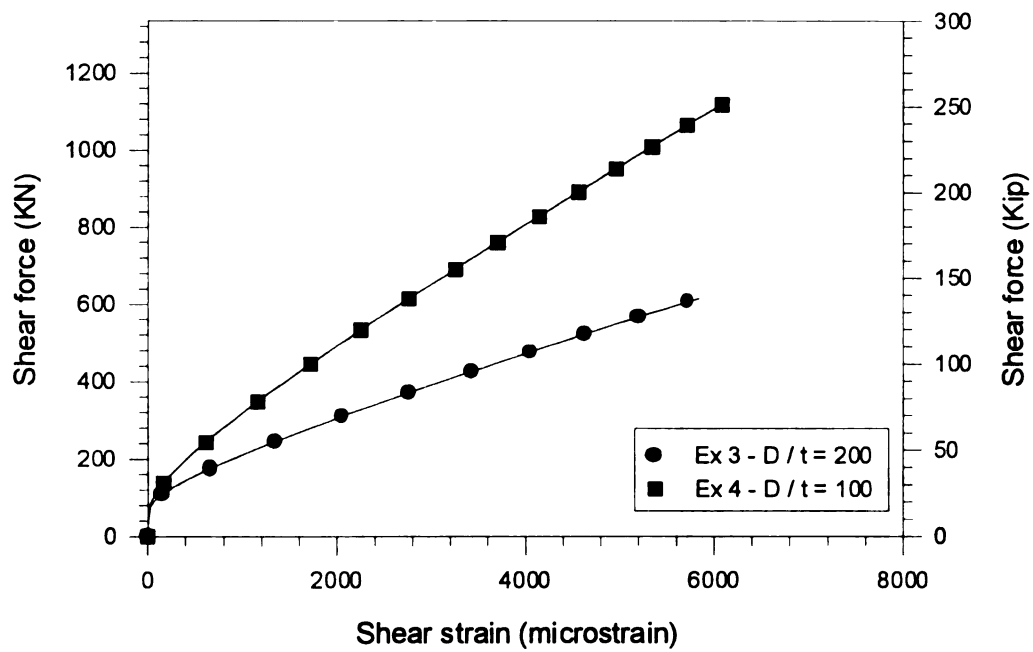
Fig. 5.3.2 Effect of Diameter to Thickness Ratio on Symm.Quasi-Isotropic
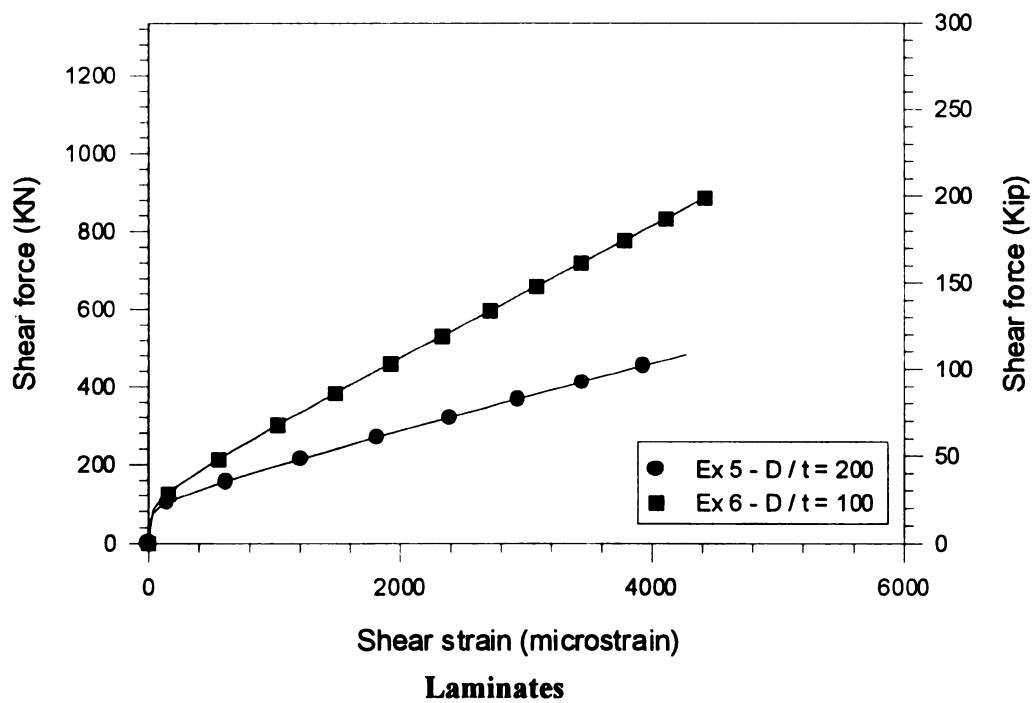
Laminates

Fig. 5.3.3 Effect of Diameter to Thickness Ratio on Anisotropic Laminates

90

Table 5.3.1 Effect of Diameter to Thickness Ratio (D/t)

Ex. No.	Laminate Type	D/t	Max. shear strength V_u KN (Kip)	Maximum/Ultimate Shear strain (x10^6)
1.	Symm. General Orthotropic	200	683 (153.47)	12060
2.	Symm. General Orthotropic	100	1154.2 (259.38)	12630
3.	Symm. Quasi Isotropic	200	614.5 (138.08)	5850
4.	Symm. Quasi Isotropic	100	1131.1 (254.18)	6165
5.	Symm. In-plane Anisotropic	200	482.38 (108.4)	4278
6.	Symm. In-plane Anisotropic	100	883.77 (198.6)	4421

It is clear from the responses that shear carrying capacity of circular concrete filled FRP tubes increases significantly with a decrease in the D/t ratio. With increase in the laminate thickness, the increased FRP shell shear stiffness allows the FRP shell to carry more shear stresses. Although the thicker FRP shell can provide higher confinement levels to the concrete core, this effect is not significant on the shear response of the section as seen by noticing that the responses follow a secondary slope (mainly the tube shear stiffness) at approximately the same point (kink).

5.4 Effect of Axial load

The effect of axial load was studied by considering all six examples with and without axial load. The values of the axial load ratio (P/f_c A_g) were equal to zero and 0.10 (1007 KN [226 Kips]). The zero axial load value provided a baseline for comparison and is a typical condition in beam applications. An axial load ratio of 0.10 represents a nominal design value considered in typical existing bridge columns.
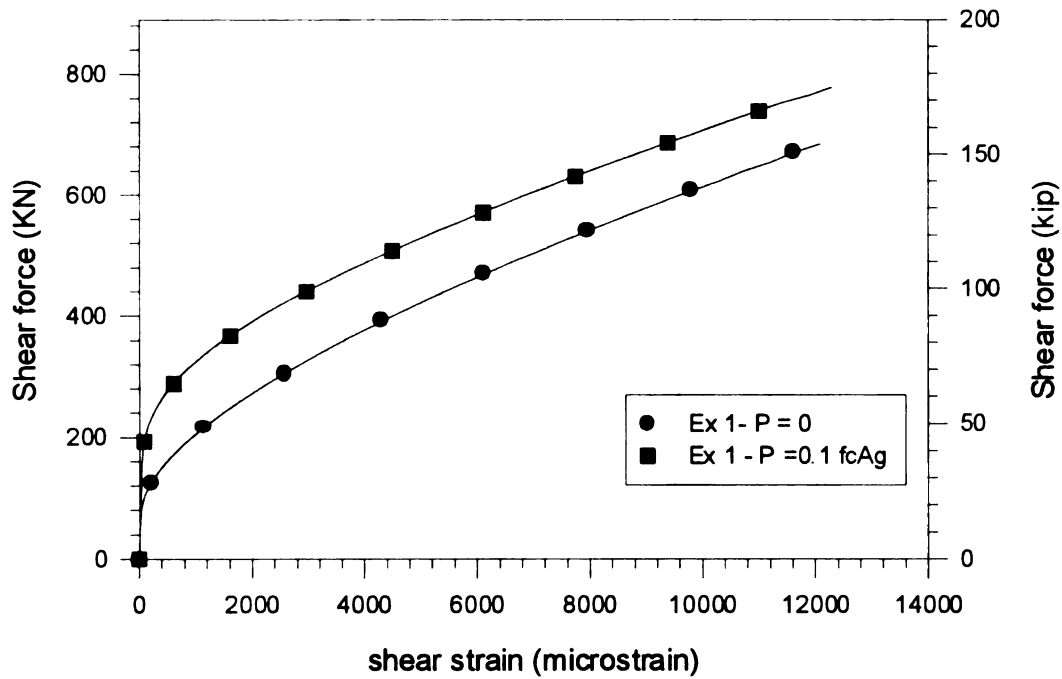
Fig. 5.4.1 Effect of axial load on General Orthotropic Laminates
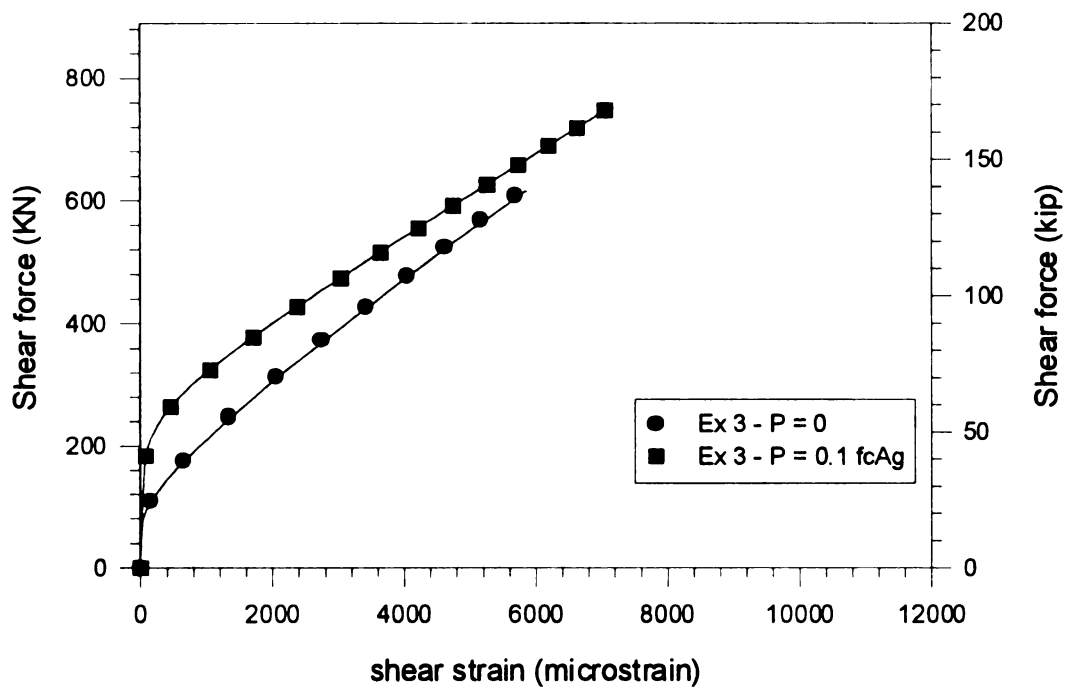
Fig. 5.4.2 Effect of axial load on Symm. Quasi-Isotropic Laminates
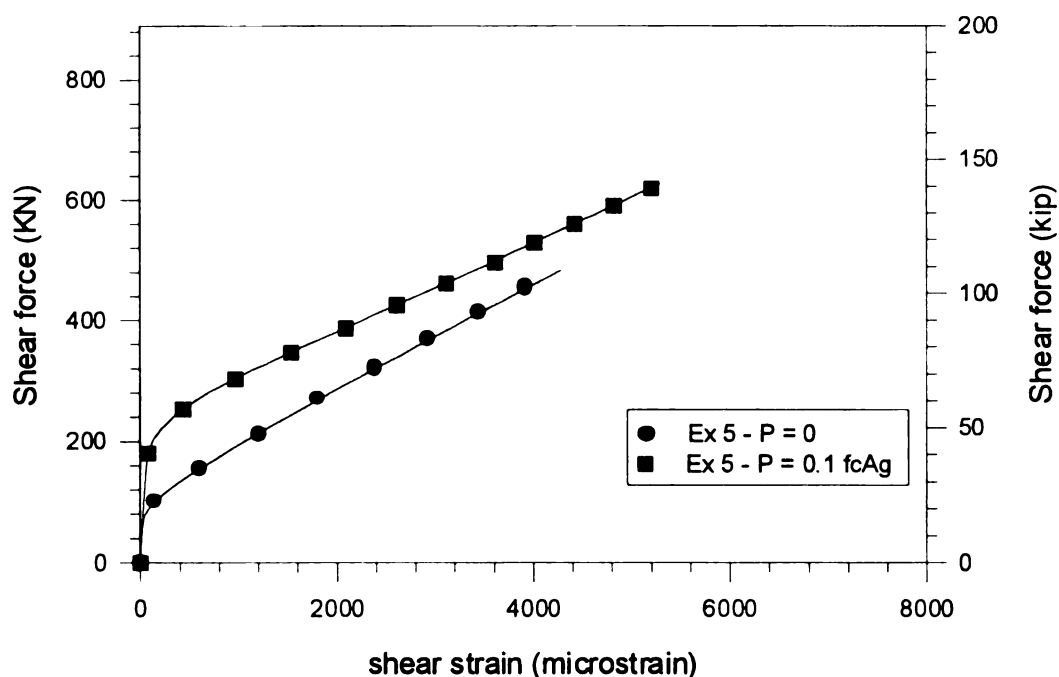
Fig. 5.4.3 Effect of axial load on Anisotropic Laminate

The analytical shear force to maximum shear strain response for examples with equal laminate types are compared in Figure 5.4.1 through Figure 5.4.3. A summary of maximum response quantities and failure types is given in Table 5.4.1. From these figures and tables, it is observed that shear carrying capacity is clearly increased when an axial load is applied. It can be noted that, as expected, the presence of axial load has an effect in delaying the cracking of the section by effectively pre-stressing the concrete core. This enhances the initial shear stiffness of the full section as observed in the initial slope of the shear load-deformation response.

Table 5.4.1 Effect of axial load

Ex no.	Axial Load KN (kip)	Thickness. mm (in.)	V_u KN (kip)	Max. Shear strain (x 10^6)	Lamina Failure Type
1	0	3.05 (0.12)	683 (153.47)	12060	Shear
1	1007 (226)	3.05 (0.12)	776.5 (174.49)	12300	Shear
3	0	3.05 (0.12)	614.5 (138.08)	5850	Fiber Tension
3	1007 (226)	3.05 (0.12)	746.3 (167.71)	7050	Fiber Tension
5	0	3.05 (0.12)	482.38 (108.4)	4278	Fiber Tension
5	1007 (226)	3.05 (0.12)	626.3 (140.75)	5290	Fiber Tension

5.5 Effect of concrete modulus of rupture

The effect of the concrete modulus of rupture was studied by evaluating the shear response of Design #1 from the large-scale test data (see Section 4.2 and 4.3) with different values of concrete modulus of rupture, f_r. The concrete modulus of rupture is taken to range from $f_r = 0.33\sqrt{f_c'}$ (MPa) [$f_r = 4\sqrt{f_c'}$ (psi)] to $f_r = 0.75\sqrt{f_c'}$ (MPa) [$f_r = 9\sqrt{f_c'}$ (psi)]. The analytical responses are compared with the experimental trace in Figure 5.5.1.
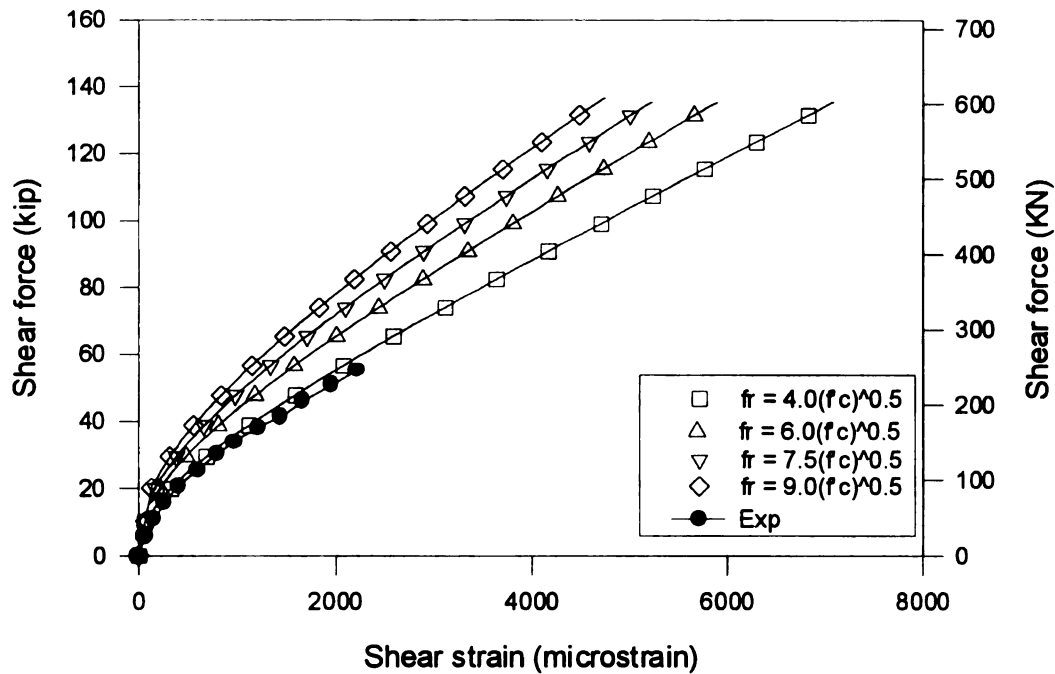
Fig. 5.5.1 Effect of concrete modulus of rupture (Design #1)

It is clear from Figure 5.5.1 that, as the tension stiffening factor increases, the concrete cracks at a higher value of shear load. Also, with the increase in the modulus of the rupture, the hybrid system fails at lower value of shear strain. Comparison of the analytical responses with the experimental trace shows that in the experiment, the concrete cracks at an early stage of loading. The experimental response agrees well with the analytical response with a tension-stiffening factor of 0.33 in MPa (4.0 in psi). Based on this study, the analytical model presented in Chapter 3 used a modulus of rupture value of $f_r = 0.33\sqrt{f_c'}$ (MPa) [$f_r = 4\sqrt{f_c'}$ (psi)].

5.6 Effect of Anisotropic Shell Behavior

The effect of in-plane anisotropic behavior (extension/ shear coupling) of the FRP

tube laminate on the shear response was evaluated by observing the response of examples

5 and 6 (laminates with anisotropic properties). The shear force to maximum shear strain

response for Example 5 (D/t = 200) and Example 6 (D/t = 100) is shown in Figure5.6.1

and Figure5.6.2, respectively. The figure features two traces. One trace shows the shear

response of the section without consideration of the shear coupling terms (i.e. A_{16} and A_{26}

are set equal to zero). The second trace shows the response with consideration of the

extension/ shear coupling terms as prescribed in the proposed formulation in Section 3.3.

A summary of the maximum response quantities is given in the Table 5.6.1.
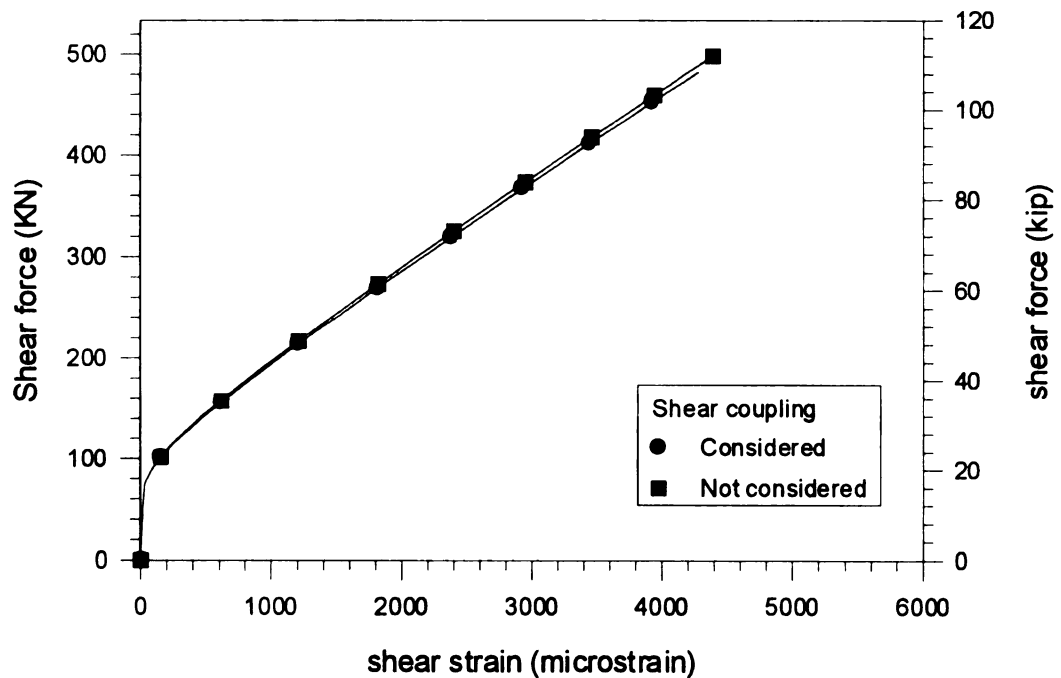
Fig. 5.6.1 Effect of Anisotropic shell behavior (Ex.5)
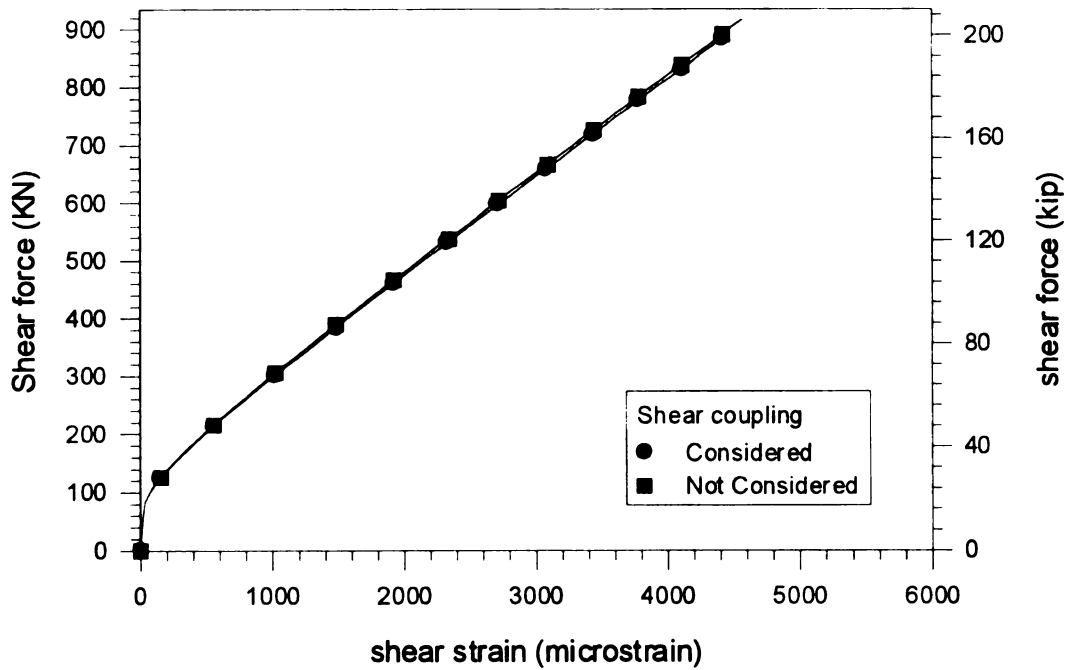
Fig. 5.6.2 Effect of Anisotropic shell behavior (Ex.6)

Table 5.6.1 Effect of Anisotropic shell behavior

Ex. no.	V_u KN (Kip)	Shear strain (x 10^6)	Remarks
5	482.38 (108.4)	4280	Coupling
5	498.3 (111.98)	4390	No Coupling
6	883.77 (198.6)	4420	Coupling
6	916.8 (206.0)	4570	No Coupling

From both examples it is observed that the ultimate shear carrying capacity is reduced by 3.3% and shear strain value is reduced by 3% when anisotropic shell behavior is considered in the analysis. Hence, it is clear from the comparison that, although small for these examples, the anisotropic properties of the FRP shell do influence the shear behavior and shear carrying capacity of concrete filled FRP tubes.
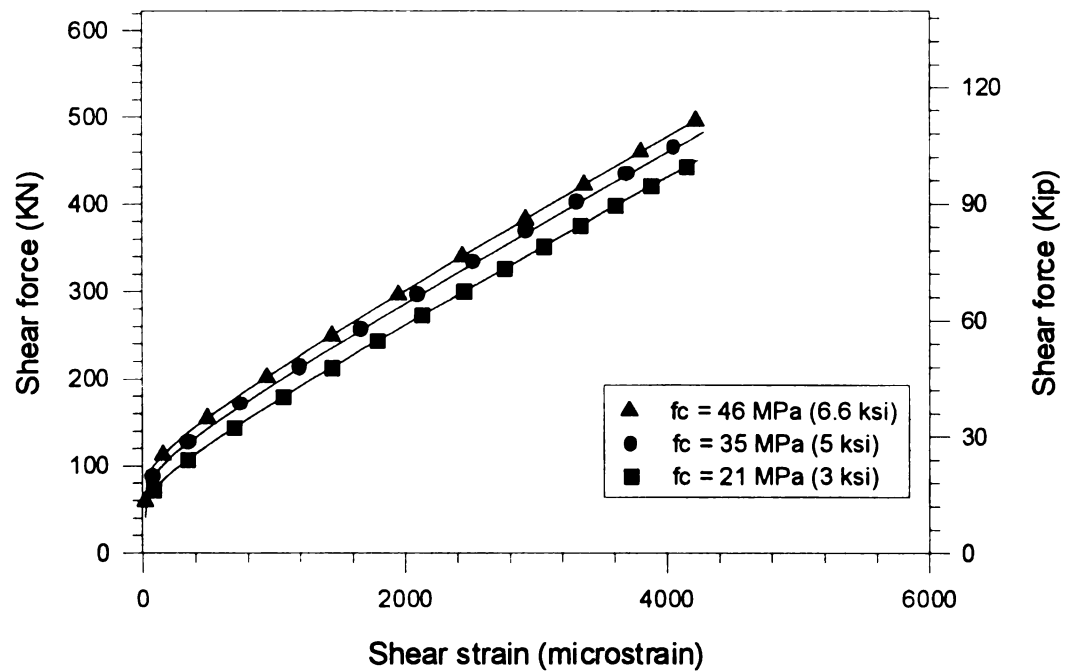
5.7 Effect of compressive strength of concrete

The effect of compressive strength of concrete was studied on examples 1, 3 and 5 by using three values of compressive strength equal to 21 MPa (3 ksi) and 35 MPa (5 ksi) and 46 MPa (6.6 ksi). Normal-weight concrete is considered for the analyses. The analytical shear force to maximum shear strain response for examples 1, 3 and 5 with different concrete compressive strengths is compared in Figure 5.7.1 through Figure 5.7.3 respectively. A summary of maximum response quantities is given in Table 5.7.1
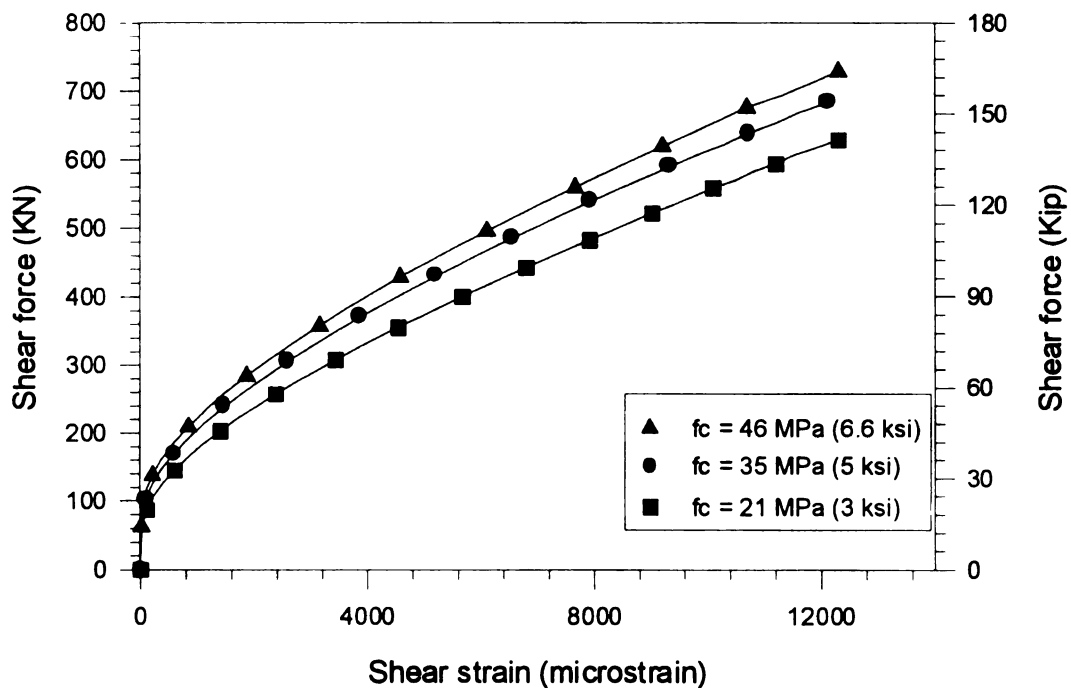
**Fig. 5.7.1 Effect of concrete compressive strength on shear response (Ex.1)**
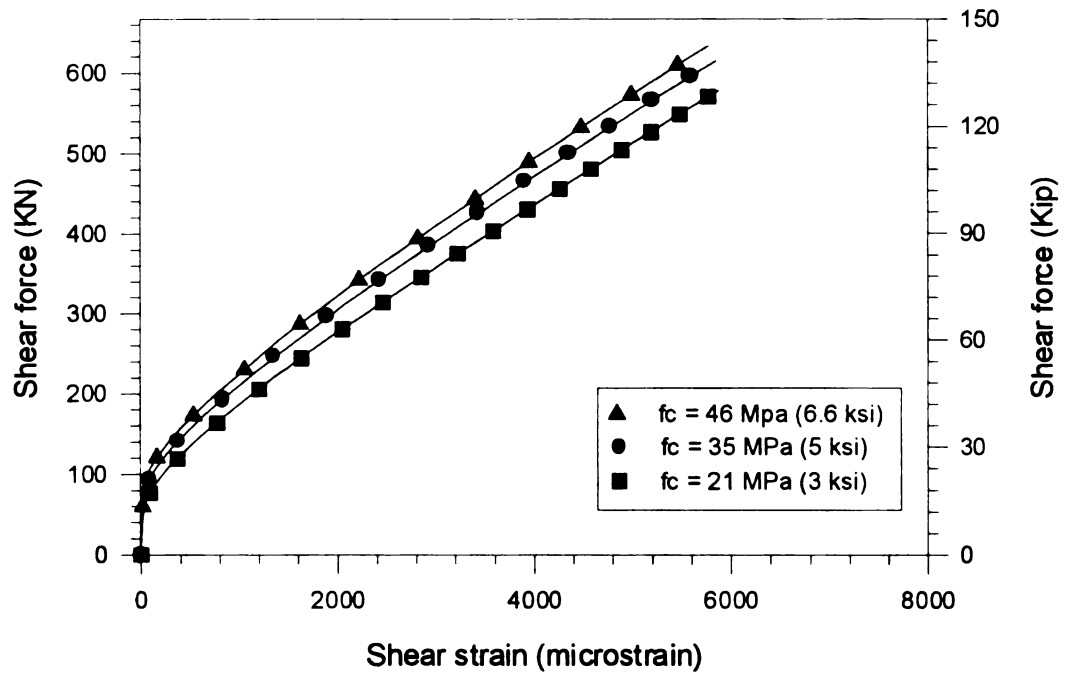
Fig. 5.7.2 Effect of concrete compressive strength on shear response (Ex.3)

Fig. 5.7.3 Effect of concrete compressive strength on shear response (Ex.5)

Table 5.7.1 Effect of Concrete Compressive Strength

Ex. no.	f_c MPa (ksi)	V_u KN (Kip)	Max. Shear strain $(x\ 10^6)$
1	21 (3)	628.6 (141.25)	12300
1	35 (5)	682.9(153.5)	12100
1	46 (6.6)	728.6 (163.74)	12300
3	21 (3)	577.6 (129.8)	5870
3	35 (5)	614.5 (138.08)	5850
3	46 (6.6)	633.4 (142.35)	5770
5	21 (3)	449.7 (101.06)	4230
5	35 (5)	482.4 (108.39)	4280
5	46 (6.6)	495.5 (111.35)	4220
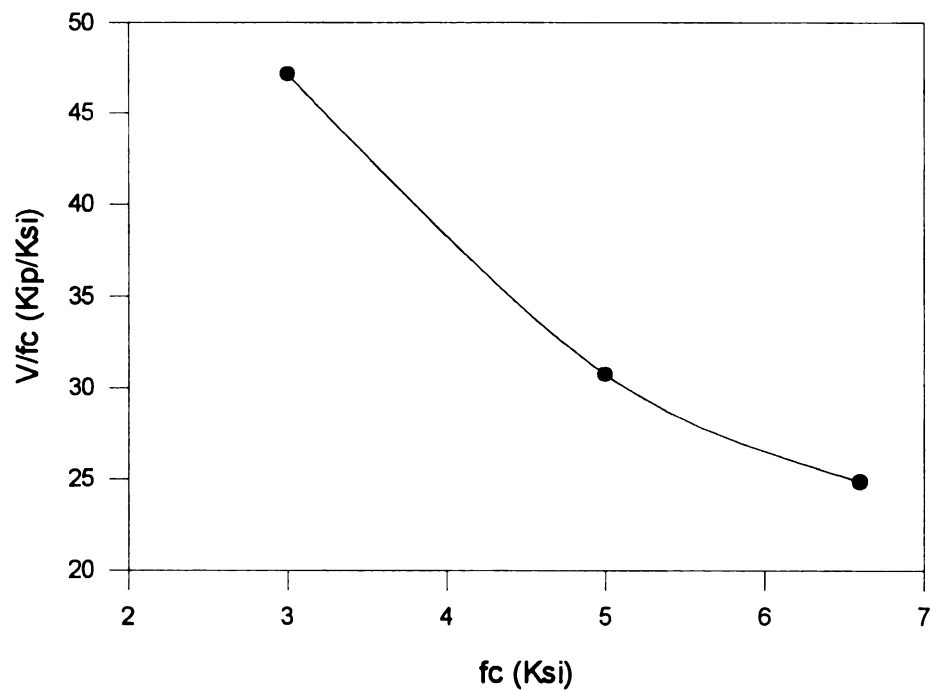
Fig. 5.7.4 Compressive strength and Shear strength to compressive strength ratio

From above examples it is clearly observed that the ultimate shear carrying capacity is only moderately increased with an increase in compressive strength of concrete. The influence of concrete compressive strength on the shear carrying capacity of Example 1 is compared in Figure 5.7.4. It can be observed that the relationship between compressive strength and shear force carrying capacity is not directly proportional. In fact, the ratio of maximum shear force to compressive strength decreases with increase in the concrete compressive strength. This indicates that the increase in the concrete compressive strength doesn't have a significant effect on the shear carrying capacity of concrete filled FRP tubes.

CHAPTER 6: SUMMARY AND CONCLUSIONS

6.1 Summary

This thesis has presented a simple, yet rational analytical procedure to evaluate the shear load–deformation response of concrete filled circular FRP tubes. This procedure was based on previously developed analytical models for the axial and flexural behavior of concrete filled circular FRP tubes. The analytical model follows the fundamental mechanics of shear behavior of structural members in combination with a smeared shear modulus of cracked concrete determined from average principal strains and stresses. The computational procedure is based on a sectional layered analysis with an iterative algorithm to satisfy equilibrium and compatibility conditions in parallel to the well-known modified compression field theory.

To adequately capture the shear stress in the FRP tubes, the existing axial/flexural model was modified to include the extension/shear coupling effects of anisotropic FRP laminates. The concrete constitutive model in tension was modified to include tension-stiffening effects after cracking. Constitutive models for confined concrete in compression and concrete in tension are based on normal stresses and strains. Average principal stresses and strains are then calculated based on equilibrium and compatibility conditions. The shear modulus of concrete is then calculated from these principal values, thus obtaining a smeared shear modulus for the cracked concrete.

The developed model captures the shear load-deformation response of the system throughout the loading history until first ply failure of the FRP composite. A procedure capable of analyzing the shear behavior of concrete filled circular FRP tubes with

composite and non-composite behavior between the concrete core and the FRP tube was implemented. The model was validated using available experimental data from two full-scale and two small-scale tests with composite and non-composite connection detailing, respectively.

6.2 Conclusions

Based on the research study as summarized above, the following conclusions were reached:

1. The analytical response of large-scale concrete filled carbon/Epoxy circular FRP tubes with composite behavior (Design #1 and Design #2) agreed well with the experimental response. The largest discrepancy in the shear force to shear strain response was observed in the tension zone of Design #2 (at −30° location). Unfortunately, an explanation to this discrepancy could not be reached as the remainder load deformation histories and section strain profiles at different stages of loading showed consistent trends and were, in general, in good agreement with the experimental values.

2. The analytical responses of small-scale concrete filled carbon/Epoxy circular FRP tubes with non-composite behavior (Design #3 and Design #4) are considered to agree well with the experimental response although some discrepancies exist with the response of Design #4. Most significantly, at location 6 (tension zone) of Design #4, the analytical response deviated significantly from the experimental response. The sources for these differences are thought to be a faulty strain gage and limitations of the developed model. It can be observed that, the shear strain

gauge at that location in the experiment consistently recorded lower values. In addition, the experimental shear stress to shear strain response showed a transition from fully composite to a partial-composite behavior when the response was compared with the analytical traces with full- and non-composite action. As discussed above, the presented model does not consider this state of partial shear interaction. Despite this discrepancy, the shear strain profile across the section for both designs followed the expected trends throughout the loading history when compared with the experimental values.

3. The behavior of concrete, both before and after cracking, under tensile stresses has a considerable effect on the computation of the shear load deformation response of concrete filled circular FRP tubes. Following the currently available constitutive models, parameters such as concrete type, cracking strength and tension stiffening behavior are consequently heavily influential in the presented analytical procedure.

4. Inclusion of extension/shear coupling effects on the considered case (symmetric in-plane anisotropic laminate) showed only a small influence on the shear deformation response. The ultimate shear force and shear strain capacities were reduced by only 3.3% and 3% respectively. Thus, while an effect is quantifiable, the case considered showed only a small influence on the overall response. While laminate designs with higher extension/shear coupling term values might exhibit greater effects, their use for actual designs is doubtful and were not considered.

5. As expected, the shear carrying capacity of circular concrete filled FRP tubes increases with increase in compressive strength of concrete. However, it was

observed that the ratio of maximum shear force to compressive strength decreases with increase in the concrete compressive strength. This indicates a small influence of concrete compressive strength on the shear carrying capacity. The increase in the shear carrying capacity was found to be in the range of 10-15% when the compressive strength was increased from 21 MPa (3 Ksi) to 46 MPa (6.6 Ksi).

6. The effect of axial load on shear force to maximum shear strain response on examples with symmetric general orthotropic laminates, symmetric quasi isotropic laminates and symmetric in-plane anisotropic laminates types were compared. For all the examples, the shear carrying capacity was increased when an axial load was applied. The presence of axial load has an effect in delaying the cracking of the section by effectively pre-stressing the concrete core. For symmetric general orthotropic laminates, the shear carrying capacity was increased by 13% while ultimate shear strain value was increased by 2% when the axial load was applied. Also, the shear carrying capacity of the symmetric quasi isotropic laminate was increased by 20% while ultimate shear strain value was increased by 20% and the shear carrying capacity of symmetric in-plane anisotropic laminates was increased by 30% while ultimate shear strain value was increased by 23%.

7. The effect of shear interaction between the FRP shell and the concrete on the shear load-deformation response of the small-scale test units was studied. It was observed that, for Design #3, the ultimate shear force capacity was reduced by 18% and the ultimate shear strain value was increased by 72% when considering

non-composite behavior versus composite behavior. In the same way, for Design #4, the ultimate shear force capacity was reduced by 25% and the ultimate shear strain value was increased by 60%.

6.3 Recommendations for Future Research

The following issues are identified as areas for future research to improve the analytical evaluation of the shear behavior of concrete filled FRP tubular members.

1. In this research work, a full bond between concrete and FRP tube was considered in the first analytical model while in the second analytical model no bond was considered between concrete and FRP tube after cracking of concrete. However, it was observed that, the bond between concrete and FRP tube has a considerable effect on the shear carrying capacity of the section. This research study did not consider partial shear interaction between concrete and FRP tube in the analysis. It is designated as a future research area to understand and model the effect of partial bond over the shear response of the section. This will probably require experimental testing to develop a correlation between shear stress transfer and slip between the FRP tube and the concrete core.

2. Further research work is required to characterize the compressive and tensile stress-strain response of *FRP-confined cracked concrete* subjected to biaxial stress demands. This will also require experimental testing and formulation of average stress-strain relationships for the *FRP-confined cracked concrete*.

3. Efforts were made to formulate the capacity of the member to transmit forces across the cracks by limiting value of f_{c1} for the concrete core system. However,

its influence on the tensile stresses in the concrete was not fully identified. This formulation was based on preliminary assumptions of modified compression field theory. Further studies are thus required to appropriately formulate this effect for FRP reinforced structures and to evaluate its effect.

REFERENCES

[1] American Concrete Institute, Building Code Requirements for Reinforced Concrete (ACI 318-95) and Commentary (ACI 318R-95), Detroit, 1995.

[2] Burgueno, R., "System Characterization and Design of Modular Fiber Reinforced Polymer (FRP) Short and Medium-Span Bridges", Doctoral Dissertation, University of California, San Diego, La Jolla, California, March 1999.

[3] Collins, M.P., Mitchell, D., Pre-stressed Concrete Structures, Response Publications Canada, 1997

[4] Davol A., "Mechanical Characterization of Concrete Filled FRP Members", Doctoral Dissertation, University of California, San Diego, La Jolla, California, June1998.

[5] Davol, A., Burgueno, R., and Seible, F., "Flexural Behavior of Circular Concrete Filled FRP Shells", *Journal of Structural Engineering*, July 2000.

[6] Elwi, A.A., Murray, D.W., (1979), "A 3D Hypoelastic Concrete Constitutive Relationship", Journal of the Engineering Mechanics Division, Proceedings of the American Society of Civil Engineers, Vol.105, No.EM4, August, pp. 623-641.

[7] Hartog Den, J.P., Strength of Materials, McGraw-Hill Book Co., New York, 1949.

[8] Jones, Robert M., Mechanics of composite materials, Scripta Book Company, Washington, D.C., 1975.

[9] Mander, J.B., Priestley, M.J.N., and Park, R. (1988), "Theoretical stress-strain model for confined concrete", *Journal of Structural Engineering*, Vol.114 No.8, August, pp. 1805-1826.

[10] Mirmiran, A., Shahaway, M., El Khoury, C., and Naguib, W., "Large Beam-Column Tests on Concrete Filled Composite Tubes", *ACI Structural Journal*, Vol. 97 No. 2, March-April 2000, pp. 268-276.

[11] Popov, E.P., Introduction to mechanics of solids, Prentice-Hall Inc., New Jersey, 1968.

[12] Priestley, M.J.N., Verma, R., and Xiao, Y., "Seismic Shear Strength of reinforced Concrete Columns", *Journal of Structural Engineering*, Vol.120 No.8, August 1994, pp. 2310-2329.

[13] Priestley, M.J.N., Seible, F., Xiao, Y., and Verma, R., "Steel Jacket Retrofit of Squat RC Bridge Columns for Enhanced Shear Strength – Part I – Theoretical Considerations and Test Design", *ACI Structural Journal*, Vol. 91 No. 4, July-August 1994, pp. 394-405.

[14] Priestley, M.J.N., Seible, F, And Calvi, G.M., Seismic Design and Retrofit of Bridges, John Wiley & Sons, New York, NY, 1996.

[15] Rizkalla, S.H., Fam, A., "Confinement Model for Axially Loaded Concrete Confined by Circular Fiber-Reinforced Polymer Tubes", *ACI Structural Journal*, Vol. 99, No. 3, May/June 2002, pp. 386-390.

[16] Seible, F., "Design of structures with Advanced Composites for the 21st century" Proceedings of the International Symposium on Conceptual Design of structures, University of Stuttgart, Stuttgart, Germany, October 1996, pp. 945-952

[17] Seible, F., Karbhari, V. M. and Burgueno, R., "Kings Stormwater Channel and I-5/Gilman Bridge", Structural Engineering International, *Journal of the International Association for Bridge and Structural Engineering*, Vol. 9, No. 4, November 1999.

[18] Sokolnikoff, I.S., Mathematical Theory of Elasticity, Providence, R. I., 1941

[19] Tsai, S.W., Introduction to composite materials, Technomic Publishing Company, Inc., Pennsylvania, 1980.

[20] Vecchio, J.V., Collins, M.P., (1986), "The Modified Compression Field Theory for Reinforced Concrete Elements Subjected to Shear", *ACI Structural Journal*, Vol. 83 No 2, March-April, pp. 219-231.

[21] Vecchio, J.V., Collins, M.P., (1988), "Predicting the Response of Reinforced Concrete Beams Subjected to Shear Using Modified Compression Field Theory", *ACI Structural Journal*, Vol. 85 No.3, May-June, pp. 258-268.

[22] Volterra, E., Gaines, J.H., Advanced Strength of Materials, Prentice-Hall, N.J., 1971

[23] Zhu, R.H., Hsu, T.C., and Lee, Jung-Yoon, "Rational Shear Modulus for Smeared-Crack Analysis of Reinforced Concrete", *ACI Structural Journal*, Vol. 98 No. 4, July-August 2001, pp. 443-450.